EVALUATION OF LIQUEFACTION POTENTIAL IN RELATION TO THE SHEARING HISTORY USING SHEAR WAVE VELOCITY

劉, 国軍

https://doi.org/10.15017/2534440

出版情報：Kyushu University, 2019, 博士（工学）, 課程博士
バージョン：
権利関係：

EVALUATION OF LIQUEFACTION POTENTIAL IN RELATION TO THE SHEARING HISTORY USING SHEAR WAVE VELOCITY

劉　国軍

GUOJUN LIU

SEPTEMBER 2019

EVALUATION OF LIQUEFACTION POTENTIAL IN RELATION TO THE SHEARING HISTORY USING SHEAR WAVE VELOCITY

A THESIS SUBMITTED

IN PARTIAL FULFILLMENT OF THE REQUIREMENTS

FOR THE DEGREE OF

DOCTOR OF ENGINEERING

BY

GUOJUN LIU

TO THE

DEPARTMENT OF CIVIL AND STRUCTURAL ENGINEERING
GRADUATE SCHOOL OF ENGINEERING
KYUSHU UNIVERSITY
FUKUOKA, JAPAN
2019

GEOTECHNICAL ENGINEERING LABORATORY
DEPARTMENT OF CIVIL AND STRUCTURAL ENGINEERING
GRADUATE SCHOOL OF ENGINEERING
KYUSHU UNIVERSITY
FUKUOKA, JAPAN

CERTIFICATE

*The undersigned hereby certify that they have read and recommended to the Graduate School of Engineering for the acceptance of this dissertation entitled, "**EVALUATION OF LIQUEFACTION POTENTIAL IN RELATION TO THE SHEARING HISTORY USING SHEAR WAVE VELOCITY**" by **GUOJUN LIU** in partial fulfillment of the requirements for the degree of **DOCTOR OF ENGINEERING**.*

Dated: August 2019

Supervisor:

_____
Prof. Noriyuki YASUFUKU, Dr. Eng.

Examining Committee:

_____
Assoc. Prof. Yukihide KAJITA, Dr. Eng.

_____
Prof. Hideo NAGASE, Dr. Eng.

Abstract

The serious disasters caused by the recurrence of soil liquefaction during the 2016 Kumamoto Earthquakes, is the primary motivation in this study. The potential cause of these disasters was considered mainly with two directions by researchers. Most opinions supposed the foreshock as the pre-shearing impact on the ground greatly when mainshock came. In this concern, the changes of particle structure and excess pore water pressure, which were produced by the foreshock, influenced the liquefaction potential significantly. On the other side, some of researchers concerned from the special geological conditions in Kumamoto-Aso area. The volcanic grains may play an important role to affect the soil behaviors in liquefied sites. However, the mechanism is still not clear now. More importantly, the investigation method needs to be developed urgently for the future earthquakes, which could evaluate liquefaction potential and the changes quickly and reliably.

According to these concerns, Kuroboku, a typical volcanic soil distributed in Kumamoto-Aso, was selected as one of the test materials to detect the liquefaction behaviour. This is for discussing the potential influence from volcanic component in liquefied sites. Boiled sand was carried into the tests to represent the typical soil condition for the liquefied sites in the 2016 Kumamoto Earthquakes. Fine sand also was used to represent a sandy ground where is very prone to be liquefied generally. These samples tested by using cyclic tri-axial apparatus assembled with bender elements. The liquefaction and re-liquefaction behaviours were investigated by cyclic tests. Meanwhile, the velocity of shear wave in samples was measured by bender elements accompanied with the cyclic tests. The velocity was discussed on the correlation with the liquefaction potential, concerning the effects from shearing history particularly.

The contents of each chapter in this dissertation are arranged briefly as follows:

In Chapter 1, the research background and motivation were described. The damages induced by soil liquefaction were considered as one of the most destructive

disasters in earthquakes. Meanwhile, the recurrence of liquefaction also was not uncommon. Two typical issues of the 2011 Earthquake off the Pacific coast of Tōhoku and the 2016 Kumamoto Earthquakes were introduced for the recurrences of liquefactions in Japan. The objectives and research flow of this study were also presented in this chapter.

In Chapter 2, the literatures were reviewed from the researches related to the changes of liquefaction behaviours by pre-shearing and the shear-wave-based evaluation on liquefaction potential. Two dominant explanations were described briefly for the changes of liquefaction resistance effected by pre-shearing. Their considerations based on the views from the stress-strain relation and from the micro changes of particles structure respectively. Some previous studies related to the basic physical properties of Kuroboku and the boiled sand also were presented.

In Chapter 3, the setup of test equipment was introduced firstly. Secondly, several preparation methods for samples were discussed with the influences on saturation degrees. The general test conditions and test progresses were introduced finally.

In Chapter 4, liquefaction and re-liquefaction behaviours of the fine sand were investigated. The saturated sand was discussed primely. Some results from partially saturated sand were compared. The main results indicated the great reduction of liquefaction resistance in saturated sand if it was liquefied once. The excess pore water pressure *EPWP* and axial strain produced much faster in re-liquefaction stages. At the same time, the *EPWP* increased much faster than axial strain in re-liquefaction stage. The re-liquefaction behaviour of partially saturated sand was affected by cyclic load ratio *CSR* potentially.

In Chapter 5, Kuroboku and boiled sand were tested for detecting the liquefaction and re-liquefaction behaviours. The results indicated the Kuroboku owned a very high liquefaction resistance even if the fines were removed. The liquefaction resistance increased significantly after first liquefaction stage. The boiled sand owned the lowest liquefaction resistance in the three soils though it contained approximately 10% of fines.

In Chapter 6, the shear-wave-based evaluation on liquefaction potential was discussed with different soils and shearing histories. The effect of shearing history was

concerned as two situations, that the excess pore water was completely discharged or remained in soil. The results expressed that this shear wave velocity cannot clearly indicate the change of liquefaction resistance between first and second liquefaction stages. However, the velocity performed a well relationship with the residual effective stress in soils. In a determined soil, this method could indicate the reduction of liquefaction resistance quantitatively when *EPWP* produced. Furthermore, in a simulated in-situ condition, the correlation became closer that the shear wave velocity increased with the increasing of liquefaction resistance generally. In previous researches, the method was very limited to identify a saturated ground, which could be liquefied or not by the proposed boundaries. Based on the laboratory results in this study, the scope of application was significantly extended to the grounds with the different saturation degrees, relative densities, and shearing histories.

In Chapter 7, the achievements and the discussion for the whole dissertation were presented. And some recommendations for further work were proposed.

ACKNOWLEDGEMENTS

I have the gratitude to the following people, because no body of the research could be completed in isolation during the doctoral works of three years. Without their encouragement and supports, this study should never have been done.

First and foremost, I would like to appreciate my supervisor, Prof. Dr. Noriyuki Yasufuku of Kyushu University. He gave me a precious opportunity to continue the study of soil liquefaction after the 2016 Kumamoto earthquake. He let me explore freely the research direction and always encouraged me when I dropped the trough in study. Finally, he guided me how to find the right direction by scientific approaches to keep me being motivated.

Secondly, specially thanks to Assoc. Prof. Dr. Ryohei Ishikura, Kyushu University. He took me into the world of soil liquefaction in my master period. And he kept shearing his ideas and suggestions in the group seminars and academic conferences. I am also grateful to Assoc. Prof. Dr. Yingbin Zhang of Southwest Jiaotong University and Lecturer Dr. Qiang Liu of Shandong University of Science and Technology, for his valuable suggestions during all the stages of this study. At the same time, I would like to appreciate Assoc. Prof. Dr. Xing Xu and Mr. Jinhui Xiao of University of Electronic Science and Technology of China, who provided many indispensable suggestions and supports in the analysis works for test results.

I owe a great debt to my dissertation committee members, Assoc. Prof. Yukihide Kajita of Kyushu University and Prof. Hideo Nagase of Kyushu Institute of Technology for their time in reviewing and providing the guidance, advices and comments on this study.

I am grateful to Prof. Dr. Hideo Nagase of Kyushu Institute of Technology again for providing the boiled sand from 2016 Kumamoto earthquake. And I am also grateful to Mr. Yamashita and the company *Kumagaigumi* he worked for. They

conducted a meaningful situ investigation and provided mass of volcanic soil (Kuroboku). These materials were indispensable for experiments in this study.

I would like to heartfelt thanks to Prof. Dr. Masayuki Hyodo, Prof. Dr. Yukio Nakata of Yamaguchi University, Prof. Dr. Satoshi Murakami of Fukuoka University and Prof. Dr. Michael Brown of University of Dundee. their worthful suggestions concerned on the problems of soil liquefaction.

I would like to express my sincere gratitude to Mr. Michio Nakashima, who worked as the technician in the laboratory belong to Geotechnical Research Group. He supported me countlessly for ensuring the experiments conducted smoothly during the three years. Administrative assistance from Ms. Aki Ito during my study is also greatly appreciated.

I would like to thank all student who I am studying with in Geotechnical Research Group. They created a harmony environment and let me really enjoy my life and study. There are special thanks to Dr. Okri Asfino Putra, and Mr. Chengqiong Qin, Dr. Chunrui Hao from Global Geo-disaster and environment Group for their great help in experiments. There are also special thanks to Post Dr. Manafi K.P. Siavash and Mr. Gobin Mukteshwar who gave the useful suggestions in English writing. There are also special thanks to my friends, Dr. Kunpeng Wang, Dr. Yi Fei , Dr. Chi Lu, Dr. Yi Li, Miss Weiwen Wang, Miss Chu Chu, Mr. Dalei Shi, Mr. Jie Liu, and Mr. Yutao Hu, who were studying and living together during the three years at the same floor of 11th of West-2, Kyushu University.

Finally, I would like to thank my wife, for having always respected and supported my decision and giving me the confidence in completion of the study in Japan. This study took me far away from her where she lives with our daughter in China. She has been patient to wait me and provided her continuous encouragement and support in the past years.

Contents

List of Figures

List of Photos

List of Tables

Nomenclature

ϕ Angle of friction.

σ' Effective total stress

MSF magnitude scaling factor

σ'_c Effective confining pressure

σ'_h Effective horizontal effective stress

σ'_v Effective overburden stress

C_r Conversion factor

C_s Constant determined empirically

C_v Conversion factor to correct V_s for overburden pressure

D_0 Diameter of specimen after forming by mould

H_0 Height of specimen after forming by mould

P_a Reference stress

σ'_1, σ'_3 Major and minor principle effective stresses, respectively

$\sigma'_a, \sigma'_b, \sigma'_c$ Principal effective stress acts along the propagation direction, in the direction of particle motion, on the plane, respectively

σ_c Confining pressure

σ'_m Mean effective stress

ΔT Travel time

B.P. Backpressure

c Cohesion

C.P. Cell pressure

CRR Cyclic resistance ratio

CRR_{tx} Cyclic resistance ratio in tri-axial tests

CSR Cyclic stress ratio

DA. Axial strain with amplitudes in double directions

D_r Relative density

e_{max} Maximum void ratio

e_{min} Minimum void ratio

Fc Content of fines

F(e) Void ratio function

Gs Specific gravity

K_0	Lateral earth pressure coefficient at rest
L	Length between Top-to-Top of bender elements
LFT	Line of phase transformation
LL	Liquid Limit
$N.P.1$	Negative pressure access (No.1)
$N.P.2$	Negative pressure access (No.2)
Nc	Number of load cycles
p'	Effective mean principal stress
PI	Plastic Index
PL	Plastic Limit
q'	Shear stress
$Sr.$	Saturation degree
u	Excess pore water pressure
u/σ_{c0}'	Excess pore water pressure ratio
V_s	Shear wave velocity
V_{s1}	Stress-corrected shear wave velocity

CHAPTER 1

INTRODUCTIONS

1.1 Earthquakes and liquefaction disasters in Japan

1.1.1 Earthquakes in history of Japan

Japan is one of the most vulnerable nations to earthquakes in the world for the special geographical position that locates at the border between Eurasian plate and pacific plate. *Chronological Scientific Tables,* edited by National Astronomical Observatory of Japan (NAOJ), recorded the number of earthquakes which was greater than M6.1 in history from 416 *AD* in Japan[1)]. More than 300 events were recorded by now. Moreover, in recent years, the number of earthquakes occurred in japan occupied about 10%~15% in total number in the world, and if the magnitude raises to M6.0, occupancy increases to around 20% by record. Table 1.1 summarized some greatest earthquakes by order of lost people after having the observing recorded (Japan Meteorological Agency, *JMA* Report a and Report b).

Table 1.1 Top 10 earthquakes in Japan by dead people including the lost

Rank No.	Name	Year	Dead & Loast	Magnitude(M)
1	Great Kantō earthquake	1923	105,385	7.9
2	2011 earthquake off the Pacific coast of Tōhoku	2011	22,199	9.0
3	1896 Sanriku earthquake	1896	21,959	8.2
4	1891 Mino–Owari earthquake	1891	7,273	8.0
5	Great Hanshin earthquake	1995	6,437	7.3
6	1948 Fukui earthquake	1948	3,769	7.1
7	1933 Sanriku earthquake	1933	3,064	8.1
8	1927 Kita Tango earthquake	1927	2,912	7.3
9	1945 Mikawa earthquake	1945	1,961	6.8
10	1946 Nankai earthquake	1946	1,443	8.0

*Data was quoted from Japan Meteorological Agency.

1.1.2 Disasters induced by soil liquefaction in earthquakes

Many research and development were conducted by researchers for preventing the structure damages when attacked by earthquakes. The developed countermeasures were applied in buildings' designs and constructions, that exactly saved people lives from the disasters from violent earthquakes. However, the disaster induced by ground liquefaction had not be attracted enough attention, until the great liquefaction appeared in the widespread in Niigata, Japan, where the great earthquake struck in 1964. After that event, the ground failure induced by soil liquefaction become to be pied more and more attentions by researchers.

Photo 1.1 Building's collapse caused by ground liquefaction in Niigata earthquake, 1964. (Japan National Committee on Earthquake Engineering)

Photo 1.1 was photographed in the Niigata earthquake that showed the most popular photo in research filed of soil liquefaction. Although the upper structure of these buildings was not expressing the serious damages by the shakings in this earthquake, the collapses were induced by foundations losing the entire sustaining strength when soil was liquefied by ground movement in earthquakes. Liquefaction is

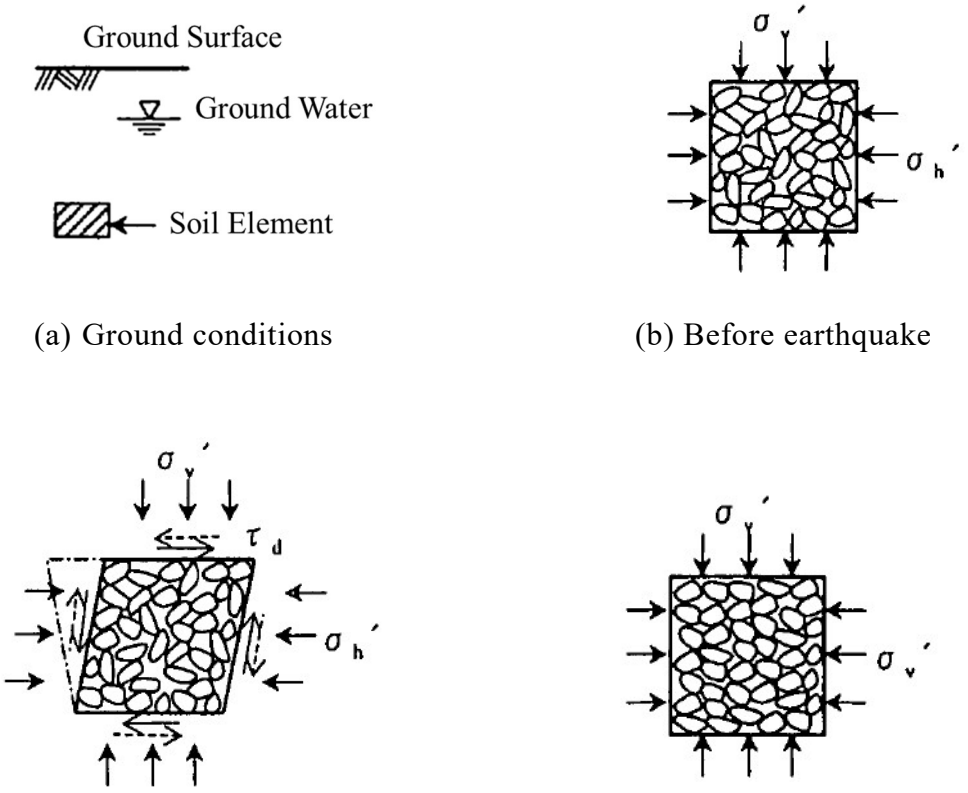

(a) Ground conditions

(b) Before earthquake

(c) During earthquake (Non-liquefaction)

(d) During earthquake (Liquefied)

(e) After earthquake (Deposition)

(f) After earthquake (accumulations on ground surface)

Figure 1.1 Mechanism of soil liquefaction (S. Yasuda 1988)

a transient response when soil loses the all effective stress and ground would become a liquid state at that moment. Certainly, the duration of liquefaction and the extent of damage to structures were also depended on the earthquakes. The mechanism of soil liquefaction could be demonstrated by Figure 1.1.

Soil liquefaction is commonly considered to be easily caused in the saturated environment. Thus, the soil element is carried from under the ground water as showed in Figure 1.1 (a). The stress state of this element could express by the Figure 1.1 (b), that the element is suffered by the vertical pressure (effective overburden pressure σ_v') and from the surrounding pressure (effective horizontal pressure σ_h'). At the same time, the shape of element is kept by the contact force(friction). In this state the shear strength could be expressed by,

$$\tau_f = c + \sigma' \tan\phi \tag{1.1}$$

Where, c is the cohesion, σ' is the effective total stress, ϕ is the angle of friction.

Figure 1.1 (c) indicates the soil is being suffered the cyclic shear force when earthquake is coming. This cyclic loading causes the deformation of the soil element, that lead to a decrement of contact force inter particles, meanwhile the soil tends to shrink from initial shape. However, the produced pore water can not run out from void formed from initial shape. The excess pore pressure would increase during process of the cyclic loading until it completely replaces the contact force inter particles. At this moment, the soil particles lose effective stress $\sigma' = 0$, and are suspended in water. The shear strength $\tau_f = c$ as well. c normally is considered as 0 for sandy soil, therefore, $\tau_f = 0$, and the sand would be completely liquefied in final. The shaking from earthquake keeps in seconds to tens of seconds normally, thus, the element keeps in a undrain environment.

After the earthquake, the soil particles start to deposit within the discharge of excess pore water. In the other hand, the excess pore water flow to the ground surface to dissipate the excess pore pressure. Finally, the water erupts from ground which is carrying the suspended soil particles.

Within the dissipation of excess pore water pressure, the soil particles would deposit to Figure 1.1 (e) or (f) in the end. If the soil particles deposit as (e), the sand became denser than initial state, which is supposed to own a greater strength. And if he soil particles deposit as (f), the soil particles accumulated on the surface of ground and developed a new layer with a loose state. It is considered owning a less strength than initial.

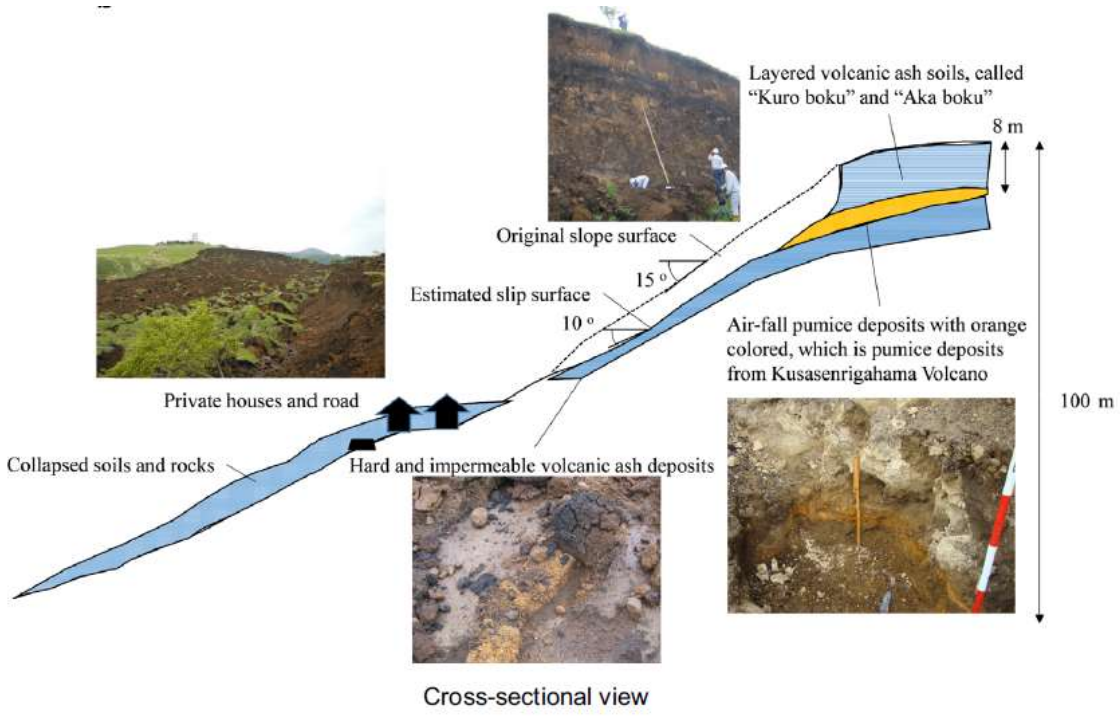

Figure 1.2 Cross view of a landslide in Takanodai with the gentle slope and long runout （T. Mukunoki et al. 2016）

The disasters induced by soil liquefaction was generally concerned with that causing the loss of support from structure's foundation such as the collapse in Niigata

earthquake. And the movement of soil particles, that directly impacted on the structure's foundation or sub ground structures (Y. Yoshimi 1998).

In recent years, some landslide with gentle slope and long distance also were considered by affected by potential liquefaction layer below the surface. In the 2016 Kumamoto earthquakes, the landslide which occurred in Takanodai, Minami-Aso village, had only 10 degrees of potential slip surface. That is generally slight enough to remain stabilized under the horizontal inertial force of an earthquake. The produced excess pore pressure in the potential liquefaction layer was looked as the major factors in this landslide. (T. Mukunoki et al. 2016).

1.1.3 Typical re-liquefaction events in Japan

As mentioned in above, the earthquake is very frequent in Japan. Meanwhile, by the considering about the two approaching for the deposition of liquefied soil particles after earthquakes, it could not be avoided that the liquefaction occurred repeatedly in a same place or the near area. E. Kuribayashi, and F. Tatsuoka, (1975) summarised the liquefied sites from Meiji era in Japan. There were 7 sites were verified to be re-liquefied which was recorded.

Besides, S. Yasuda and I. Tohno (1983); K. Wakamatsu et al. (2012, 2017) R. Hirata (2018) investigated the liquefied sites in 1983 Nihonkai Chubu earthquake, and 2011 earthquake off the Pacific coast of Tōhoku and 2016 Kumamoto earthquake, the results proved the recurrence of liquefaction in the same sites, as shown in Figure 1.3, 1.4 and 1.5. And they also clarified that the liquefaction resistance may reduce even the earthquakes is weaker than previous earthquakes.

The investigation of 1983 Nihonkai Chubu earthquake and 2011 earthquake off the Pacific coast of Tōhoku were conducted to compare with other earthquakes in history. Such as the sites in 2011 earthquake off the Pacific coast of Tōhoku were found where also were liquefied in 1987 Chiba Tohooki earthquake (M6.7) and Miyagiken Hokubu earthquake.

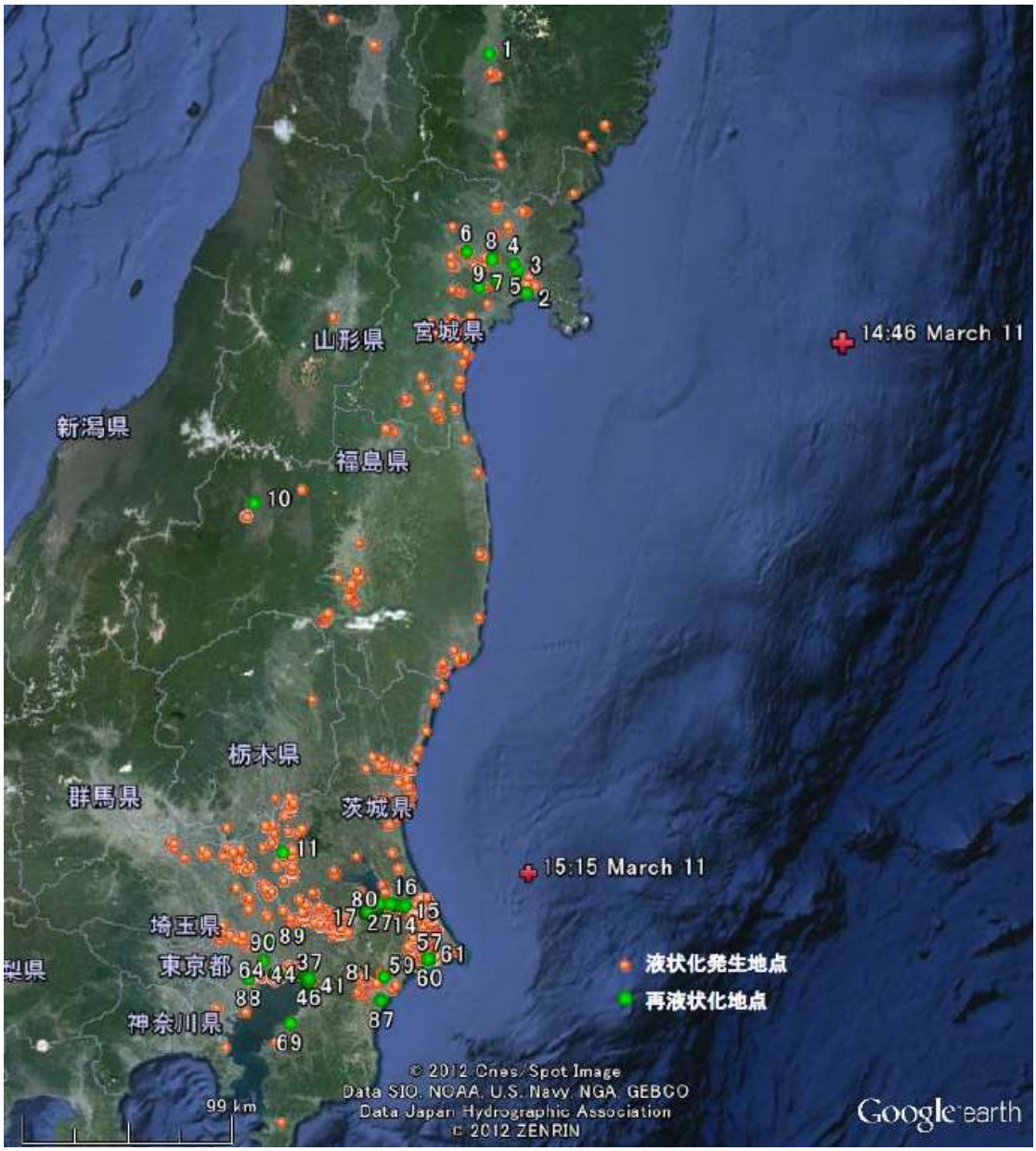

Figure 1.3 Liquefied and re-liquefied sites in the 2011 earthquake off the Pacific coast of Tōhoku. (K. Wakamatsu 2012)

However, the recurrence of liquefaction in 2016 Kumamoto earthquakes was more worth to discuss by the performances between the foreshock and mainshock, because the maximum intensity was very closed at around 7 degree between the two shocks. However, the liquefaction extent was great different. The comparison was done by Figure 1.4. The enveloped area by red line expressed where liquefaction appeared in

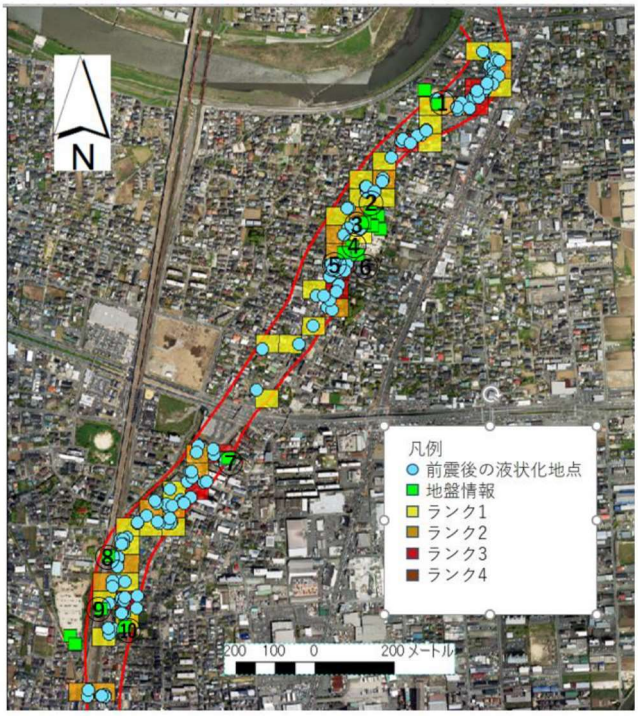

(a) Foreshock

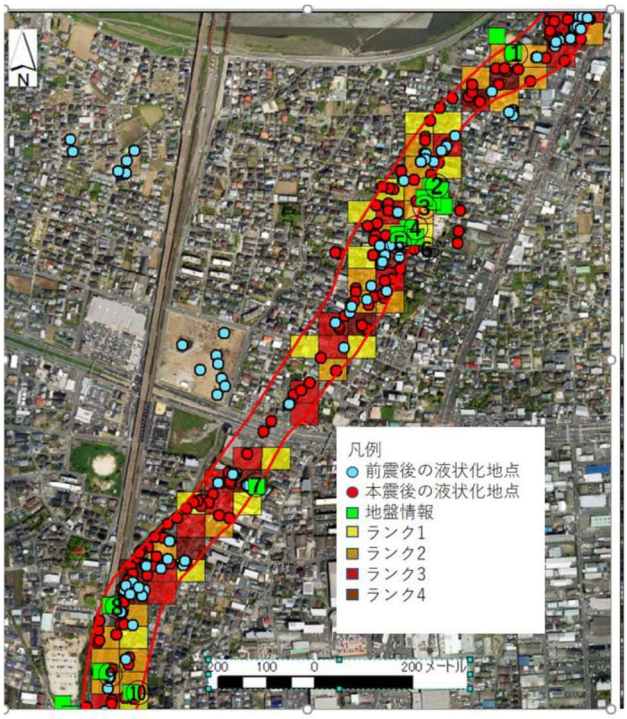

(b) Mainshock

Figure 1.4 Liquefied sties and ranks between foreshock and mainshock in the 2016 Kumamoto earthquakes (R. Hirata et al. 2018)

the two shocks. The marked colour represented 4 ranks of the liquefaction areas (the greater rank represents a larger area).

1.2 Objectives and scope of this study

The clear understanding of the risk from disasters induced by soil liquefaction caused by earthquakes was introduced in above. While because the special geographic position of Japan, the liquefaction behaviours is urging to be detected.

This study focused on the disasters of soil liquefaction occurred in the 2016 Kumamoto earthquakes to attempt to detect the liquefaction behaviours of local soils in Kumamoto-Aso region firstly. The difference of the behaviours between foreshock and mainshock was discussed primarily, because the investigation results indicated the expended disasters in mainshock compared to foreshock. This phenomenon was more notable at the sites where liquefaction recurred in both two shocks.

K. Wakamatsu et al. (2017) supposed that the great reduction of liquefaction resistance was because that the excess pore water pressure which produced in foreshock remained in ground when mainshock came. Meanwhile, it was regardless the occurrence of liquefaction in foreshock or just increasing of excess pore water pressure in ground.

According to their assumption, there is a difficulty to evaluate the soil state and liquefaction behaviours after foreshock which could be looked as the pre-shearing for mainshock. The traditional test method by the sample's boring and laboratory test would disturb the deposited state of particles and residual excess pore pressure with a great possibility.

Therefore, the propagation of shear wave with small strain was carried in this study to discuss the possibility of evaluation on liquefaction potential. It was based on these considerations:

1) Shear wave is very small and without destructiveness.
2) It has been used in situ-investigation previously. The convenience and

reliability were verified by previous works.

3) The most important point is that the propagation of shear wave was affected by the factors which is as similar as soil liquefaction in ground.

Based on these, the correlation between shear wave and liquefaction behaviours is very worth to be discussed. As so, this study attempts to provide a method to evaluate the liquefaction potential, particularly for the soils with a shearing history.

1.3 Layout of the thesis

In order to detect behaviours, cyclic tri-axial test was adopted in this study for detecting the liquefaction behaviours including liquefaction and re-liquefaction for soils, which was introduced in Chapter 3.

There were three soil samples were adopted as the test materials in this study:

1) Toyoura sand as reference material was discussed firstly. The saturated samples were conducted mainly, and the comparison with un-saturated samples also was conducted. These results were summarised in Chapter 4.
2) Chapter 5 discussed the liquefaction behaviours of typical soil of Kuroboku (volcanic soil) in Kumamoto-Aso region and the boiled sand in the 2016 Kumamoto earthquakes. And there were also some basic tests were conducted to investigate the physical properties of these soils.

The correlation between propagation of shear wave and liquefaction potential was discussed in Chapter 6. The correlation was investigated with the three types of soils carried in this study. at the same time, the correlation was investigated by the samples as following conditions:

1) Samples were without pre-shearing;
2) Samples were with pre-shearing but didn't causing liquefaction. (excess pore water pressure produced).
3) Samples were with pre-shearing and were completely liquefied. The excess pore water was completely discharged, and the soil particles were re-

consolidated sufficiently.

Finally, some factors, such as void ratio and fines content, were discussed in Chapter 6 as well. The research flow was demonstrated by chart as Figure 1.5.

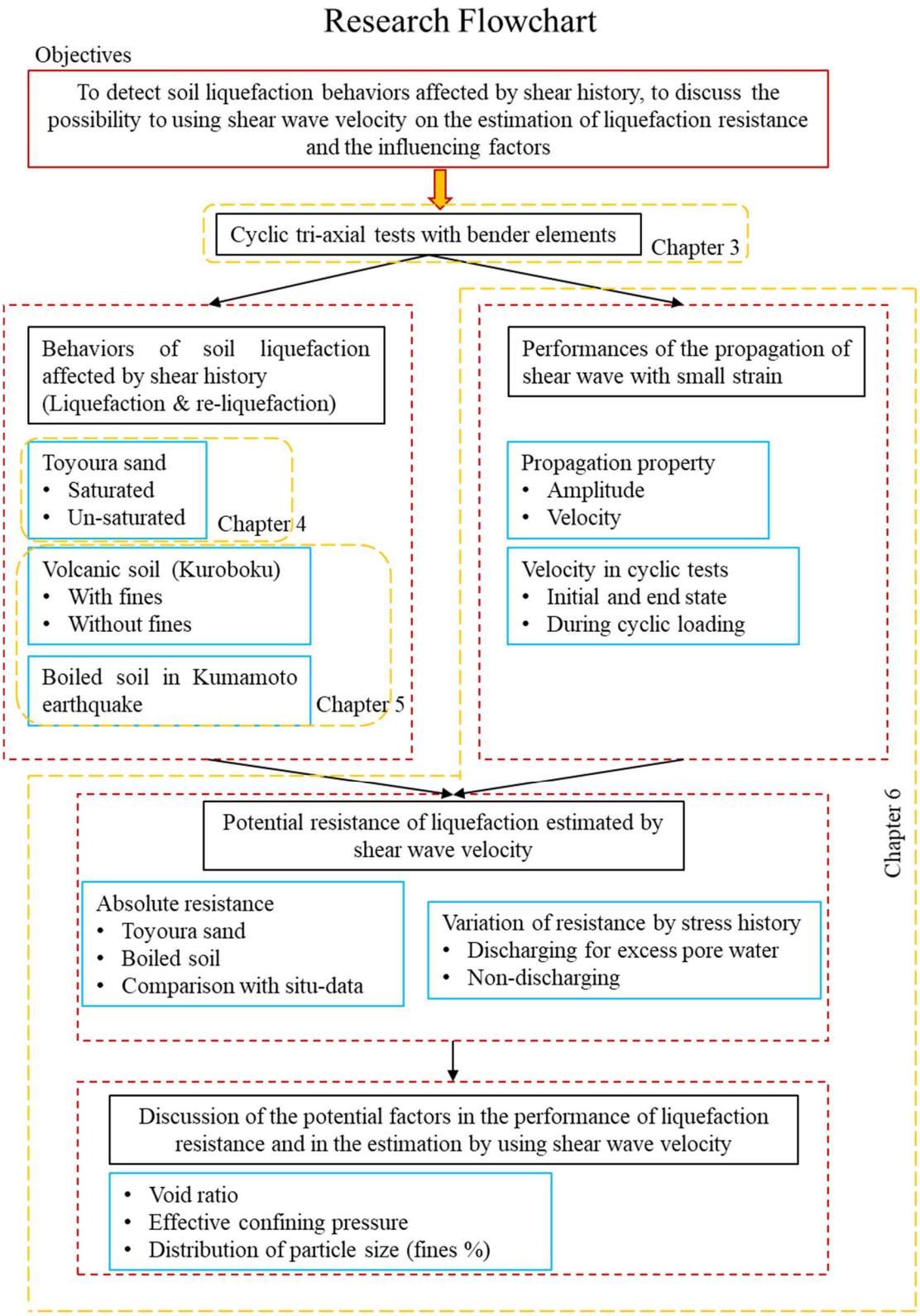

Figure 1.5 Research flow chart for this study

Note

1) The number and magnitude in ancient were used by extrapolation.

References

Chronological Scientific Tables. Serious book from 1925. Editor: National Astronomical Observatory of Japan (NAOJ). In Japanese.

E. Kuribayashi, and F. Tatsuoka, 1975. Brief Review of Soil Liquefaction during Earthquakes in Japan, *Soils and Foundations*, Vol. 15, No. 4, 1975, pp81-92.

Japan Meteorological Agency, JMA Report a: The disasters by earthquakes and Tsunami in past. *http://www.data.jma.go.jp/svd/eqev/data/higai/higai-1995.html*. In Japanese.

Japan Meteorological Agency, JMA Report b: Major earthquakes occurred near Japan from H 8. *http://www.data.jma.go.jp/svd/eqev/data/higai/higai1996-new.html*. In Japanese.

Japan National Committee on Earthquake Engineering. Niigata Earthquake, 1964. *Proceedings of the 3rd World Conference in Earthquake Engineering*, Volume III, pp s.78-s.105. In Japanese.

K. Wakamatsu, 2012. Recurrent Liquefaction Induced by the 2011 Great East Japan Earthquake, *Journal of JAEE*, Vol. 12, No. 5, pp 69-88. In Japanese.

K. Wakamatsu, S. Senna, and K. Ozawa, 2017. Liquefaction and its Characteristics during the 2016 Kumamoto Earthquake. *Journal of JAEE*, Vol. 17, No. 4, pp 81-100.

R. Herata, S. Murakami, H. Utsugihara, and Y. Nomiyama, 2018. H28 熊本地震において現れた液状化帯内における液状化層の調査, Japan Society of Civil Engineering 2018 Annual Meeting, Cs12-042, pp 83-84. In Japanese.

S. Yasuda, and I. Tohno, 1988. Sites of Reliquefaction caused by the 1983 Nihonkai-Chubu Earthquake, *Soils and Foundation*, Vol. 28, No. 2, pp. 61-72.

S. Yasuda. 1988. Liquefaction: From investigations to countermeasures, pp 13.

In Japanese.

T. Mukunoki, S. Kasama, H. Murakami, H. Ikemi, R. Ishikura, T. Fujikawa, N. Yasufuku, and Y. Kitazono, 2016. Reconnaissance report on geotechnical damage caused by an earthquake with JMA seismic intensity 7 twice in 28 h, Kumamoto, Japan. *Soils and Foundations*, JGS, **56**(6), 947-964

Y. Yoshimi. 1998. Simplified design of structures buried in liquefiable soil, *Soil and foundations*, JGS. Vol. 38, No. 1, pp 235-240.

CHAPTER 2

LITERATURE REVIEW

2.1 Introduction

The escalation of the disasters included by soil liquefaction in the 2016 Kumamoto earthquakes was discussed primally as the argument in this study. The great change of behaviours was considered affected by foreshock potentially when mainshock came. The foreshock caused the soil liquefaction or excess pore water pressure increment which could be looked as the pre-shearing. The liquefaction behaviours had a great possibility influenced by the remained excess pore pressure and the re-organization of soil particles. For these purposes, the literature review is illustrated as the following three major parts.

1) Related research concerned on the liquefaction behaviours for soils by pre-shearing or liquefied once.
2) Performance of shear wave propagating in soils and the clarified correlations with soil liquefaction potential.
3) The results of Kuroboku (volcanic soil) and boiled sand investigated by previous researchers.

In the end of this chapter, some interpretation for potential concerns for cyclic tri-axial tests was expressed finally.

2.2 Liquefaction behaviours of sandy soil with pre-shearing

The pre-shearing could be divided to the it caused liquefaction and did not caused liquefaction as mentioned previously. Ishihara et al. released a serious of founding from 1974 to 1978, to investigate and summarized the general behaviours for sand including the pre-shared samples under undrain test condition. Their results also were referred and discussed by other researchers for the analysis of the re-liquefaction behaviours using different test methods and test materials (B. Ye et al 2015). In the other hand, the liquefaction resistance of sand might be reduced when it was liquefied firstly, even if the relative density became denser. Finn et al. (1970) revealed this kind of phenomenon

firstly which was investigated by tri-axial tests.

Different to the investigation by cyclic tri-axial compression tests or the similar tests depending on the stress path performances, B. Ye et al. (2018) conducted the sharing table tests to try to investigate the behaviours from the movement of soil particles. The results tested by two typical experiment method conducted by Ishihara et al. and B. Ye et al. were introduced typically in this section.

2.2.1 Behaviours of sand with pre-shearing in cyclic tri-axial tests

Ishihara et al. released three representable articles (1974, 1975, 1978) to explain the behaviours of sand after pre-shearing under the undrain condition.

1) The existence of yielding of sand was verified by cyclic tri-axial tests firstly (1974).
2) The line of phase transformation (*LFT*) was found from the yielding state of sand in cyclic tri-axial tests (1975).
3) They found that the performance in second cyclic tests were greatly affected by relative relation between the stress path and *LFT* in first cyclic tests. At the same time, the direction in the final half of load cycles during first cyclic tests seriously affected the performance in the first load cycle during second cyclic tests (1978).

The LFT was depended by the families of yield loci for sand with different relative density. The results of the tests performed exclusively in the domain of tri-axial compression shown that, for a given density of sand, the yield loci in the space of shear stress *q'*- effective mean principle stress *p'* can be uniquely determined irrespective of the stress history to which the sample had previous been subjected. The typical shear stress *q'*- effective mean principle stress *p'* was plotted by different relative densities, showed in Figure 2.1. Some of the yield loci obtained for the yielding in tri-axial test were shown in Figure 2.2. The yield loci also were verified in extension direction which had the similar characteristics.

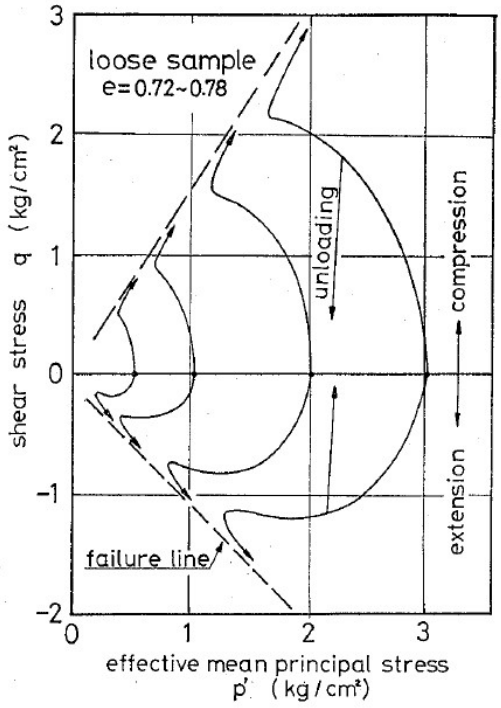

Figure 2.1 Typical undrained stress paths for sand (K. Ishihara et al. 1975).

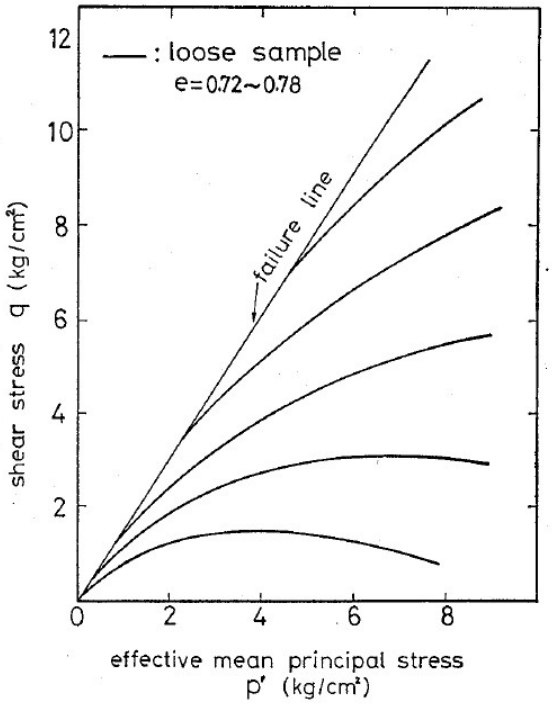

Figure 2.2 Yield in compression for typical samples (K. Ishihara et al. 1975).

Based on these understanding, the line of phase transformation could be defined by the *q-p'* stress path and yield state, that was introduced in Figure 2.3. Curve A-B-C was performed as a general pattern of stress path when a sand subjected to a shear stress in a cyclic tri-axial tests in the stress space of *q-p'*. It was to be noted that there always exists a point such as point B where the stress path changes its direction and bends upwards to right. This line straight pass through the origin and point B was defined as the "line of phase transformation *LFT*", which is also unique for a given relative density of sand. This lie was named as such because a sand sample doesn't develop large strains and behaves in the manner of a soiled plastic material when the stress changes are limited to the stress space bounded by two of this line. If the stress goes cross this line and enter the yielding state, the stress would be considered that the sand tends to develop a large strain and behaves in the manner of a viscous fluid.

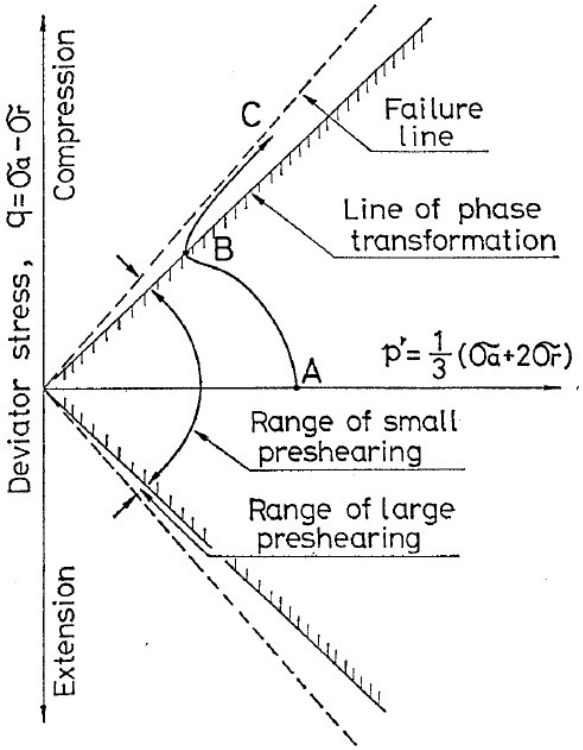

Figure 2. 3 Description of line of phase transformation LFT (K. Ishihara and S. Okada 1978).

By considering the pre-shearing condition, if the variation of stress is restricted by the boundary of two lines of phase transformation, it is defined as “small pre-shearing”. On the contrary, if the change in stress crosses the lines of phase transformation is defined “large pre-shearing”. The sand was sheared by the two serious of pre-shearing; then was discharged of the pore water pressure and re-consolidated. Finally, the similar shear stresses were applied again to investigate the change of behaviours. The major outcomes indicated that:

1) The liquefaction resistance increased if the sand experienced by the small pre-shearing.
2) Oppositely, the liquefaction reduced greatly if the sand experienced by the large pre-shearing.

Their researches proposed a reasonable explanation from the relation of stress-strain in pre-shearing process, to solute the indecipherable phenomenon in laboratory experiments.

2.2.2 Micro view on re-liquefaction behaviours of sand in shaking table tests

Recently, Bin Ye et al. (2018) released a new finding for the behaviours of re-liquefaction from the observable micro changes of soil particles’ structure. They focused on the changes of long-axis of soil particles, before and after liquefaction, second liquefaction or third liquefaction and so on. The test apparatus was set upped as the illustration shown in Figure 2.4. Each part in this test system is that: 1) shaking table; 2) model box; 3) data collector; 4) stereomicroscope; 5) industrial camera; 6) fiber tube halogen lamps; and 7) computer.

The Fujian sand was sieved out grain size greater than 355 μm as the test material to produce the sand more prone to liquefaction. The physical properties could refer to original articles. The samples were made to 42cm x 20cm x 25 cm by water pluviation (A.B. Huang et al. 2015) for the achievement of simulated the alluvial deposition while

owning a high saturation degree. The initial relative density of the specimens was approximately 42%. 11 groups of tests were carried out to investigate the liquefaction behaviour of the specimen of the test material. The shaking duration was the only difference between the 11 groups, which is listed in Table 2.1. In each test cases, the specimen was successfully vibrated several times (named with event 1, 2, 3…) using the same input motion until it no longer re-liquefied.

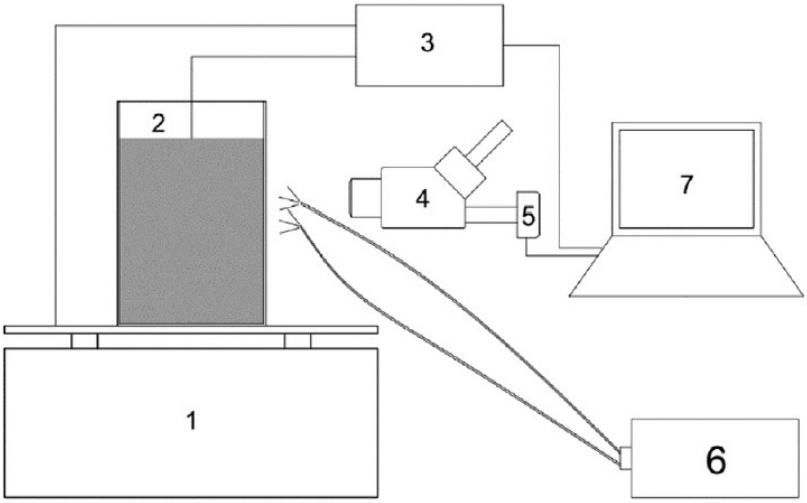

Figure 2.4 Illustration of test equipment for observing the micro changes of soil structure (B. Ye et al. 2018).

Table 2.1 The shaking duration of each test

Test number	Shaking duration	Test number	Shaking duration
1	1.5s	7	7.5s
2	2.5s	8	8.5s
3	3.5s	9	9.5s
4	4.5s	10	10.5s
5	5.5s	11	42s
6	6.5s		

The typical results were carried from test 1 by produced excess pore water pressure in their article as shown in Figure 2.5, that there were 5 shaking events in total until there was not the re-liquefaction occurred in specimen.

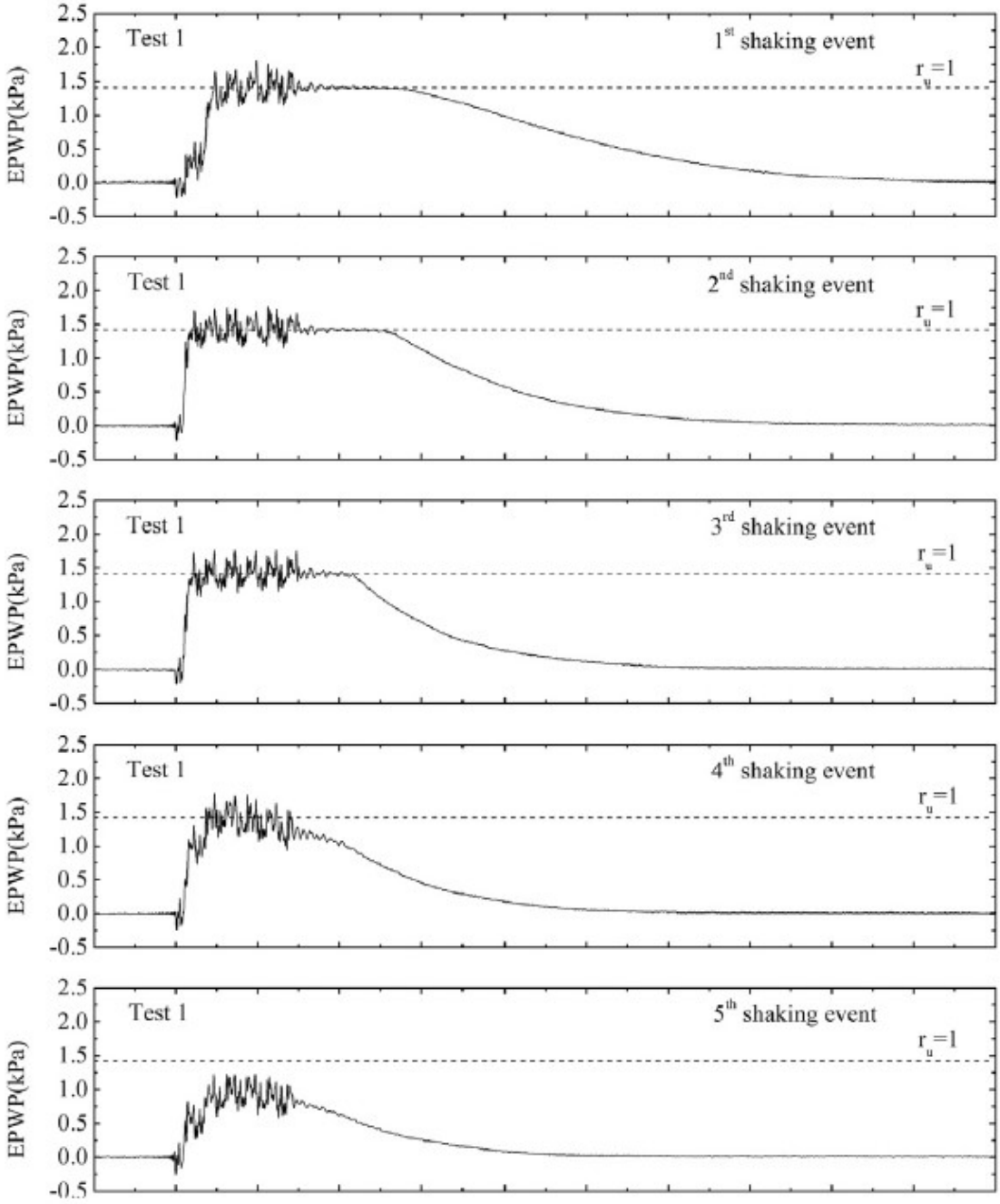

Figure 2.5 Typical results of the time history of the EPWP in Test 1 (B. Ye et al. 2018)

Within the shaking table tests, a digital image processing method called watershed transformation was adopted to extract the outline of sand particles. The watershed transformation method treats an image as a topographic map, with the brightness of each point representing its height, and finds the lines that run along the tops of the simulated ridges. Based on the principle of watershed transformation, the algorithm called watershed flooding was used to process the sand particle images in their study. The disadvantage of this algorithm leading to over-segmentation was fixed by some pre-treatment and after-treatment, which could be widely found in the literature (A.K. Jain, 1989; R.C. Gonzalez et al. 2004; L. Vincent, and P. Soille, 1991). The results after each image processing step were presented, which were summarized and displayed in Figure 2.6.

Figure 2.6(a) shows an original grayscale image taken during Test 1. Figure 2.6(b) shows the same image after histogram equalization processing, which improved the brightness and contrast of the original image. As a result, the sand particles and voids can be identified more easily. Figure 2.6(c) displays the gradient image which is obtained by applying the I. Sobel, and G. Feldman (1968) operator algorithm on Figure 2.6(b). It can be seen that many redundant details remain in Figure 2.6(c), which will result in over-segmentation. Therefore, another pre-treatment measure called region marking was applied on Figure 2.6(b), and the result is shown in Figure 2.6(d). By overlaying Figure 2.6(d) onto Figure 2.6(c), the redundant details can be removed, as shown in Figure 2.6(e). After the above pre-treatment steps, the watershed transformation algorithm can be applied, and Figure 2.6(f) displays the edge image after image segmentation. The black line in Figure 2.6(f) is the watershed ridge line and, clearly, over-segmentation is still apparent, especially in the unmarked void areas. Next, an aftertreatment measure called region merging was adopted to remove the over-segmentation, and the precise edge image is shown in Figure 2.6(g). The accuracy of extracted sand particle edges can be verified by overlaying Figure 2.6(g) onto Figure

2.6(b), as shown in Figure 2.6(h). It is clear that the segmented edges are consistent with the contour of sand particles. Finally, the sand granular edge image shown in Figure 2.6(i) was obtained by changing the colour of the voids to gray; this figure was used to calculate the mesoscopic parameters of the sand.

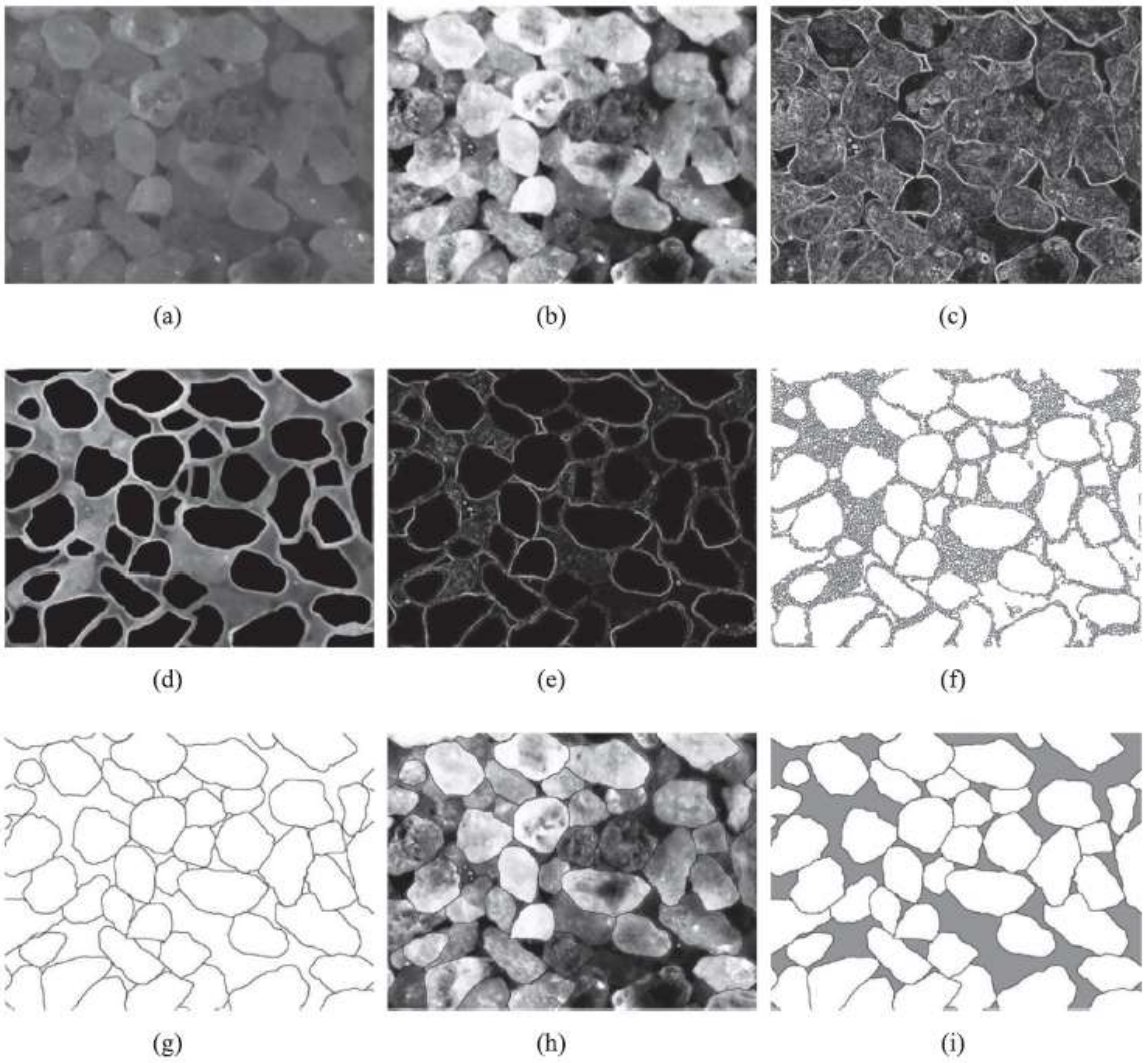

Figure 2.6 Results of each image processing step: (a) original image; (b) histogram equalization; (c) gradient image; (d) region marking; (e) gradient image after removing redundant; (f) watershed transformation; (g) region merging; (h) verification of the accuracy; and (i) sand granular edge image (B. Ye et al.2018).

Based on this process, the long axis of the sand particle was defined as the

longest line segment that linked two points on the edge if the particle. Its inclination angle of 0 ~ 180° in the plane was defined as the long-axis direction. Figure 2.7 demonstrated the granular edge images before each shaking event in Test 2. It can be seen the void space among the sand particles decreased with number of shaking events. The results showed that the directions of long axes of the sand in Figure 2.7(a) were different to the those in Figure 2.7(b) ~ (d), that were prone to be horizon before first shaking. On the hand, the inclination of long axes of sand particles are more prone to be vertical while sand experienced liquefaction and re-liquefaction.

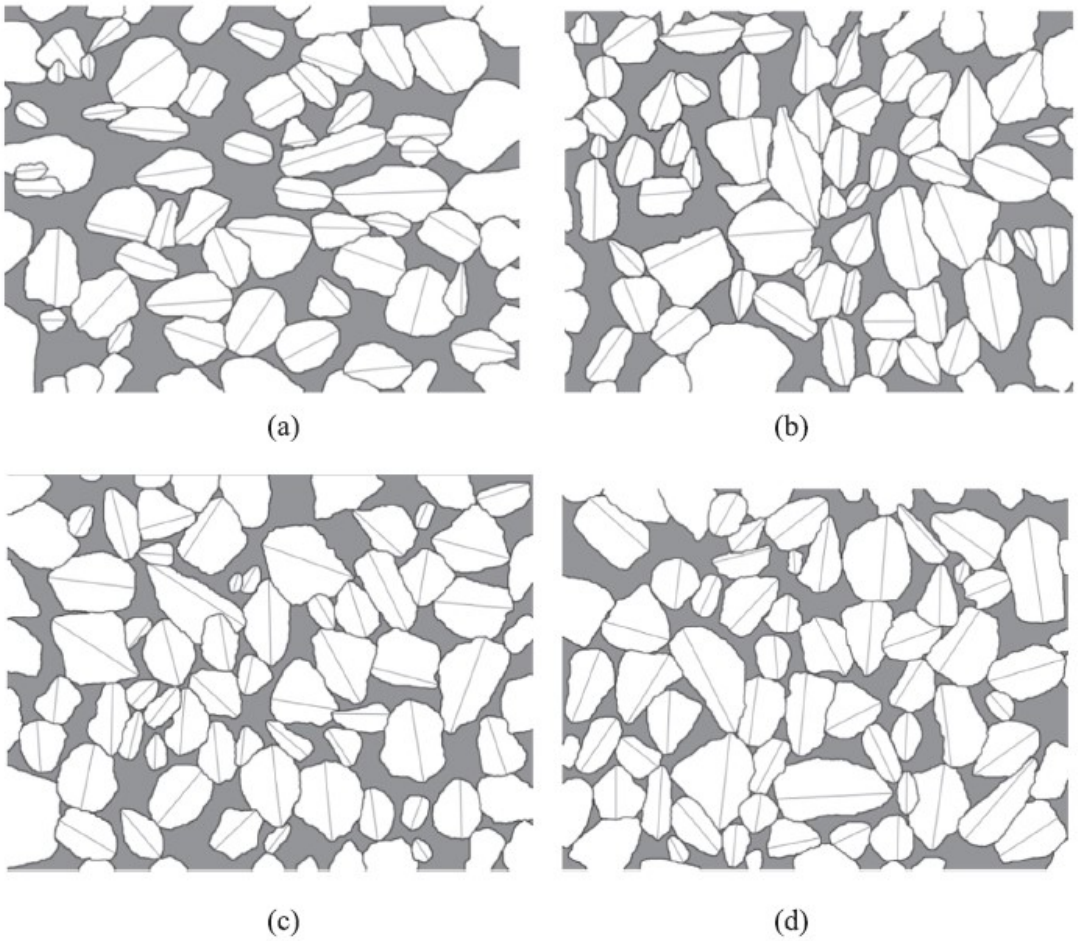

Figure 2.7 Typical granular edge images in Test 2: (a) before 1st shaking event; (b) before 2nd shaking event; (c) before 3rd shaking event; (d) after the 3rd shaking event(B. Ye et al.2018).

Their considers was that the faster increase in the excess pore water pressure in re-liquefaction events was mainly caused by the changes of the distribution of the long-axis direction. Moreover, the change of distribution was the difference of deposition ways between it before first event and liquefaction or re-liquefaction events. For the state before first event, they thought that the long axes of particles trend to be horizontal. When the sand was during liquefying or re-liquefying, the sand particles would suspend in the water due to the excess pore pressure producing. After that, because the surface of the specimen was a drainage boundary, the water would flow up to the surface. The sand particles were influenced by the upward flow, and trend to rearrange with the vertical direction of long-axis. The new structure was less stable than that of the initial deposit and can be collapsed more easily.

According to their interpretation, the author still has an uncertain. They considered the relative movement between water and sand particle was vertically to lead to long axes of particles trended to be vertical as well. However, the state before first event, the specimen which was prepared by water pluviation, also dissipate from the top of water surface to the bottom. The water also could be looked as flowing upward relating to sand particles. The behaviours trended to be different greatly. This point also needs more investigation in future works.

2.2.3 Re-liquefaction behaviours of sand using shear box with shaking table

There are also some result public by S. O-hara and T. Yamamoto (1981, 1982) using the shear box with shaking table test. They obtained opposite results that the liquefaction resistance increased after sand was liquefied firstly. The liquefaction performances should be as the results shown in Figure 2.9 based on their study.

For these performances, the shear strain γ = 10% produced during first liquefaction and second liquefaction was looked as the pre-shearing to second and third liquefaction tests respectively. By the opinion from author in this study, the pre-shear strain is too great, meanwhile, the shaking duration is too long to perhaps cause the soil

particles start to deposit when shaking was keeping, meanwhile, there were very fewer particles deposited after first and second liquefaction. As the result, the relative density became very great, there were not the sufficient void space for collapsing, that lead to have the higher liquefaction resistance with the number of liquefaction tests gradually.

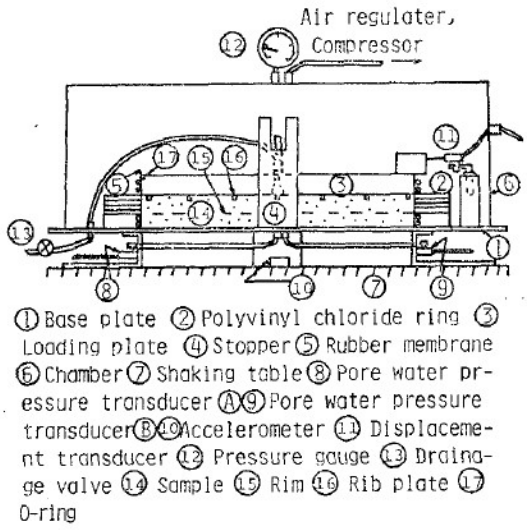

Figure 2.8 Equipment of shear box with shaking table tests (S. O-hara and T. Yamamoto 1982).

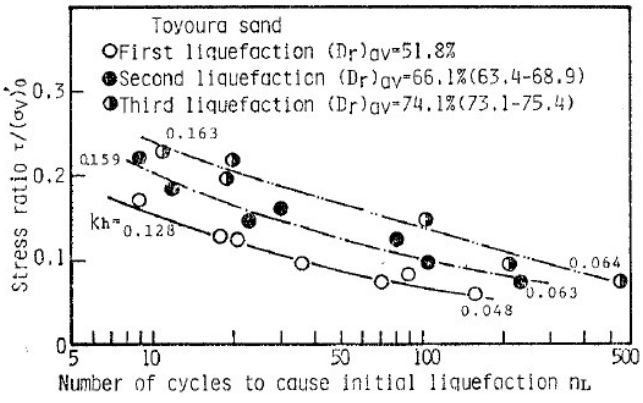

Figure 2.9 Comparison of liquefaction resistance among 1st, 2nd, and 3rd liquefaction for saturated Toyoura sand (S. O-hara and T. Yamamoto 1982).

2.3 Propagation of shear wave applying on the estimation for liquefaction potential

Table 2.2 Earthquakes used to establish the correlation between shear wave velocity and liquefaction resistance (R.D. Andrus and K.H. Stokoe 2000)

Earthquake (1)	M_w (2)	NUMBER OF CASE HISTORIES BY FINES CONTENT				
		Sands and Silts			Gravels	
		≤5% (3)	6–34% (4)	≥35% (5)	≤5% (6)	6–34% (7)
1906 San Francisco, Calif.	7.7	—	4	4	4	—
1957 Daly City, Calif.	5.3	3	2	—	—	—
1964 Niigata, Japan	7.5	4	—	—	—	—
1975 Haicheng, China	7.3	—	—	6	—	—
1979 Imperial Valley, Calif.	6.5	—	9	2	—	—
1980 Chiba-ibaragi, Japan	5.9	—	1	1	—	—
1981 Westmorland, Calif.	5.9	—	9	2	—	—
1983 Borah Peak, Idaho	6.9	—	—	—	17	1
1985 Chiba-ibaragi, Japan	6.0	—	1	1	—	—
1986 Event LSST2, Taiwan	5.3	—	—	4	—	—
1986 Event LSST3, Taiwan	5.5	—	—	4	—	—
1986 Event LSST4, Taiwan	6.6	—	—	4	—	—
1986 Event LSST6, Taiwan	5.4	—	—	4	—	—
1986 Event LSST7, Taiwan	6.6	—	—	4	—	—
1986 Event LSST8, Taiwan	6.2	—	—	4	—	—
1986 Event LSST12, Taiwan	6.2	—	—	4	—	—
1986 Event LSST13, Taiwan	6.2	—	—	4	—	—
1986 Event LSST16, Taiwan	7.6	—	—	4	—	—
1987 Chiba-toho-oki, Japan	6.5	—	1	—	—	—
1987 Elmore Ranch, Calif.	5.9	—	9	2	—	—
1987 Superstition Hills, Calif.	6.5	—	9	2	—	—
1989 Loma Prieta, Calif.	7.0	19	30	14	4	—
1993 Kushiro-oki, Japan	8.3	1	1	—	—	—
1993 Hokkaido-nansei, Japan	8.3	—	2	1	1	—
1994 Northridge, Calif.	8.3	—	3	—	—	—
1995 Hyogo-ken Nanbu, Japan	6.9	1	9	—	—	9

For detecting a liquefaction evaluation method with a simplified procedure, Seed and Idriss (1971) firstly proposed to use the blow count from the standard penetration test (*SPT*) correlated with cyclic stress ratio to represent the cyclic load in ground. A parallel procedure based on the come penetration test (*CPT*) was introduce by

Robertson and Campanella (1985). Although these procedures were revised and improved well (T.L. Youd, and I.M. Idriss 2001; I.M. Idriss, and R.W. Boulanger, 2006), the penetration tests were suitable and reliable for very sites. Therefore, the velocity of shear wave was developed to provide a promising alternative and supplementary tool to evaluate liquefaction. The propagation of shear wave in soil owns the similar factors with liquefaction resistance (e.g., void ratio, stress state, stress history, and geologic age) (R.D. Andrus, and K.H. stoke II, 2000), that makes a possible to be the index for liquefaction potential.

R.D. Andrus, and K.H. stoke II (2000); R.D. Andus et al. (2004) who summarised the previous related researches and based the earthquakes data in history from 1906 to 1995 (Table 2.2), developed a guide of the evaluation for liquefaction potential by using shear wave. The laboratory experiments also were conducted by K. Tokimatsu et al. (1986); Y.G. Zhou, and Y.M. Chen (2007); Y. Tsukamoto et al. (2002); and C.D.P. Baxter et al. (2008) to verify and complete the method from mechanics concerning by controllable factors such as the fines, cyclic stress ratio or void ratio.

The recommended curve from measured shear wave velocity for calculation of cyclic stress resistance *CRR* was plotted in Figure 2.10. The results were summarised by the soil condition of sands and gravels of the liquefied sites in these earthquakes. This aggregation was accomplished through an adjustment procedure, that is, the cyclic stress ratio in each case history were adjusted to the earthquake with M_w = 7.5 by divide by Equation 2.1 with n = -2.56.

$$MSF = (\frac{M_w}{7.5})^n \tag{2.1}$$

Where, *MSF* is magnitude scaling factor. It equals to 1.0 for earthquakes with a magnitude of 7.5. M_w is moment magnitude; n is exponent. The lower bound for the range of *MSFs* recommended by the 1996 NCEER workshop is

defined with n = -2.56; the upper bound of the recommended range is defined with n = -3.3.

As the operation in penetration tests, the sandy soil case history were separated into three categories: 1) sands with average fines $F_c \leq 5\%$; 2) sands with average fines F_c = 6 ~ 34%; and sands and silt with average fines $F_c \geq 35\%$.

Besides, the shear wave velocity was correlated to the overburden stress for soil element. Therefore, for a certain soil, knowing the fines content, over burden depth included the ground water level, and measured shear wave velocity, the liquefaction potential is able to be evaluated by Figure 2.10.

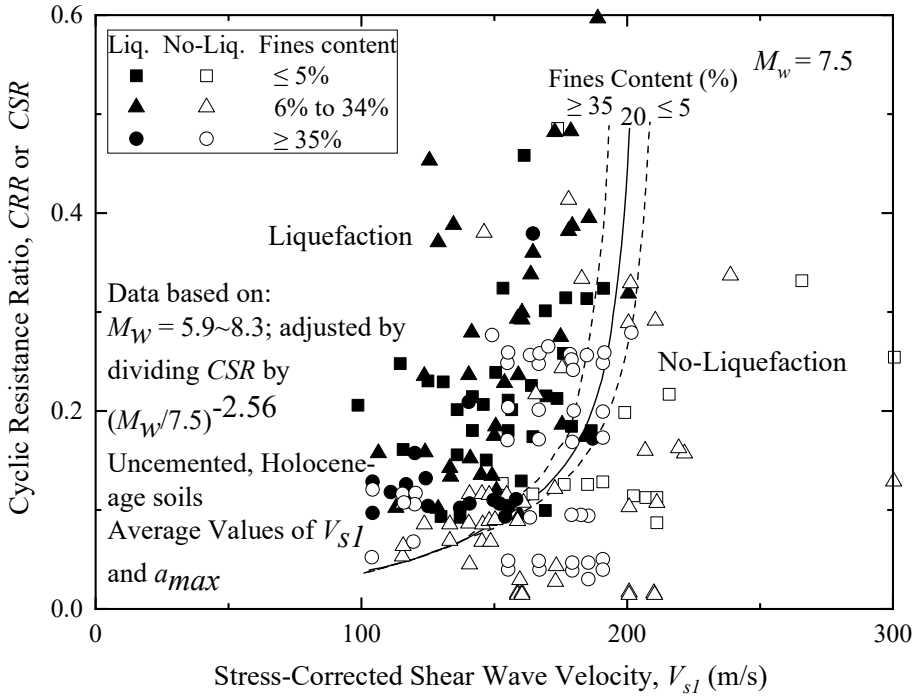

Figure 2.10 Curves recommended for the calculation of *CRR* from V_{s1} measurements in sands and gravels (R.D. Andrus and K.H. Stokoe 2000).

2.4 Previous studies for Kuroboku and boiled sand in the 2016 Kumamoto earthquakes

Figure 2.11 Distribution of volcanic soil deposition in Kyushu Island (S. Miura et al. 2005)

Based the investigation for the 2016 Kumamoto earthquakes, the Kuroboku (volcanic soil) was widely existed under the strata in the sites where liquefaction appeared. The boiled sand, which was found in these sites, presented a colour with back and gray particles. Figure 2.11 shows the distribution of volcanic soil in Kyushu Island (S. Miura et al. 2005). It indicated the Kumamoto-Aso area was widespread with volcanic soil where the deposition contained the epicentres of two great shocks.

In order to detect the influence from Kuroboku, some tests were conducted to investigate the basic physical properties for Kuroboku and boiled sand.

Photo 2.1 Sampling sites in Kumamoto-Aso area (K. Yamada et al. 2017).

Photo 2.2 Granular analysis D ≥ 1/4 mm (S. Murakami et al. 2017)

Photo 2.1 shows the sampling sites for the boiled sand where liquefaction appeared in the two shocks (K. Yamada et al. 2017); Photo 2.2 expresses a lot of black particles maxed in the sands. Figure 2.12 shows the cumulative grain size distribution of boiled sand (S. Murakami et al. 2017). The range from blue lines represents the soils have the possibility of liquefaction; while the range from orange lines represents the soils might be liquefied very easily. Therefore, the results indicated all the samples carried from the liquefied sites were belong to very easy to liquefy based on Technical standards and commentaries for port and harbour facilities in Japan (2007).

Moreover, the Kuroboku was tests separately for controlling factor of the influences on the behaviour of boiled sand (Y. Kawaguchi, 2018). The samples (A, B) were collected from the deep landslide nearby Aso-Bashi. The physical properties were arranged in Table 2.3 and Figure 2.13, that might be used as the basic information and the comparing objects with the behaviour of test materials in this study.

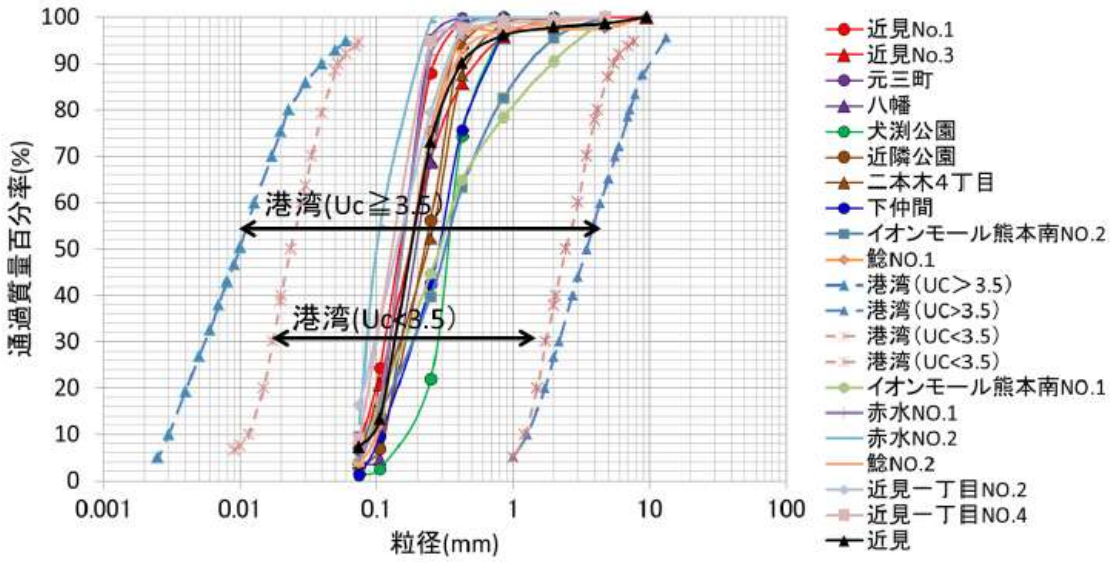

Figure 2.12 Cumulated grain size distribution of boiled sand (S. Murakami et al. 2017)

Table 2.3 Physical properties of Kurobuku collected from the landslide nearby Aso-Bashi (Y. Kawaguchi, 2018)

Place	Water content %	Dried density g/cm3	Specific density	Organic matter content %	Liquid limit %	Plastic limit %
Site A	170~190	0.52	2.28~2.31	48.6~49.3	224~229	153~159
Site B	92~101		2.27	35.8~36.9	137	94

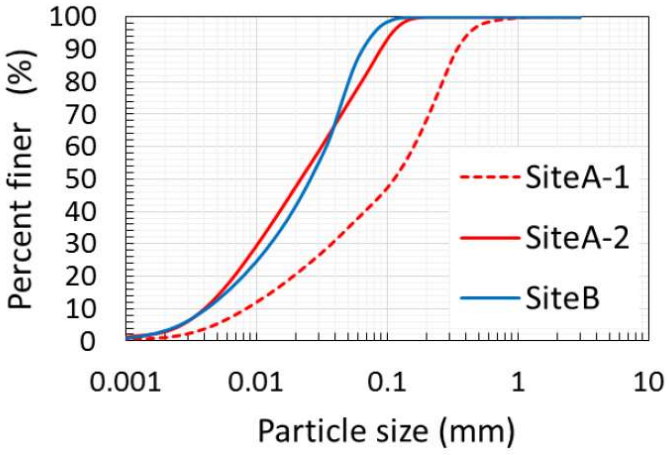

Figure 2.13 Cumulated grain size distribution of Kuroboku collected from the landslide nearby Aso-Bashi (Y. Kawaguchi, 2018)

2.5 Some interpretations for cyclic tri-axial test

Researches by S. O-hara and T. Yamamoto (1982) in section 2.2.3 also pointed out an augment to the result from cyclic tri-axial tests, that the constriction appeared in the dimeter of specimen when γ = 10% was applied as the pre-shearing. Due to this, they thought the great reduction of liquefaction resistance after first liquefaction was produced by the imperfection in test operation.

However, the axial shear with double amplitudes *DA* = 5% was commonly used as the criterion for liquefaction, because the excess pore water pressure ratio u/σ_{c0}' was mostly closed to $u/\sigma_{c0}' = 0.95$ in this state. At the same time, the specimen could remain a uniform shape when the axial strained was within the range of *DA* = 5%. This outcome, from a way of speaking, was also verified by some researchers who focus on the re-liquefaction using cyclic tri-axial test (S. Yamada et al. 2010; M. Wada, 2015). Therefore, the range of *DA* = 5% also was considered with out he un-uniform deformation after first liquefaction generally, if there were not visible defects during test process.

References

A.B. Huang, W.J. Chang, H.H. Hsu, Y.J. Huang. 2015. A mist pluviation method for reconstituting silty sand specimens. Engineering Geology, Vol. 188, pp 1-9.

A.K. Jain. Fundamentals of digital image processing. Upper Saddle River, U.S.A.: Prentice Hall, 1989.

Bin Ye, Hailong Hu, Xiaohua Bao, Ping Lu. Reliquefaction behavior of sand and its mesoscopic mechanism. Soil Dynamics and Earthquake Engineering 114 (2018) 12–21.

Bin Ye, Jiafeng Lu, Guanlin Ye, 2015. Pre-shear effect on liquefaction resistance of a Fujian sand. Soil Dynamics and Earthquake Engineering, Vol. 77, pp 15-23.

C.D.P. Baxter, A.S. Bradshaw, R.A. Green, and J.H. Wang, 2008. Correlation between Cyclic Resistance and Shear-Wave Velocity for Providence Silts. Journal of Geotechnical and Geoenvironmental Engineering, 134(1), pp 37-46.

F. Tatsuoka, and K. Ishihara. 1974. Yielding of sand in triaxial compression. Soils and Foundations, Vol. 14, No. 2, pp 63-76.

H.B. Seed, and I.M. Idriss, 1971. Simplified procedure for evaluating soil liquefaction potential. *Journal of the Soil Mechanics and Foundations Division*, 97(9), 1249-1273.

I. Sobel, and G. Feldman. A 3×3 isotropic gradient operator for image processing. Presented at a talk at the Stanford Artificial Project; 1968.

I.M. Idriss, and R.W. Boulanger, 2006. Semiempirical procedures for evaluating liquefaction potential during earthquakes. Soil Dynamics and Earthquake Engineering, 26(2-4), 115-130.

川口裕子, Master thesis: 阿蘇大橋地区における火山灰質土の力学特性と複合災害を想定した斜面の安定性評価への適用 2018.3. 九州大学. In Japanese.

K. Tokimatsu, T. Yamazaki, and Y. Yoshimi, 1986. Soil liquefaction evaluations by elastic shear moduli. Soils and Foundations, Vol. 25, No. 1, pp 25-35.

K. Ishihara, and S. Okada. 1978. Effects of stress history on cyclic behavior of sand. Soils and Foundations, Vol. 18, No. 4, pp 31-45.

K. Ishihara, F. Tatsuoka, and S. Yasuda. 1975. Undrained deformation and liquefaction of sand under cyclic stresses. Soils and Foundations, Vol. 15, No. 1, pp 29-44.

L. Vincent, and P. Soille. Watersheds in digital spaces: an efficient algorithm based on immersion simulations. IEEE Trans Pattern Anal 1991;13(6):583–98.

三浦清一, 八木一善, 石川達也: 2005. 火山灰質土-その性質と設計施工-2. 日本に分布する火山灰質土の概要と分類. 土と基礎, 53-10 (573). In Japanese.

村上哲, 永瀬英生, 大里重人, 矢ヶ部秀美: 2017. 平成 28 年熊本地震地盤災害調査報告書：5. 液状化•地盤陥没災害, pp 115-141. In Japanese.

P.K. Robertson, and R.G. Campanella, 1985. Liquefaction potential of sands using the CPT. Journal of Geotechnical Engineering. Volume 111, Issue 3, pp 384-403.

R.C. Gonzalez, R.E. Woods, S.L. Eddins. Digital image processing using MATLAB. Upper Saddle River, U.S.A.: Prentice Hall; 2004.

R.D. Andrus, and K.H. Stokoe II, 2000. Liquefaction resistance of soils from shear-wave velocity. Journal of Geotechnical and Geoenvironmental Engineering, 126(11), 1015-1025.

R.D. Andrus, and K.H. Stokoe II, and C.H. Juang, 2004. Guide for shear wave-based liquefaction potential evaluation. Earthquake Spectra, 20(2), 285–308.

S. o-hara, and T. Yamamoto, 1981. Sand liquefaction tests using shaking table. 土と基礎 29(4), p33-38. In Japanese.

S. o-hara, and T. Yamamoto, 1982. Experimental studies on reliquefaciton characteristics of saturated sands, using shaking table. 土質工学会論文報告集, vol. 22, No. 2, pp 123-132. In Japanese.

S. Yamada, T. Takamori, and K. Sato, 2010. Effects on reliquefaction resistance produced by changes in anisotropy during liquefaction. Soils and Foundations, Vo. 50,

No. 1, pp 9-25.

T.L. Youd, and I.M. Idriss, 2001. Liquefaction resistance of soils: Summary report from the 1996 NCEER and 1998 NCEER/NSF workshops on evaluation of liquefaction resistance of soils.” Journal of Geotechnical and Geoenvironmental Engineering, 127(10), 817-833.

Technical standards and commentaries for port and harbour facilities in Japan, 2007. In Japanese.

和田正寛, Doctoral dissertation: 高炉水砕スラグの強度評価および軽量地盤材料として適用性関する研究 2015.3. 山口大学. In Japanese.

W.D.L. Finn, P.L. Bransby, D.J. Pickering, 1970. Effects of strain history on liquefaction of sands. Journal of the Soil Mechanics and Foundations Division ;96(SM6), 1917-194334.

山田康平, 村上哲, 櫨原弘貴: 2017.3. 平成 28 年熊本地震における液状化噴砂の物理的特性. 土木学会西部支部研究発表会 III-057, pp 365-366. In Japanese.

Y. Tsukamoto, K. Ishihara, H. Nakazawa, K. Kamada, and Y. Huang, 2002. Resistance of partly saturated sand to liquefaction with reference to longitudinal and shear wave velocities. Soils and Foundations, Vol. 42, No. 6, pp 93-104.

Y.G. Zhou, and Y.M. Chen, 2007. Laboratory investigation on assessing liquefaction resistance of sandy soils by shear wave velocity. Journal of Geotechnical and Geoenvironmental Engineering, 133(8), pp 959-972.

CHAPTER 3

INTRODUCTION OF CYCLIC TRI-AXIAL COMPRESSION TESTS WITH BENDER ELEMENTS

3.1 Introduction

The liquefaction resistances were quietly affected by the method of researchers had done for the sample's preparation and by the ways how to modify the cross-area to obtain the cyclic stress ratio (*CSR*) after consolidation and re-consolidation. In order to solute this kind problem and ensure all of the results could be compared by the same conditions, the standard sand using in Japan of Toyoura sand and some typical soil materials were tested following a standard progress in this study. These tests were assembled up principally based on the criteria of JGS 0541-2000; JGS 0522; JGS 0520. The sections of this chapter were organized as follow:

At first, the setup of the cyclic tri-axial test apparatus assembled with bender elements was introduced.

Secondly, some preparations ways of specimens were explained to compare the advantages and disadvantages respectively. The most important and difficult step was how to achieve a high saturation degree ($S_{r.}$) within specimens' preparations. The method of double negative pressure with water pluviation, CO_2-Air replacement with air pluviation and water pluviation were introduced specifically in follow. Absolutely, for controlling the saturation degrees (B-value) in different targets, these preparations were applied flexibly in the tests.

Then, there is a part for explaining the achievement of estimated cyclic stress ratio CSR which was applied in this study. The correlation between electric voltage and vertical axial force was detected. And the modification for the relative density and cyclic stress ratio also was considered.

After that, the general test process for this study was introduced finally. In order to the consistency of explanation for the behaviour of shear wave in soils, the introductions of measurement for shear wave was conducted and included in Chapter 6 together with the related discussions of results.

3.2 Setup of cyclic tri-axial test apparatus with bender elements

Cyclic tri-axial compression tests apparatus assembled with bender elements was utilized to detecting the performance of soils under dynamic shear environment as well as the propagation features of shear wave with small strain.

The experiment equipment was consisted by two main components: 1) cyclic tri-axial test for detecting soil performances under dynamic loading; and 2) measurement of shear wave. Photo 3.1 shows the equipment used in this study, and Figure 3.1 shows the schematic diagram of the testing apparatus including the cyclic load controlling cell, PC recorder cell and shear wave measurement cell. The de-aerated water was prepared by vacuum negative pressure at -90 kPa with more than one day.

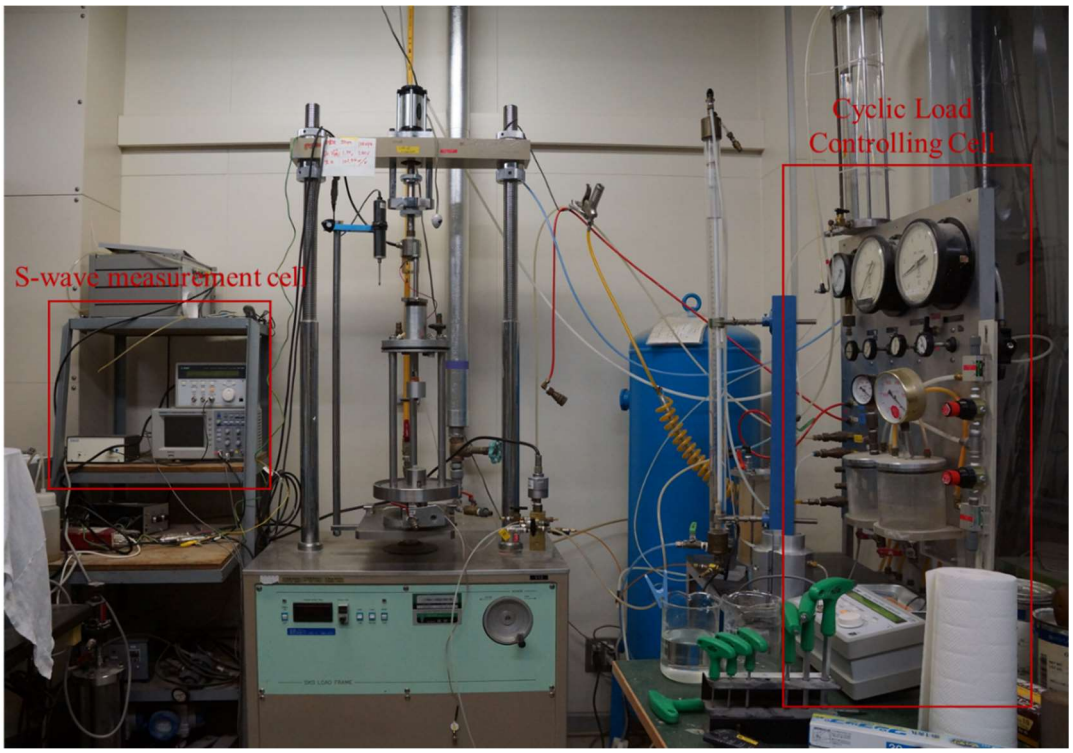

Photo 3. 1Experiment equipment utilized in this study.

The mass of samples was calculated by the target relative densities ($D_{r.}$) or target void ratio (e) for different test cases. Specimens were formed by a mould with the size of 5 cm in diameter × 10 cm in height. Commonly, soil samples were

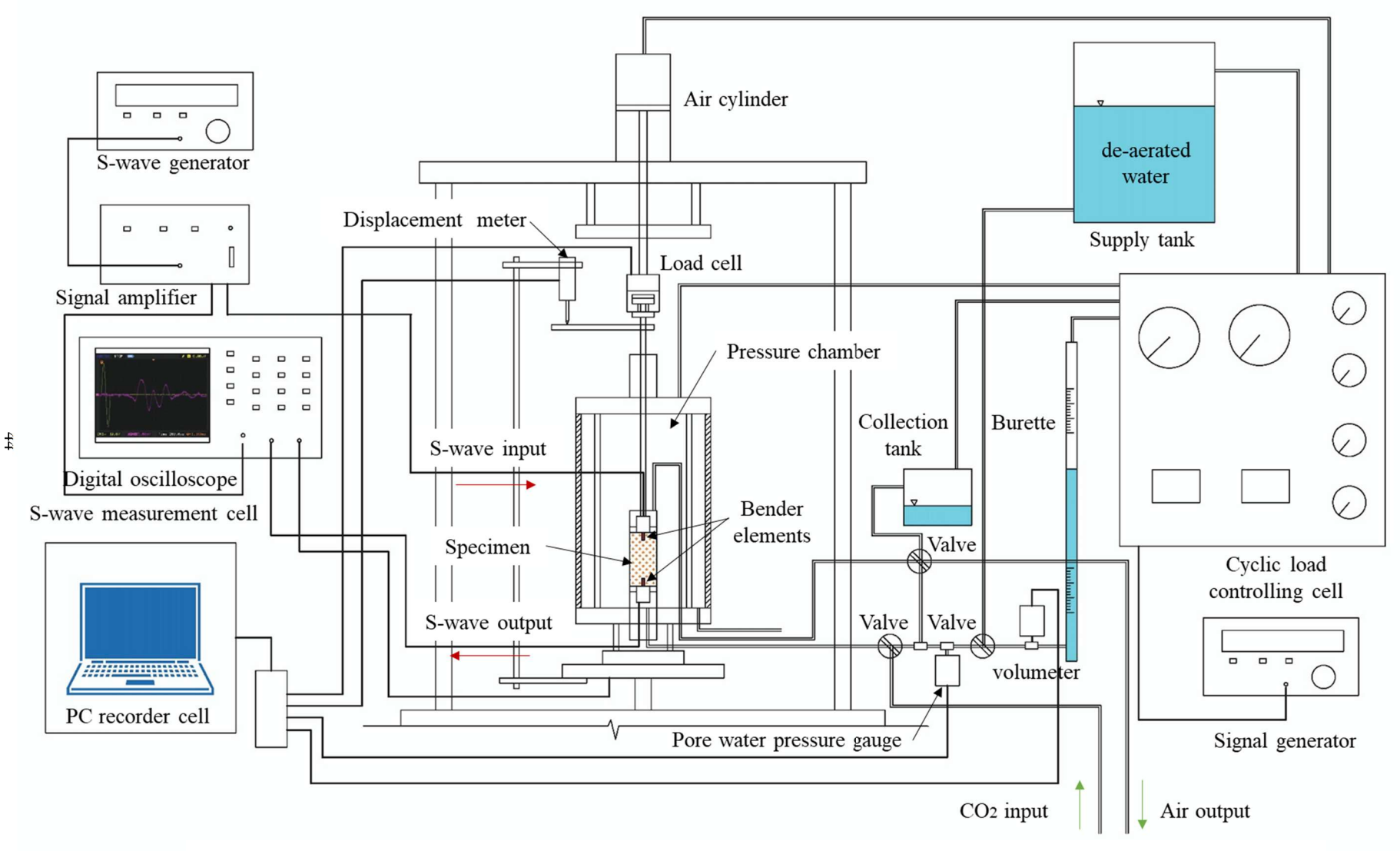

Figure 3.1 Configuration of test equipment for cyclic tri-axial tests and Vs measurement

carried into the mould by three steps with each 1/3 of total mass. A watertight rubber covered the surrounding of specimen and made it could stand by itself under a negative pressure of -20 kPa from internal of specimen while the mould was dissembled. The exact dimension of specimen was measured again to marked by D_0 as the initial diameter and H_0 as the initial height after forming by mould.

Specimens were made by two ways of air pluviation and water pluviation. The difference is defined that samples was dipped with a water environment or without water. For the cases made by water pluviation, de-aerated water was infused into mould from the lower porous stone firstly. Then soils were dipped gradually from the top opening of the mould. Water head was kept higher than soils to make sure soil particles were settled in de-aerated water environment. Contrary, soils were dipped directly into mould for air pluviation method. In both the two ways, it was needed to make the surface flat to achieve a good connection between soil and the upper porous stone. The effects of the two method will result in the difference on saturation degree which is explained accompanied with the saturation methods in follow.

3.3 Comparison of saturation methods

3.3.1 Saturation method of double negative pressure with water pluviation (二重負圧法)

This method provides a difference of negative pressure between cell pressure camber and the system of the *supply tank-specimen-collection tank* to magnify the residual air bubbles inside of specimen for first step. Then utilizes the hydraulic head difference of the de-aerated water between supplying tank and collection tank to wash the expanded air bubbles inside of specimen when water flowed through, as indicated in figure 3.2. The preparation in detail was conducted as follow:

1) Specimen was formed by water pluviation within a negative pressure of -20 kPa,

which was defined as *N.P.1*.

2) Connected another access of negative pressure to the cell pressure chamber, defined as *N.P.2*. And gradually enlarged the negative pressure in both of *N.P.1* and *N.P.2* while kept the difference of 20 kPa. In this study, author make it rise to -90 kPa at internal of specimen; and -70 kPa in the end.
3) Let it be standing within around 1 hour for making it steady.
4) Adjusted multi-way switch to build the water flowing system of the *supply tank-specimen-collection tank*. After that, carefully controlled the opening of the valve, which is near by lower water inlet, to make sure the de-aerated water flowed into specimen gently. During this operation, it should be taking the attention especially, in order to protecting the specimen avoiding from the disturbance of water flowing.
5) Observed the condition of air bubbles washed out from the access of upper porous stone by 15 min, 30 min, 45 min……until there were not any bubbles were washed out.
6) Decreased the *N.P.1* together with *N.P.2*. (keep the difference of 20 kPa) until *N.P.1* became 20 kPa meanwhile *N.P.2* became 0.
7) Switched the connection of *N.P.2* to cell pressure access; then gradually raised the cell pressure (*C.P.*) to 20 kPa and replaced internal negative pressure.
8) Adjusted the multi-ways valves at top and bottom of specimen to let them switch to bullet.
9) Applied the backpressure (*B.P.* = 200 kPa), while cell pressure raised to 220 kPa automatically. Thus, the confining pressure (σ_c) was obtained by Equation 3.1:

$$\sigma_c = \text{C.P.} - \text{N.P} \tag{3.1}$$

10) In order to provide an isotropic environment, the vertical axial force was needed to apply. The level should be corresponding to confining pressure by calculation. The relation of electric-force and the calculation method will be introduced later.
11) Specimens were consolidated at a low confining pressure σ_c = 20 kPa with about

1 hour. Then saturation degree was measured by the results of B-value.

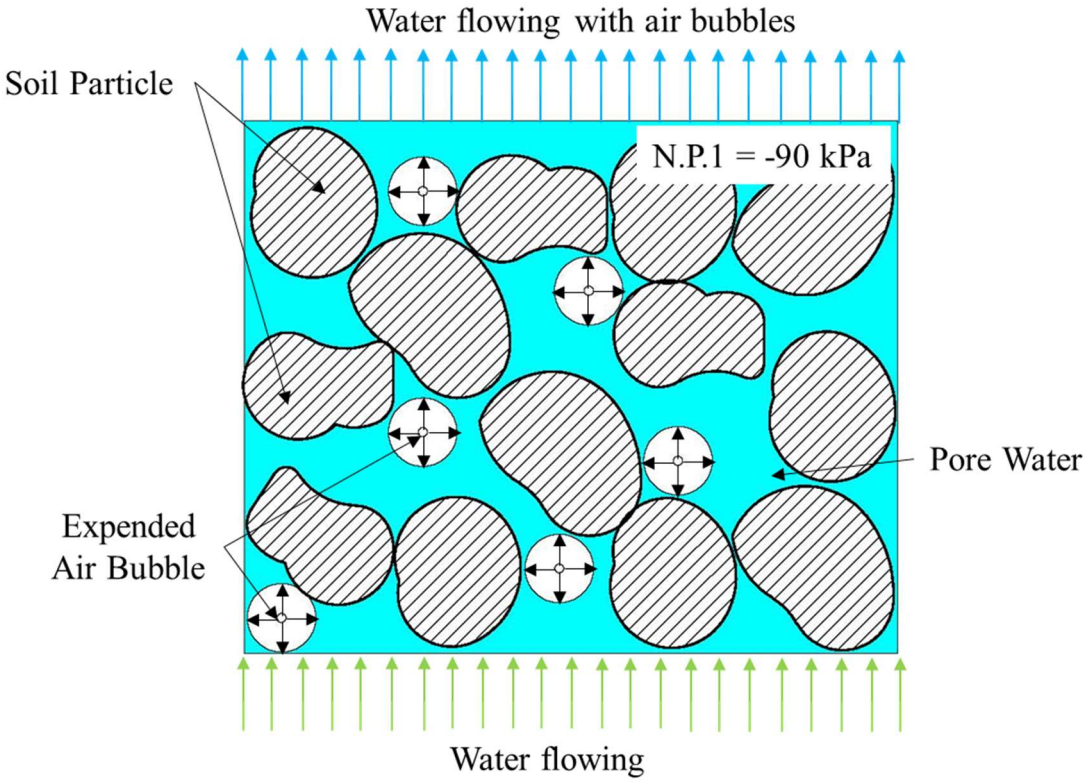

Figure 3.2 Schematic diagram of saturation method with double nagative presure (*N.P.* = 90 kPa & *N.P.2* = 70 kPa)

By this method, the saturation degrees achieved in soils was arranged in Figure 3.3. Toyoura sand prepared with the relative density from 50% to 70% as the test material was conducted for these results.

The results showed a very unsteady performance while all specimens were saturated by the same procedure. It was regardless of how much of confining pressure was applied or the relative densities. The B-value at confining pressure of 80 kPa distributed from near 0.1 to 1.0 which mostly covered the entire range. This phenomenon may be primly due to that the apparatus did not be assembled perfectly

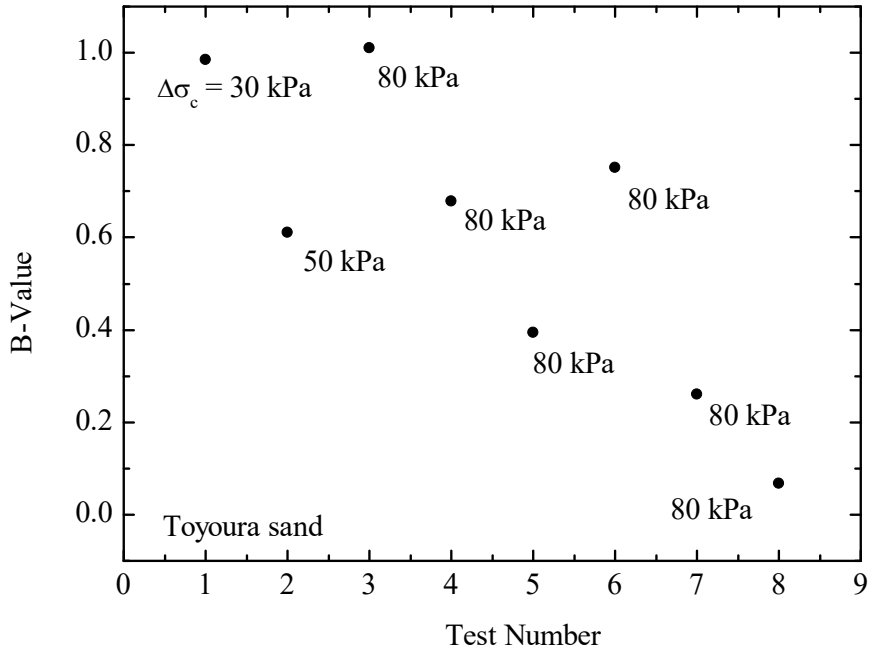

Figure 3.3 Measurement of B-value for soils saturated by double negative pressure method

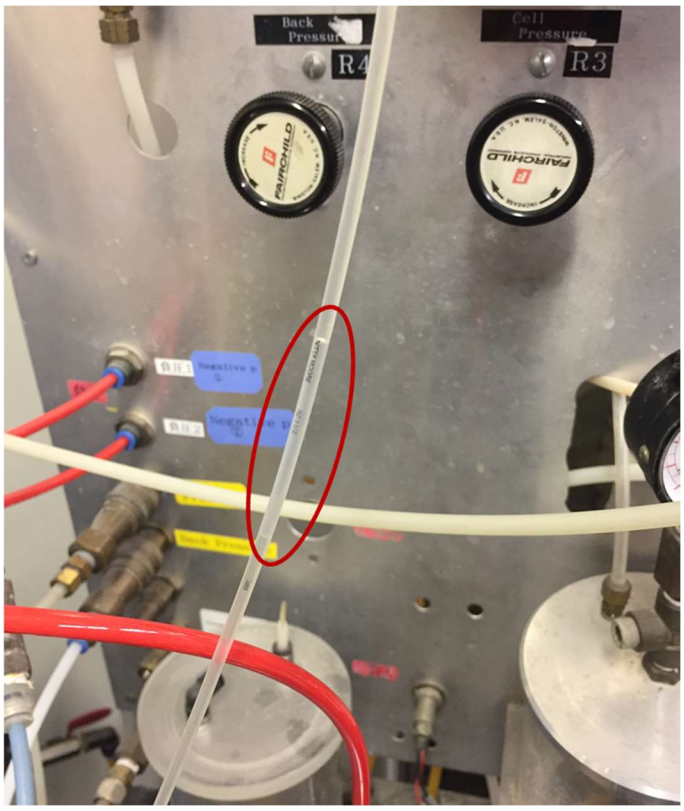

Photo 3.2 Occurrence of air bubbles in pipeline

in tightness in our laboratory. The air bubbles occurred at everywhere inside of pipelines base on the observation during saturation progress, which did not move out companied with water from the topside of specimen. The phenomenon was showed as Photo 3.2.

3.3.2 Saturation method by using CO_2 replacement

According to the physical properties, pure CO_2 could dissolve into water with the volume ratio of 1:1, which is different as air. Meanwhile, the specific gravity of CO_2 is much greater than the average gravity of air because the molecular weight of CO_2 = 48 while air (in average) = 28. These properties provide a possibility to utilize CO_2 to eject the residual air with minor gravity in specimen. There are some changes of procedures comparing with the method by using double negative pressure:

1) As same as before, measured the dimension of specimen after disassembly of mould.
2) Pressed the cell pressure into chamber gradually to instead of internal negative pressure to provide the pressure make specimen standing.
3) Connected the supply capsule of CO_2 to the tests system. The multi-ways valves were switched to make CO_2 was ejected into specimen from lower porous stone and let air leave from the upper pipeline. Because the pressure of CO_2 needs to defence the suction at some level, the pressure became much greater than the head difference in last saturation method. Therefore, the ejection needs very, very slowly and carefully, otherwise the pressure may destroy the particle structure as well as create a shortcut run out from upper pipeline.
4) The upper pipeline was access to a beaker filled with solution mixed with distilled water and calcium hydroxide ($Ca(HO)_2$) as the indicator. The solution would become turbid when amount of CO_2 flows in. This situation was considered as that air was completely ejected out from specimen. The changes of the solution before and after this process preserved in Photo 3.3.

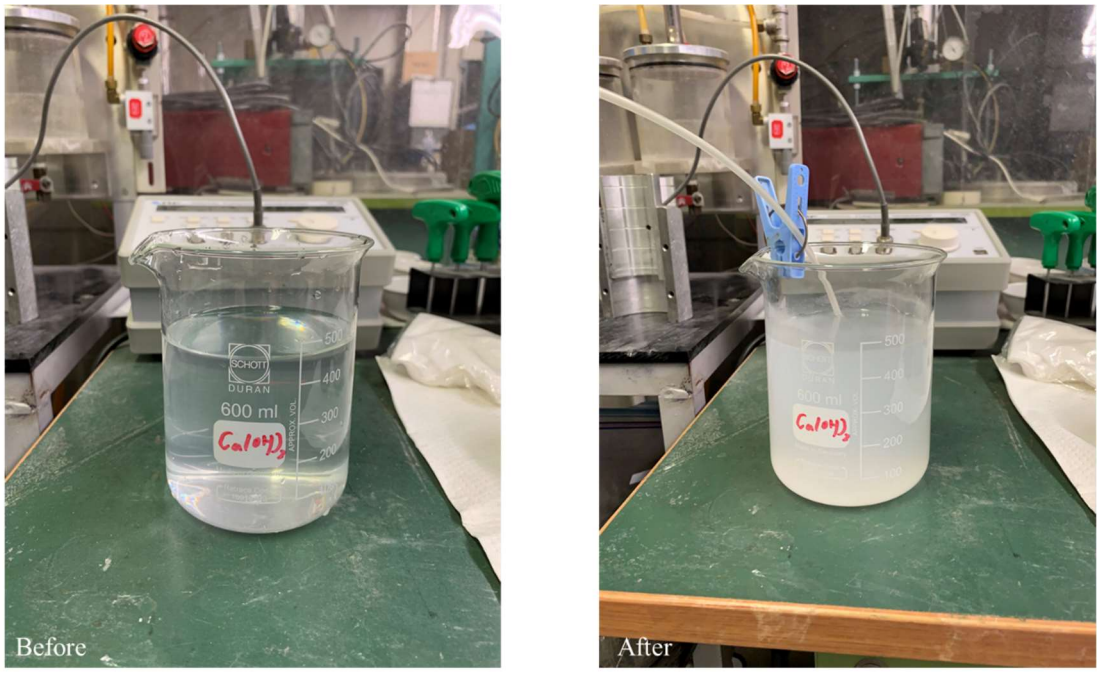

Photo 3.3 Solution of $Ca(HO)_2$ before and after filling with CO_2 in specimen

5) Repeated the steps 4) ~10) in the method of double negative pressure (skipped the operation 6) and 7) which is for negative-cell pressure switching). Then check the B-values after saturation progress.
6) B-value was measured in the sands prepared by both air pluvitaion and water pluviation ways. The results were arranged in Figure 3.4 and 3.5 and showed the different situation for the specimens saturated with double negative pressure. The B-values became steadier, that it was in the range of 0.8 ~ 0.95 for air pluviation way mostly, and in the range of 0.95 ~ 1.0 for water pluviation.
7) By comparing these saturation ways explained above, the method of double negative pressure was deprecated for the unsteady in controlling. The method by using CO_2, was utilized as the primary method to saturated soil samples. In the meantime, the specimens made by air pluvation way was adopted into the tests for un-saturated cases; water pluviation way for the completely saturated cases.

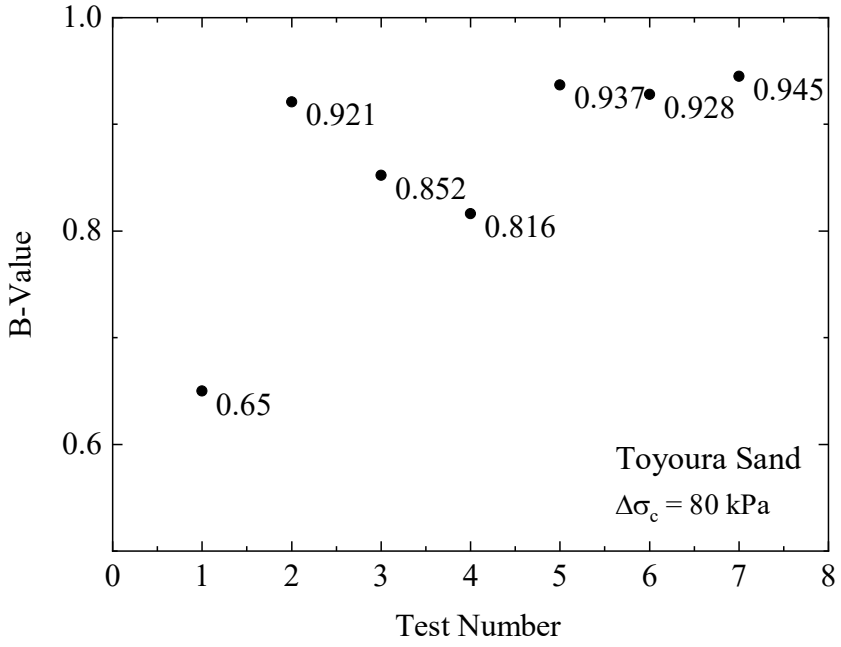

Figure 3.4 Measurement of B-value for the specimens formed by air pluviation.

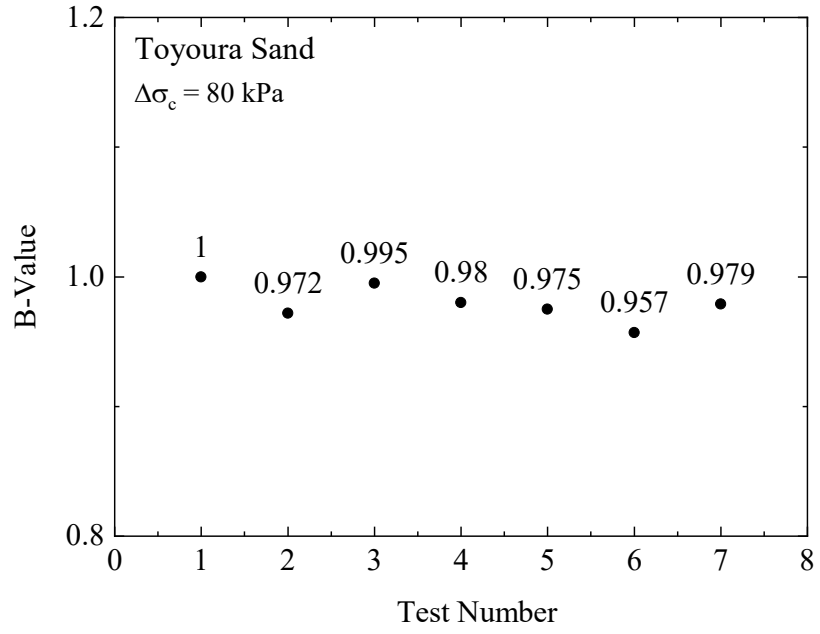

Figure 3.5 Measurement of B-value for the specimens formed by water pluviation.

3.5 Calculation of additional vertical axial force for isotropic consolidation

Because the own weight of the component parts between the load cell and top side of specimen should not be neglected for the soils during consolidation progress. At the same time, as the vertical axial force mentioned in section 3.2.2, in order to permit the specimens was consolidated with an isotropic stress environment, the force needed to be adjusted compatibly let it be corresponding to the confining pressures. Therefore, the additional force *F* should be calculated based on weight from the component parts. The weighing of these parts was photographed shown in Photo 3.4. It needs to pay an attention without missing any part, otherwise, the effect of consolidation will be influenced significantly caused by the deviate stress. Then the force could obtain with the Equation 3.2 ~ 3.3 according to the weight and dimensions indicated in Figure 3.6.

As showing in the Figure 3.6, the cell pressure only applies on area of *A2-A1*. If the target cell pressure was wanted to apply upper face of specimen, the Equation 3.2 should be built,

$$C.P. = (C.P. \bullet (A_2 - A_1) + G + F_a) / A_2 \tag{3.2}$$

Where, F_a (N)is the additional force from piston; G (N) is the weight of upper component parts; A1, A2 is the cross area of piston and porous stone respectively.

Arrange it to Equation 3.3

$$F_a = C.P. \bullet A_1 - G \tag{3.3}$$

It could be found that the additional force is only depended on the weight and cross section area of piston. In this study, weight *G* is measured at 681.03g and

cross area A_2 is measured at 1.33 cm^2. There are same typical results arranged at table 3.1, which were used in this study.

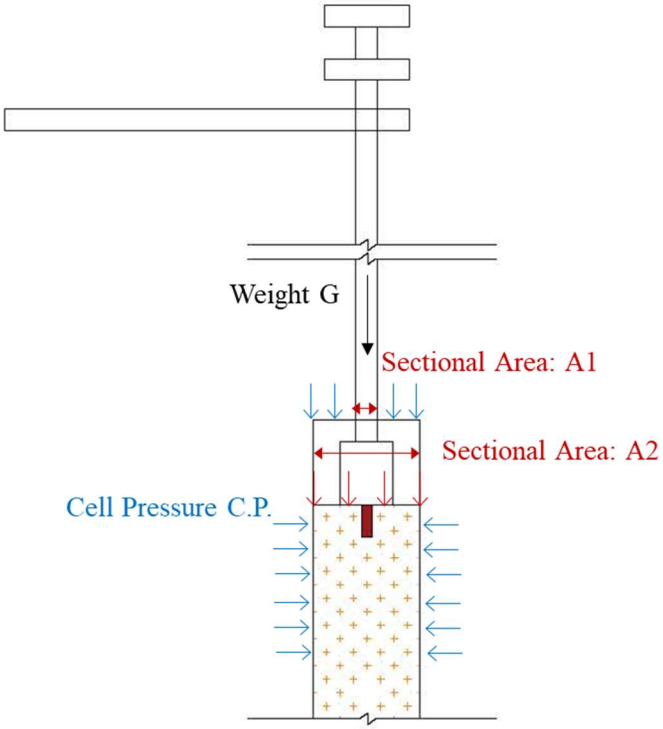

Figure 3.6 Upper schematic diagram of tri-axial tests apparatus

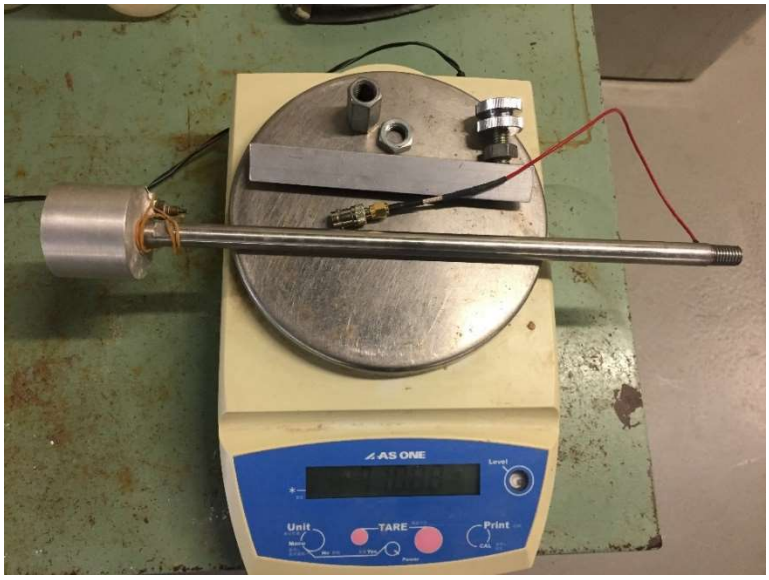

Photo 3.4 Weighment for the upper component parts in tri-axial tests apparatus

Table 3.1 Additional vertical axial forces base on different backpressures used in this study

Cell Pressure (B.P) (kPa)	100	220(200)	320(300)
Additional Force (N)	6.367	21.99	34.78

There is some increment of confining pressure ($\Delta\sigma_c = \Delta C.P.$) were arranged for the measurement of B-value or for consolidation.

Table 3.2 Additional vertical axial forces played in confining pressure

Increment of Confining Pressure (kPa)	80	50	30
Additional Force (N)	32.42	28.51	25.90

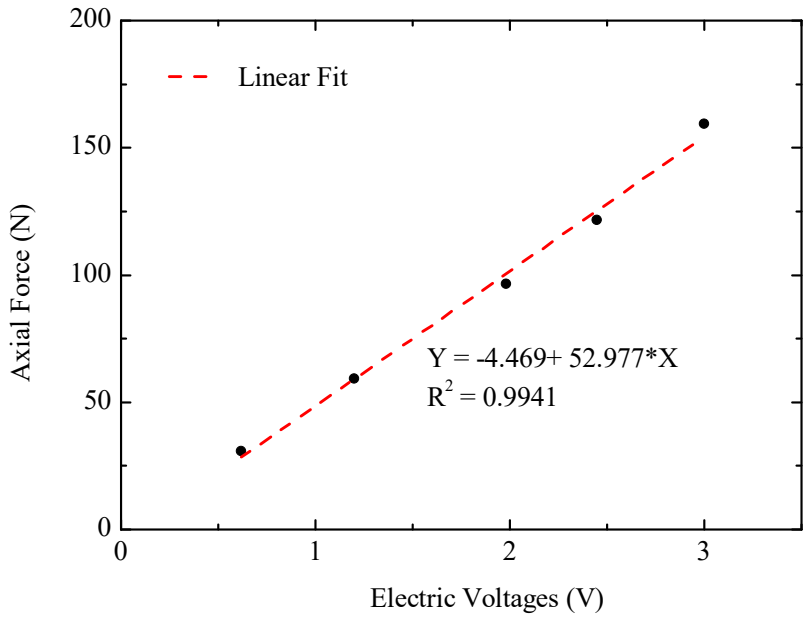

Figure 3.7 Relationship between voltage of electric and vertical axial force

3.6 Trial calculation of cyclic stress ratio (*CSR*)

In this experimental equipment, signal generator creases an electrical signal and sends it to the Electric-Air Pressure converter. This converter would produce an air pressure with the continuous varying. Finally, this air pressure drives the piston to give a continuous varying force affecting on the vertical axial direction of specimen. The confining pressure is provided by the calculation in last section. Therefore, the changes in the relationship between voltage of electric and vertical force is urgent to be detected.

Figure 3.7 shows the results obtained by that give the different voltages into the loading system to find the different levels of force recorded in load cell. The specimens were used by the real soil samples.

The linear correlation could be kindly to fit the results. And base on this relationship, cyclic stress ratio for the tri-axial tests could be easily obtained by Equation 3.4.

$$CSR = \frac{F}{2A_0 \bullet \sigma_{c0}} \tag{3.4}$$

Where, F is the vertical axial force; A_0 is the intimal area of the horizonal cut of specimen; σ_{c0} is the initial confining pressure. The changes of A_0 was neglected during the cyclic tests with the un-draining condition in this study. As the result, it is possible to control the target *CSR* by adjusting electric voltages in the signal generator.

3.7 Description of the tests progress for causing liquefaction and re-liquefaction

Most samples were tested with two serious of cyclic tests for causing the samples two times. The results were focused on detecting the performance on liquefaction

resistance, especially on the changes of the resistance between first and second cyclic tests. It was attempted to find out the effect of pre-shearing or shear history on liquefaction resistance. Then propagation of shear wave was investigated by bender elements to discussing the correlation to the factors such as the shear history, effective stress (soil situation at present), shear modulus, etc. which could influence the liquefaction resistance definitively in soils.

Though the test materials and conditions were specified in the related section and chapters, the common procedure conducted for all samples and the calculation for the changes of relative density between two cyclic tests were introduced in this section. That could void the repetition of description in the follow chapters.

The common test procedure is introduced firstly, as follow:

1) As the description in above, the size of specimen (H_0 and D_0) was measured after formed by mould. The saturated it and make it rest until the B-value measurement. The confining pressure didn't change; thus, the size was considered without any change. Therefore, the initial volume of specimen (V_0) was obtained easily.
2) Added the confining pressure to check the B-value with an un-draining condition. This pressure (σ_{c01}) was also used as the confining pressure for consolidation in most cases. When the measurement of B-value was finished, the lower valve was switched to the burette again. The volume of discharged water (ΔV_{c1}) was caught by volumeter and recorded by PC during consolidation. The volume (V_{c1}) and area of horizonal cut (A_{c1}) of specimen after consolidation could be calculated by the ΔV_{c1} and ΔH_{c1} which was recorded by PC as well. This process was express by Equation 3.5 and 3.6 respectively.

$$V_{c1} = V_0 - \Delta V_{c1} \tag{3.5}$$

$$A_{c1} = \frac{V_{c1}}{H_0 - \Delta H_{c1}} \tag{3.6}$$

3) Thus, the relative density after consolidation could be modified by using V_{c1}. Then, applied the vertical axial force base on the different *CSR* planned for the specimens to start the first cyclic test. However, the real *CSR* in the cyclic tests should be modified by using A_{c1}.
4) The cyclic tests were finished when the axial strain with amplitude in double directions (DA) raised to 5%. It is because that failure traces are very close between excess pore water pressure ratio($\Delta u/\sigma_{c01}$) > 0.95 and DA = 5%.
5) Opened lower valve to let the excess pore water discharge from specimen. Then kept the confining pressure used for second consolidation (re-consolidation). Then, volume (V_{c2}) and cross area (A_{c2}) of specimen after re-consolidation were achieved as well as in step 2). In the end, the cyclic tests would be repeated secondly until soils were liquefied again. The variation of excess pore water pressure, axial loading and axial force was recorded by PC in this progress.

References

JGS 0520-2009: Preparation of soil specimens for triaxial tests.

JGS 0522-2009: Method for consolidated-undrained triaxial compression test on soils.

JGS 0541-2000: Method for cyclic undrained triaxial test on soils.

CHAPTER 4.

COMPARISON OF THE BEHAVIOURS BETWEEN LIQUEFACTION AND RE-LIQUEFACTION IN FINE SAND

4.1 Introduction

Toyoura sand prepared with different relative densities was carried as the tests material in this chapter. The saturation degree was controlled by that B-value = 0.95~1.0 was looked as the completely saturated, and that B-value < 0.95 was looked as unsaturated principally. Besides, it is set 0.2~0.3 of error for the accuracy of measurement to divide that specimen was saturated or not.

The detailed test conditions were introduced firstly. Then, the performances of saturated samples were discussed mainly in this chapter. In final, the comparison of the performances between saturated and unsaturated samples.

4.2 Liquefaction behaviours of saturated Toyoura sand.

4.2.1 Test materials and specimen's preparations

Saturated standard sand (Toyoura sand) was tested as the baseline for comparison firstly. Some of the physical properties of Toyoura sand were expressed in Figure 4.1 and Table 4.1 which was carried in this study.

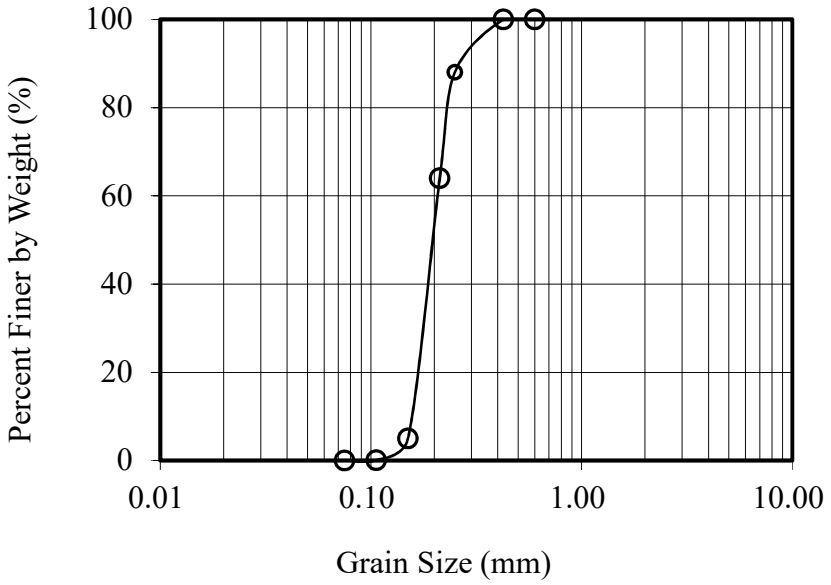

Figure 4.1 Cumulative grain size distribution of Toyoura sand

Table 4.1 Physical properties of Toyoura sand

Specific gravity *Gs*	2.643
Maximum void rate e_{max}	0.977
Minimum void rate e_{min}	0.606

The sand was weighed oven-dried condition for different target relative densities. The target weight of sand was obtained by Equation 4.2 ~4.2.

$$Dr. = \frac{e_{\max} - e_0}{e_{\max} - e_{\min}} \tag{4.1}$$

Where, e_0 is the initial void ratio for target relative density. It is also depended on the density of sand, which is achieved by,

$$\rho_d = \frac{G_s}{1+e_0}\rho_w \tag{4.2}$$

Where, ρ_d is the target density for oven-dried sand; ρ_w is the density of water. Thus, the target weight of sand could be estimated with the volume of the cavity of mould. The target relative density using in study was divided to two groups of 60%, 70% and 80%. Obviously, these relative densities were modified by the changes of volume after consolidation and re-consolidation progresses. The confining pressure of 100 kPa was applied for consolidation and re-consolidation, which resulted in the continual compression of volume.

The consolidation period for different relative density was measured and exhibited in Figure 4.2. The change of specimen's height was adopted as the indicator because the specimen was consolidated isotopically. It could be found that there is a greatly increment when discharged the excess pore water, whereafter, the increment became gentle. The displacement of both in the specimens with Dr = 60% and 80%, was approached to a flat within about 1 hour after consolidation

start. Therefore, it could be considered that the consolidation was completely in this period if the specimen made with a relative density of 60%~80%. Therefore, 1 hour was set as the period for consolidation and re-consolidation thein this study.

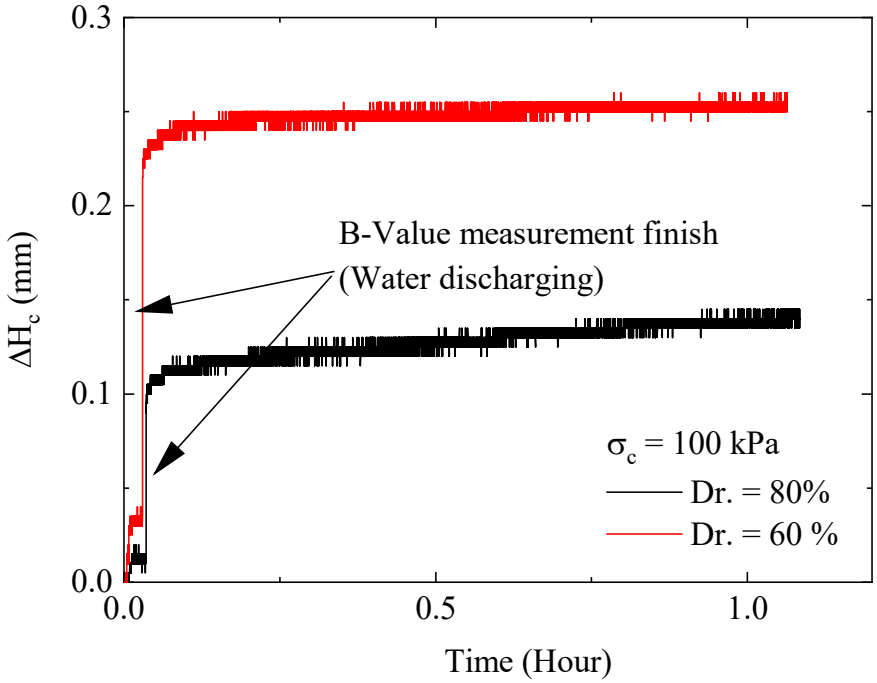

Figure 4.2 Changes of specimen's height during consolidation process for Toyoura sand.

4.2.2 Test condones and process

Based on these conditions, the test process could be introduced clearly by using the confining pressure through the schematic in Figure 4.3 The specimens and test conditions were arranged in Table 4.2. All of them were modified carefully with the changes of specimens' dimension after consolidation and re-consolidation. The specimens were sorted by the increasing relative density, which could be grouped to Dr = 60% (C-1, 2, 3, 4), 70% (C-5, 6, 7, 8), and 80% (C-9, 10, 11, 12) B-value

Table 4.2 Exact test conditions modified by the changes of specimens' dimensions in consolidations

Case No.	B-Value	Relative density after consolidation D_{r01} (%)	Cyclic stress ratio CSR_{01}	Relative density after re-consolidation D_{r02} (%)	Cyclic stress ratio CSR_{02}
C-1	0.993	57.96	0.249	63.99	0.256
C-2	0.978	55.67	0.297	63.55	0.294
C-3	0.957	61.94	0.236	67.95	0.233
C-4	0.995	63.87	0.226	70.58	0.224
C-5	0.980	65.78	0.272	70.98	0.270
C-6	0.979	69.21	0.257	74.86	0.255
C-7	0.975	70.17	0.248	75.86	0.244
C-8	0.955	70.56	0.309	74.94	0.312
C-9	0.945	79.68	0.395	83.93	0.401
C-10	0.928	80.13	0.342	85.27	0.351
C-11	0.937	81.22	0.300	86.58	0.306
C-12	0.951	81.27	0.263	86.12	0.271

respectively. is very high in each case, consequently, the specimens were perfectly saturated.

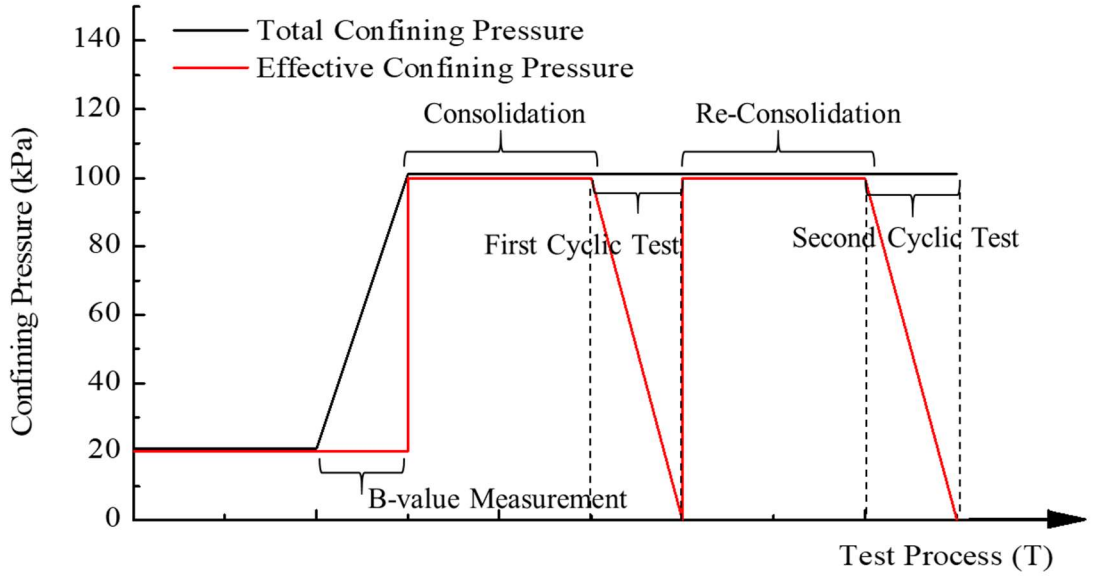

Figure 4.3 Application of confining pressure in test process

The cyclic load was triggered by the continual sinusoidal wave. The 0.1 Hz of frequency is adopted in this study which is the fastest speed for air cylinder. The *CSR* also was modified by the changes of dimension after consolidation and re-consolidation.

4.2.3 Performances on axial displacement and excess pore water pressure under cyclic loading.

The applied cyclic loading and induced changes of axial displacement and excess pore water pressure were record by PC shown from Figure 4.4 to 4.9 which were the typical results in each specimen with relative density from 60% to 80%. These results both in first cyclic tests and second cyclic test were arranged in these figures. In order to make the comparison intuitively, the start position and the time scale were adjusted appropriately between different relative densities and between first cyclic tests and second cyclic tests. Some unload stages were set during cyclic

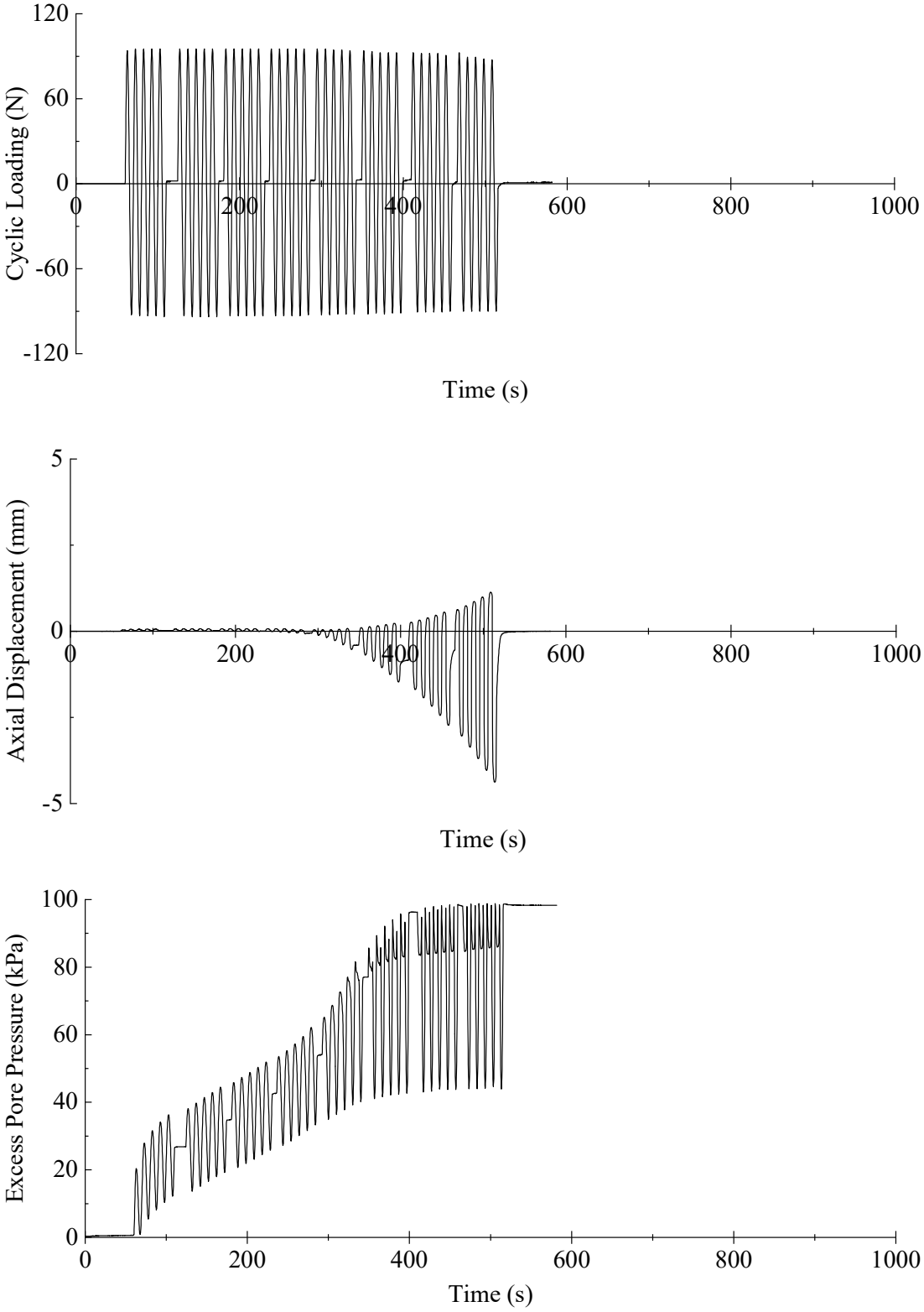

Figure 4.4 The time history of axial force, axial displacement and excess pore in first cyclic test for Toyoura sand with *Dr* = 60% (*CSR* = 0.236)

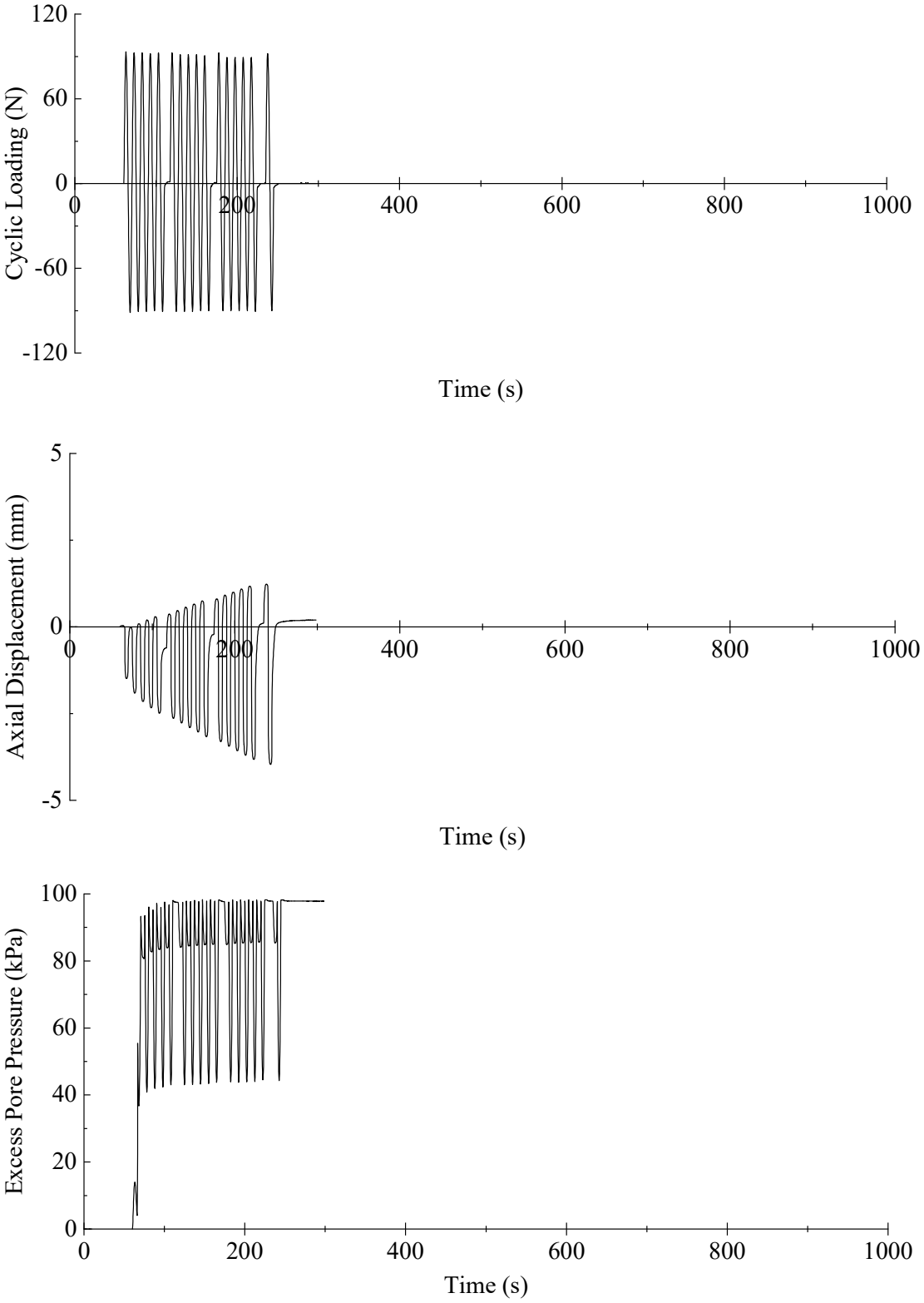

Figure 4.5 The time history of axial force, axial displacement and excess pore in second cyclic test for Toyoura sand with *Dr* = 60% (*CSR* = 0.233)

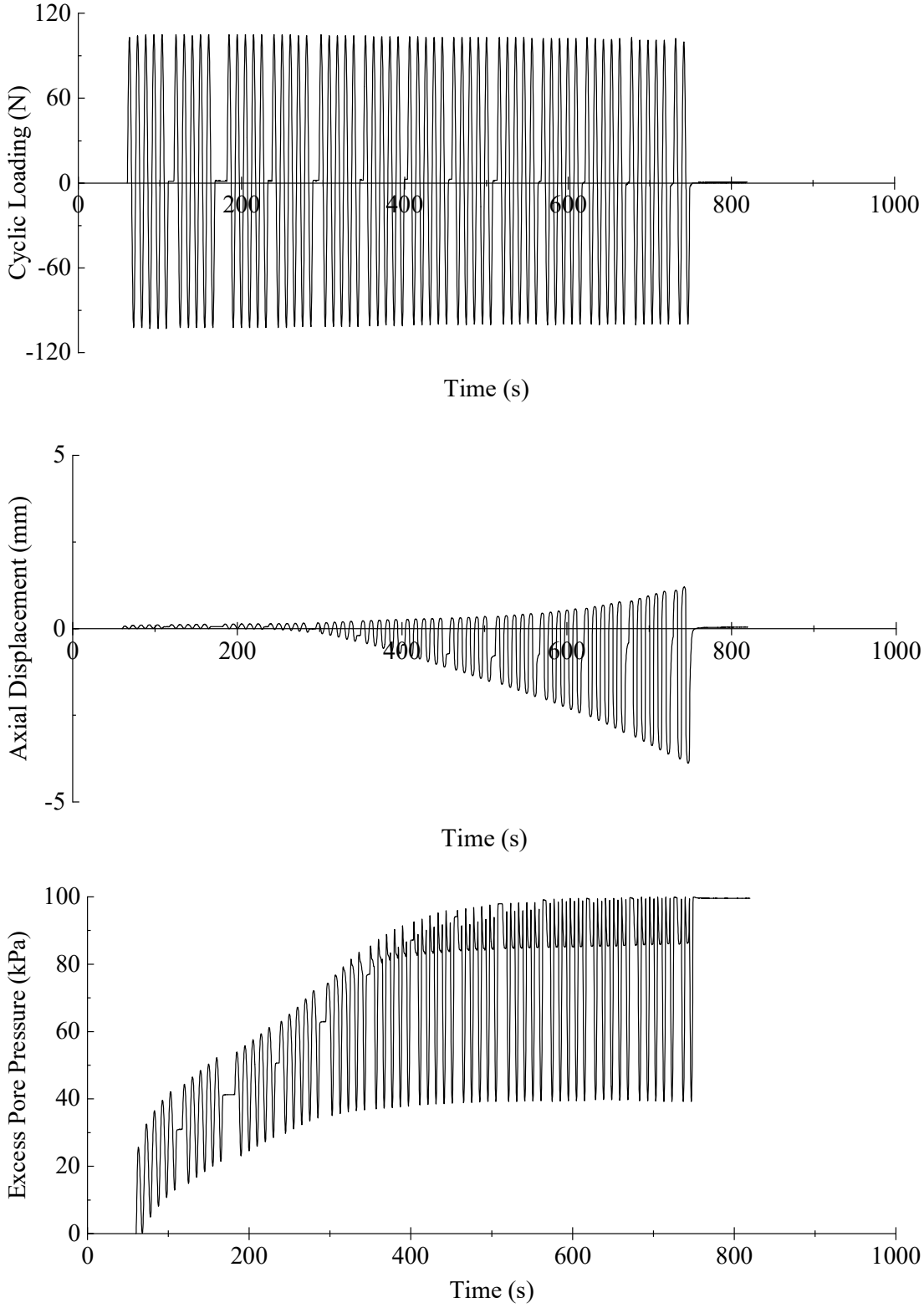

Figure 4.6 The time history of axial force, axial displacement and excess pore in first cyclic test for Toyoura sand with *Dr* = 70% (*CSR* = 0.257)

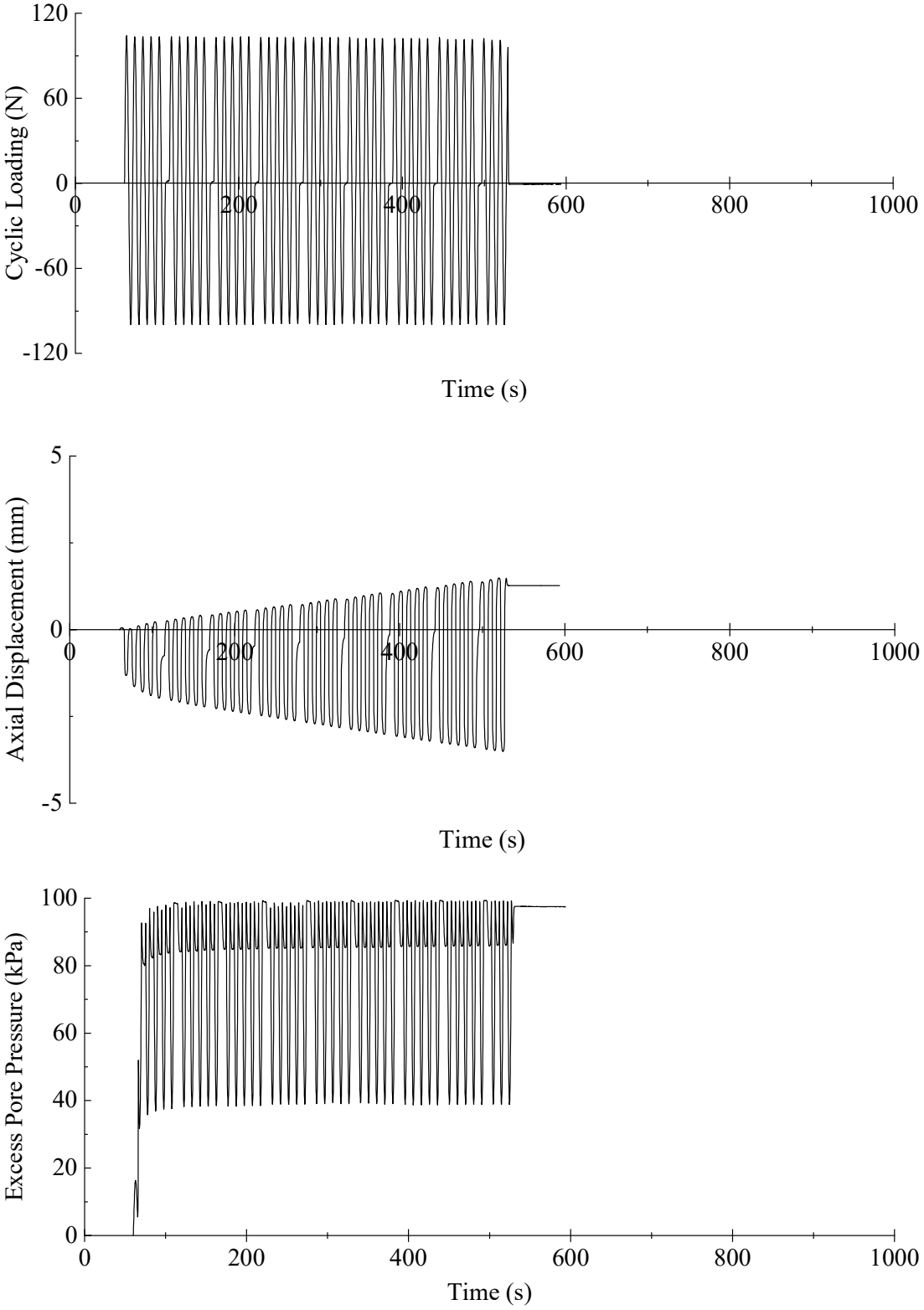

Figure 4.7 The time history of axial force, axial displacement and excess pore in second cyclic test for Toyoura sand with *Dr* = 70% (*CSR* = 0.255)

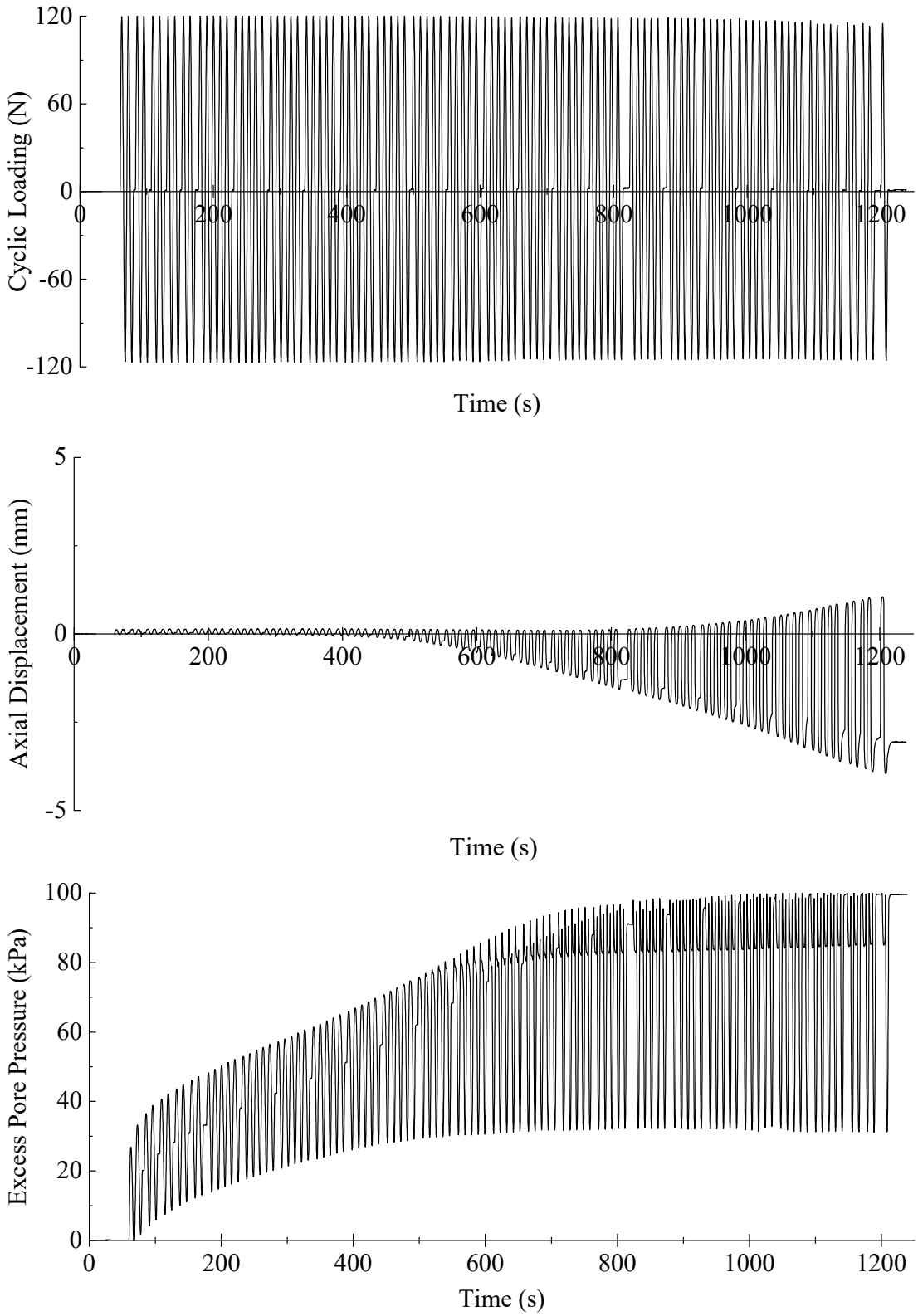

Figure 4.8 The time history of axial force, axial displacement and excess pore in first cyclic test for Toyoura sand with *Dr* = 80% (*CSR* = 0.300)

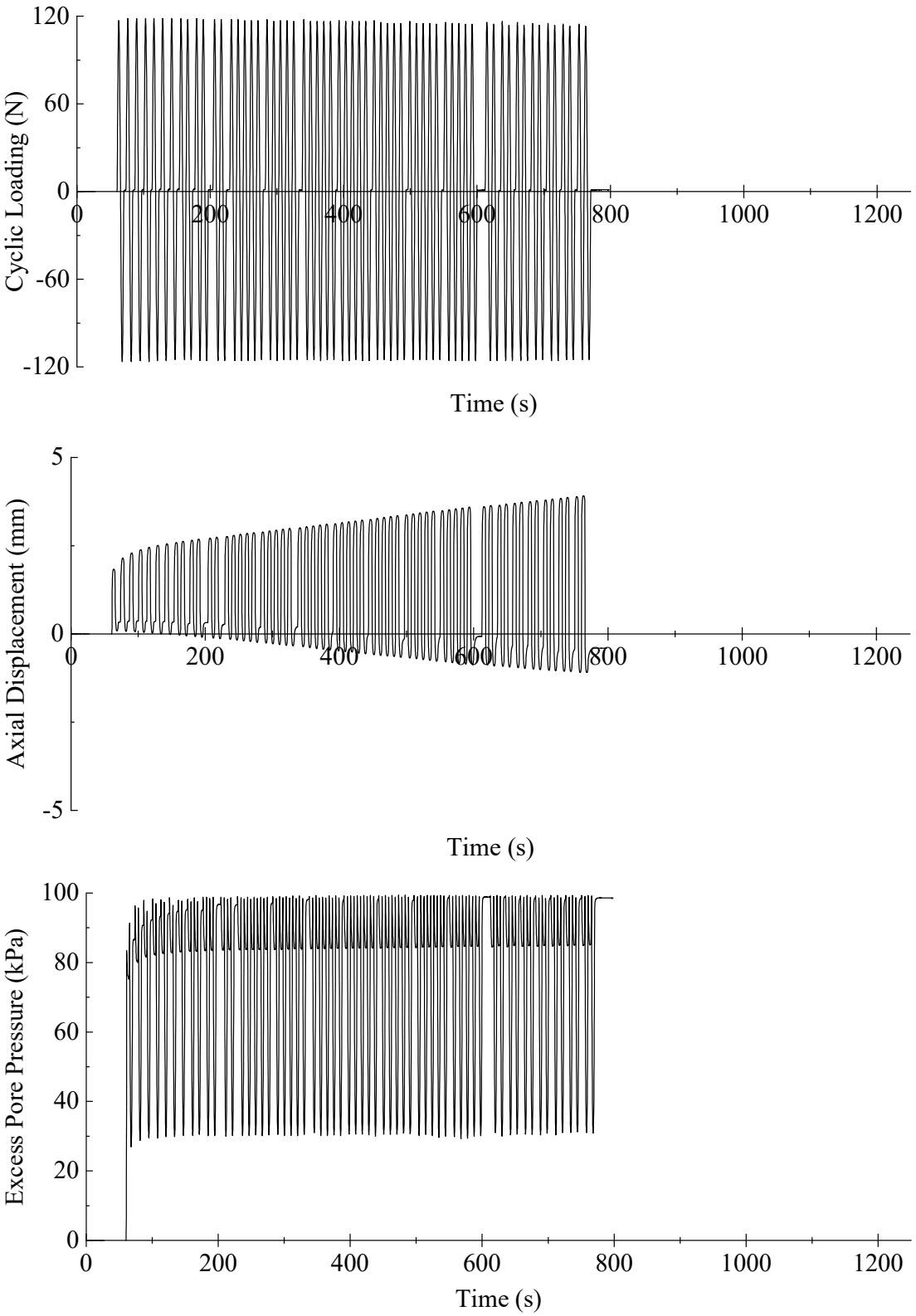

Figure 4.9 The time history of axial force, axial displacement and excess pore in second cyclic test for Toyoura sand with *Dr* = 80% (*CSR* = 0.306)

loading which is for purpose of measuring the propagation of shear wave during the process. The detailed conditions would be explained in Chapter 6 where focused on the performances of shear wave velocity in soils. Finally, the cyclic loading was stopped when DA = 5% where was considered failing by liquefaction as mentioned in above.

It could be easily to found that the necessary cycles were affected by relative density significantly where they were in first or second cyclic tests. Moreover, the necessary cycles greatly decreased in second cyclic tests regardless the changes of relative density in Toyoura sand.

The variation tendency of axial strain and excess pore water pressure also was very different between first and second cyclic tests. The tendency in the sands with the three typical relative densities were very closed which was shown in Figure 4.10 ~ 4.13 summarised as follow:

1) For the axial displacement, the growth rate increased patulously with the increasing of loading cycles in first cyclic tests. On the contrary, this rate performed with the greatest level in first few cycles in second cyclic tests, then it became slow and the displacement increased convergent with loading cycles increasing.
2) For the excess pore water pressure, in first cyclic tests, the pore pressure increased gradually with the loading cycles increasing in general speaking. The maximum pore pressure was produced at u/σ_{c0}' = 1.0 where was very closed to 5%. However, pore pressure raised very fast and approaching to the maximum level with fist few cycles in second cyclic tests. After that, it glowed very slowly with the increasing of loading cycles and displacement.

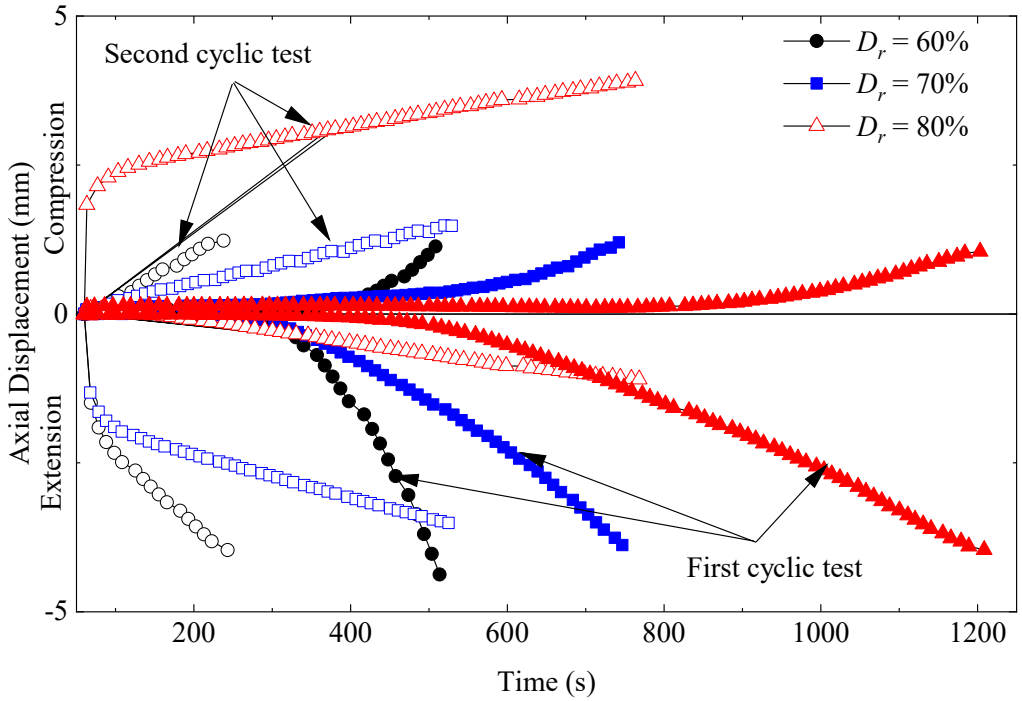

Figure 4.10 Comparison of envelope curve of axial displacement between first and second cyclic tests for different relative densities.

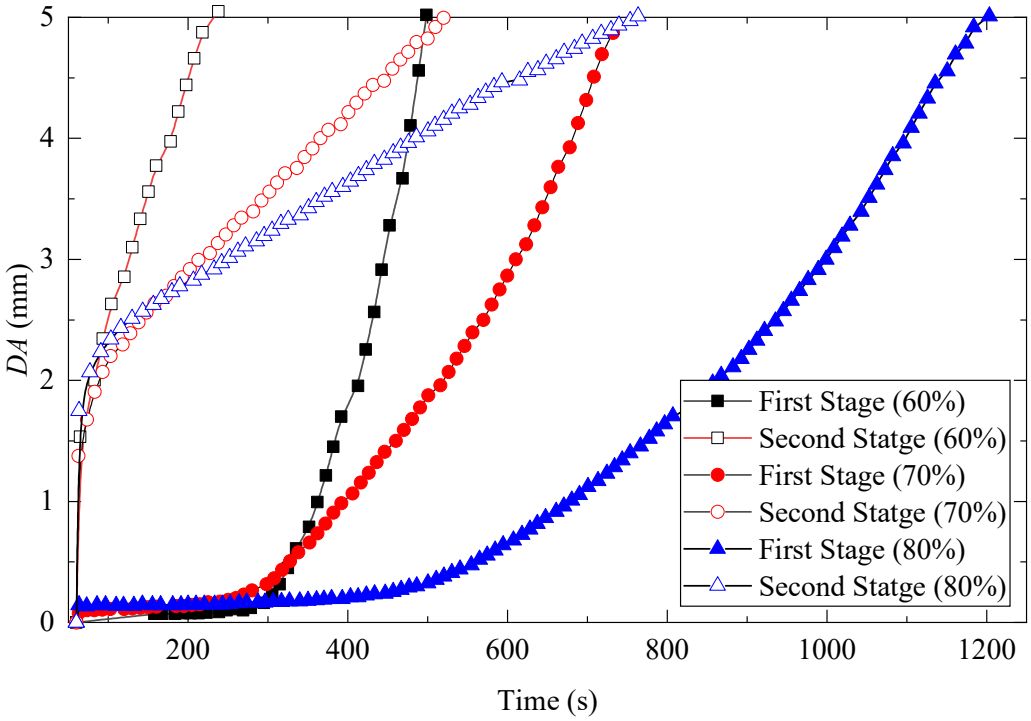

Figure 4. 11 The maximum axial strain producing in each loading cycle between first and second cyclic tests for different relative densities.

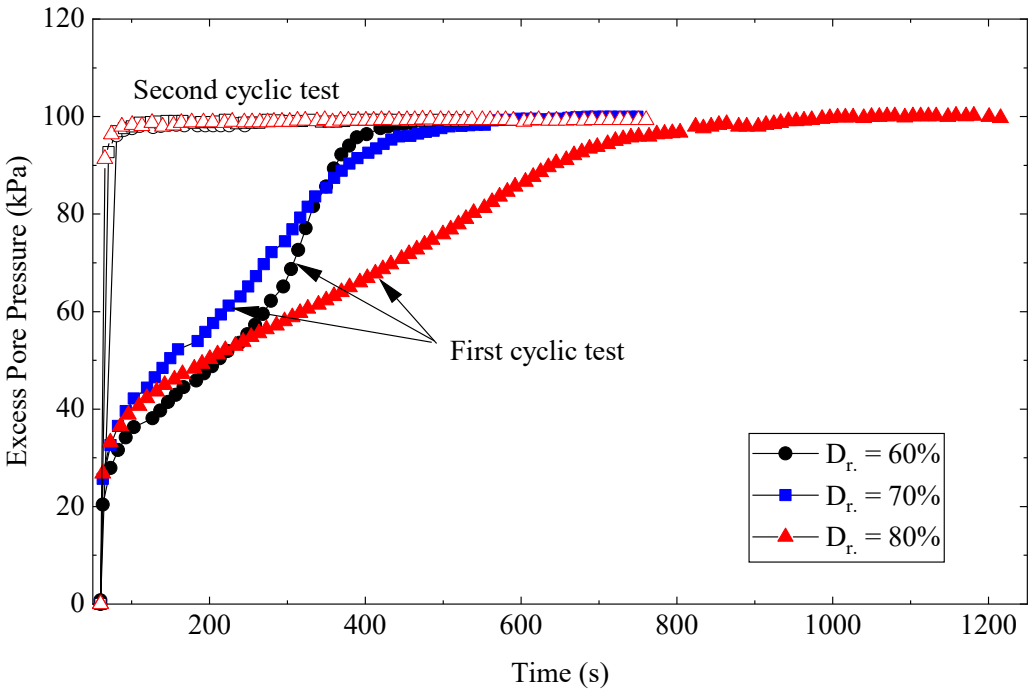

Figure 4.12 The maximum *EPWP* producing in each loading cycle between first and second cyclic tests for different relative densities.

These results could strongly prove the liquefaction resistance of Toyoura sand was influenced after the pre-shearing which caused a liquefaction once time. The performances could be understood more directly to use the stress path and the relationship of shear stress-strain during the cyclic tests. Figure 4.13~4.18 showed this kind of results corrected from Dr = 60%, 70% 80%.

These figures clearly indicate the difference of both excess pore water pressure and axial strain developing between the two cyclic tests. The performances during the first cycle became most important for the second cyclic tests. The excess pore pressure raised to near 100% of mean effective stress in this period, at the same time, the axial strain produced near 1/3 in total. After the first or second load cycles, the changes became uniformly and tightly until these reached the failure criteria respectively.

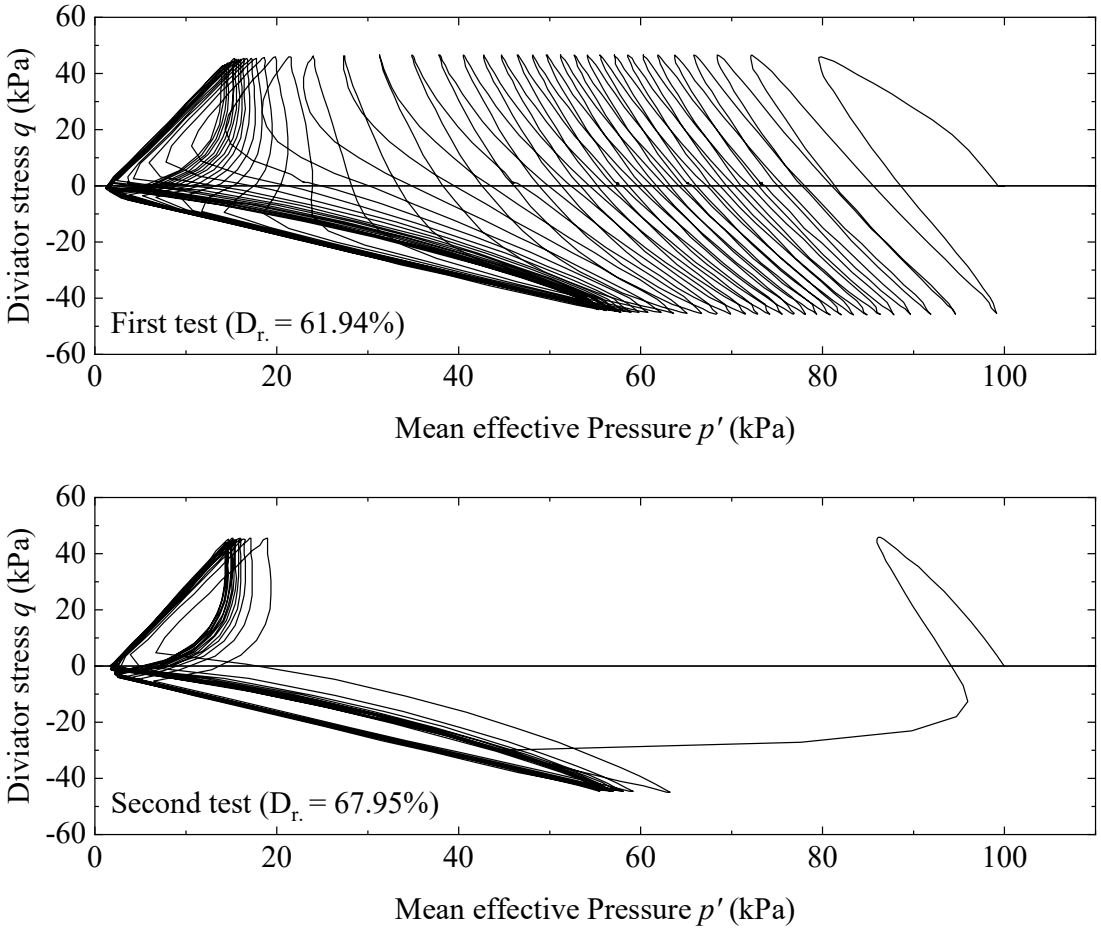

Figure 4.13 Stress path of first and second cyclic tests for the Toyoura sand with the initial relative density = 60%.

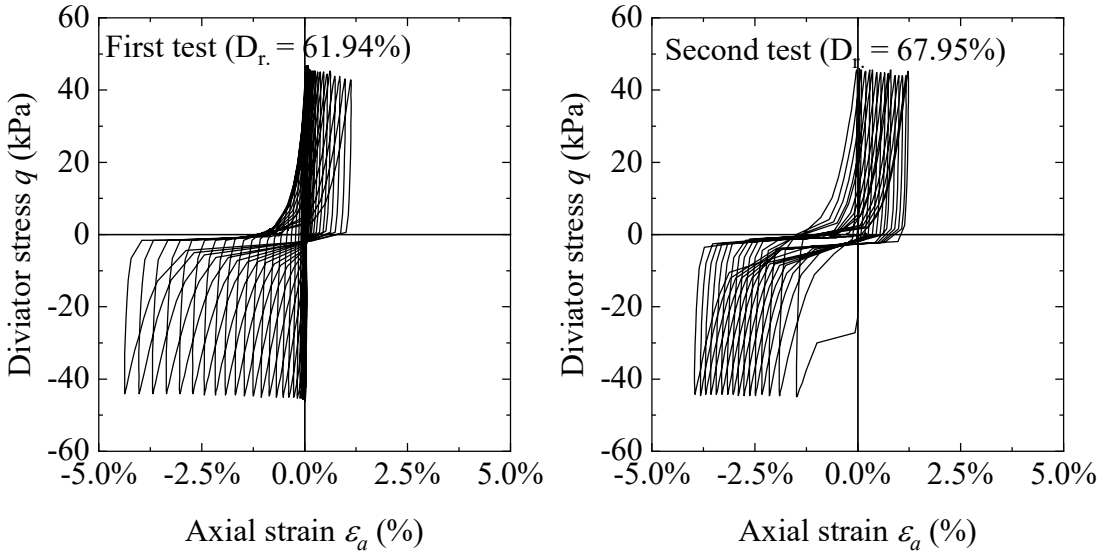

Figure 4.14 Shear stress-strain relation between first and second cyclic tests for Toyoura sand with initial relative density = 60%

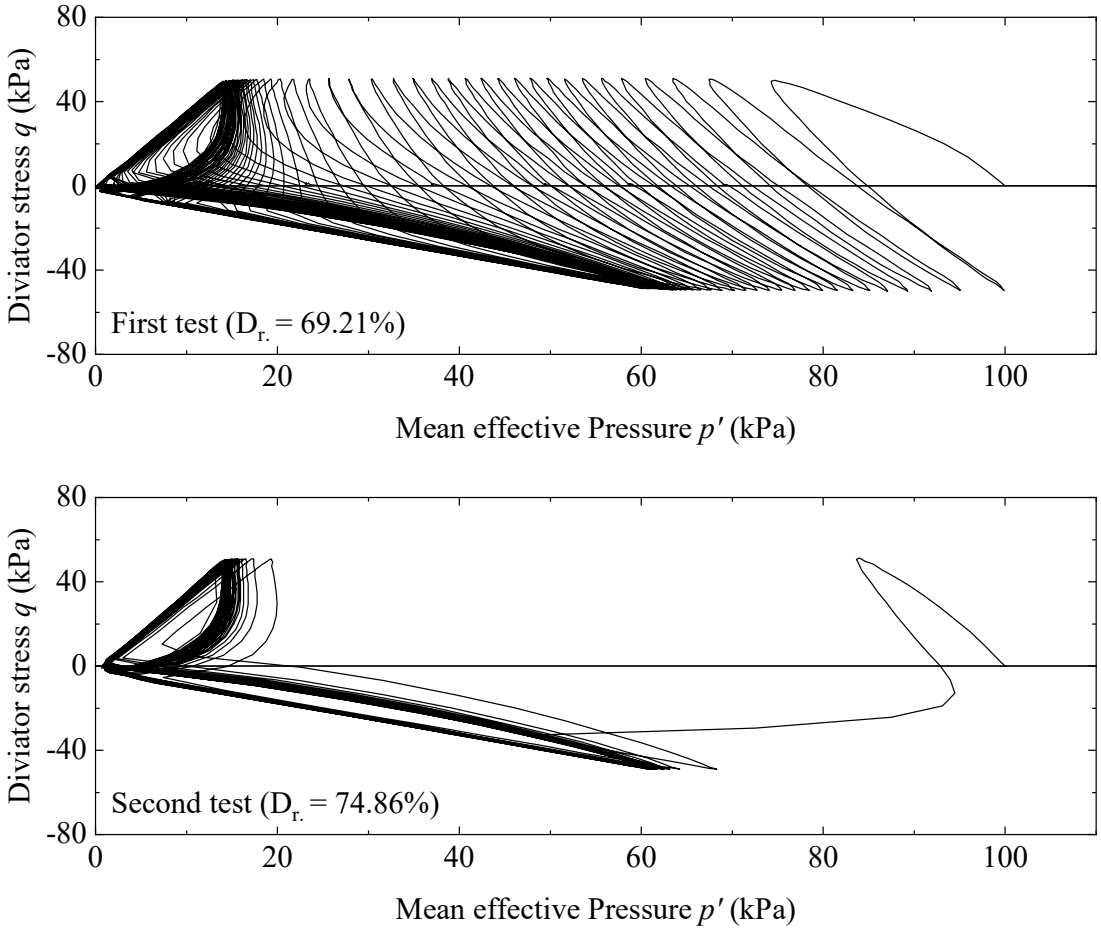

Figure 4.15 Stress path of first and second cyclic tests for the Toyoura sand with the initial relative density = 70%.

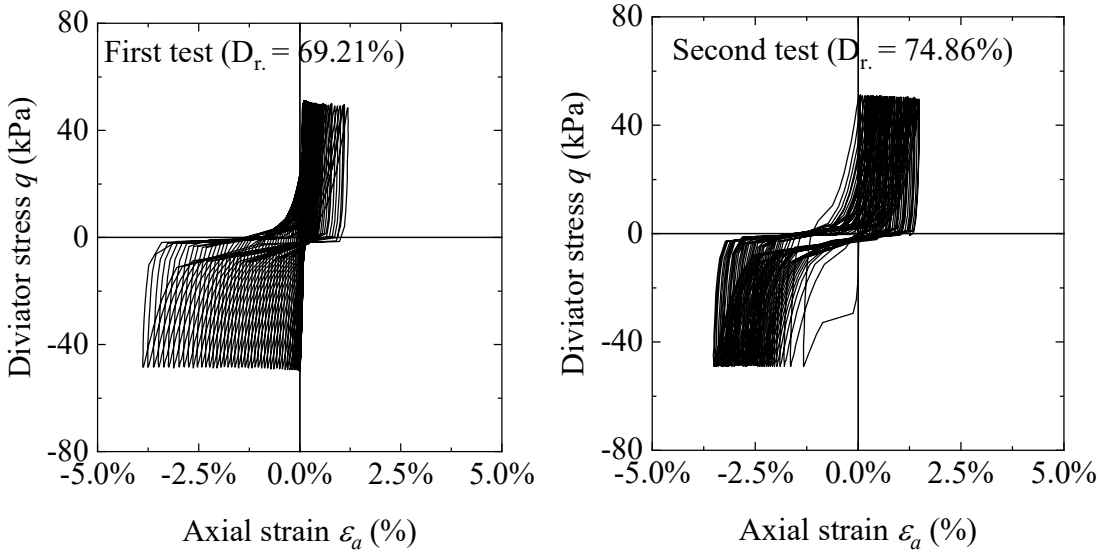

Figure 4.16 Shear stress-strain relation between first and second cyclic tests for Toyoura sand with initial relative density = 70%

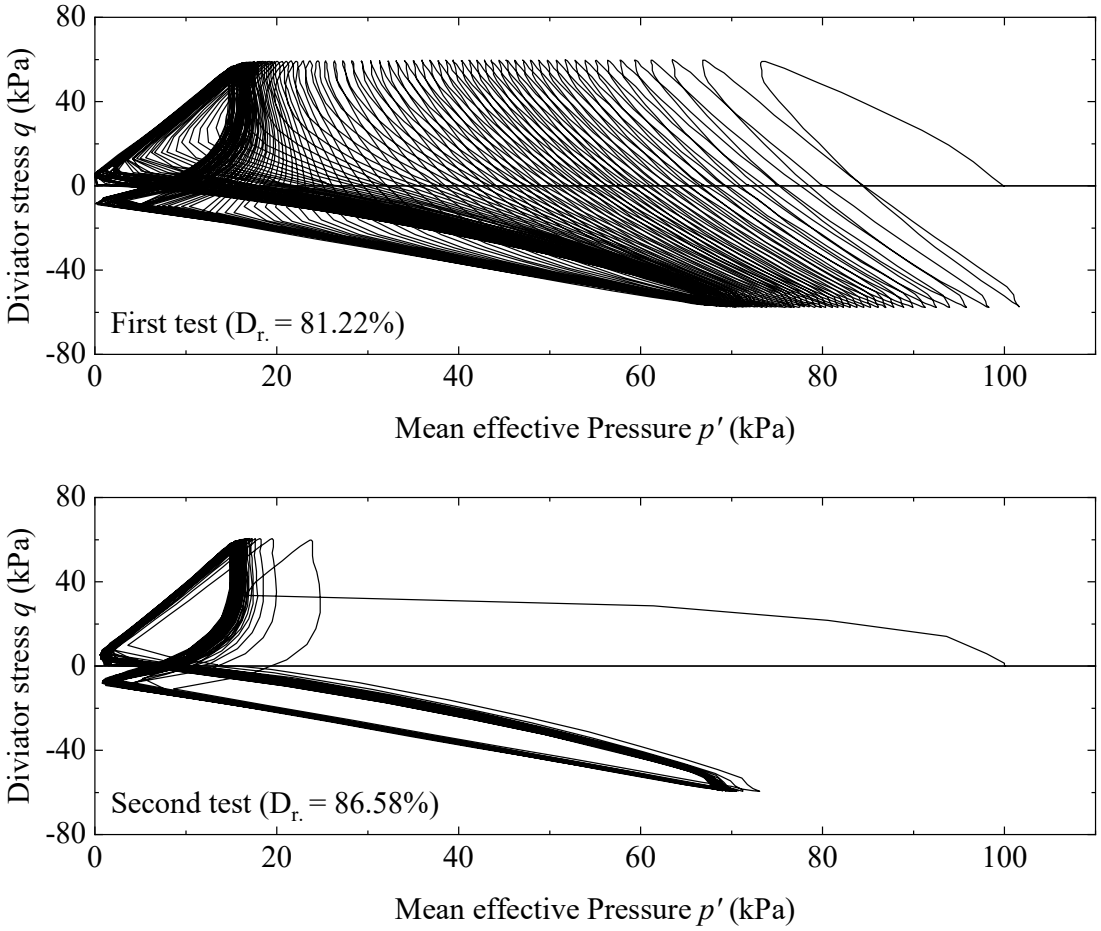

Figure 4.17 Stress path of first and second cyclic tests for the Toyoura sand with the initial relative density = 80%.

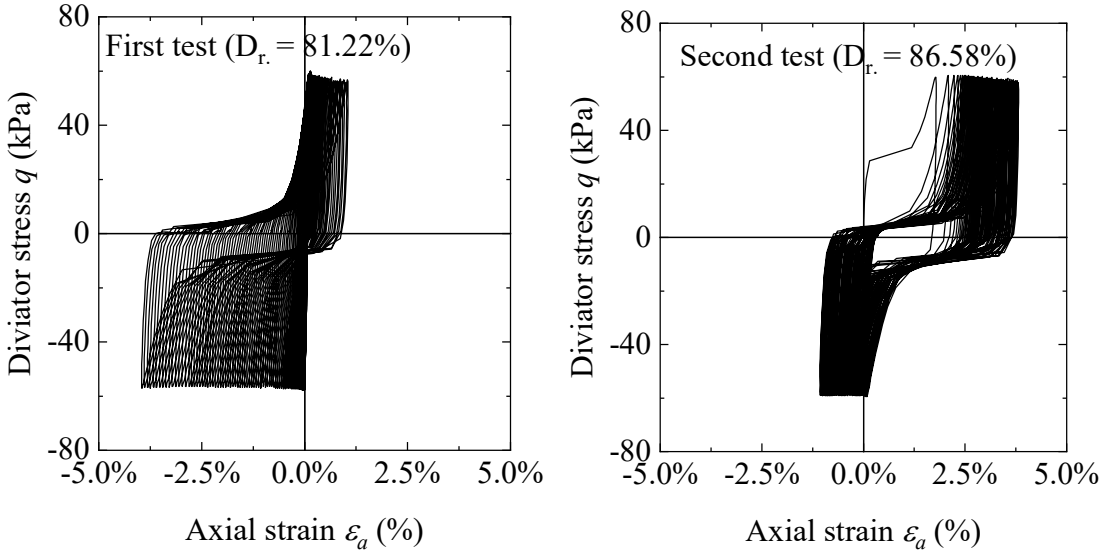

Figure 4.18 Shear stress-strain relation between first and second cyclic tests for Toyoura sand with initial relative density = 80%

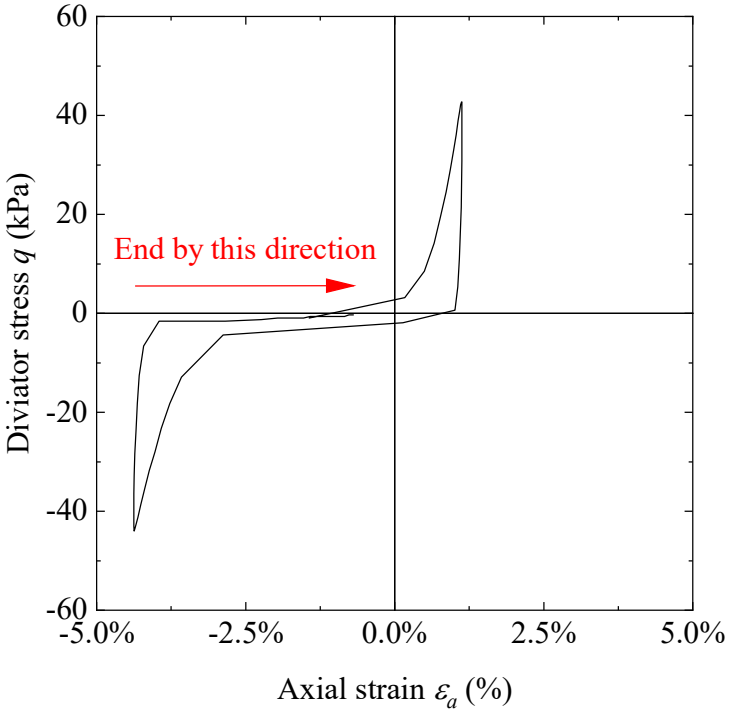

(a) In the final load cycle during first stage

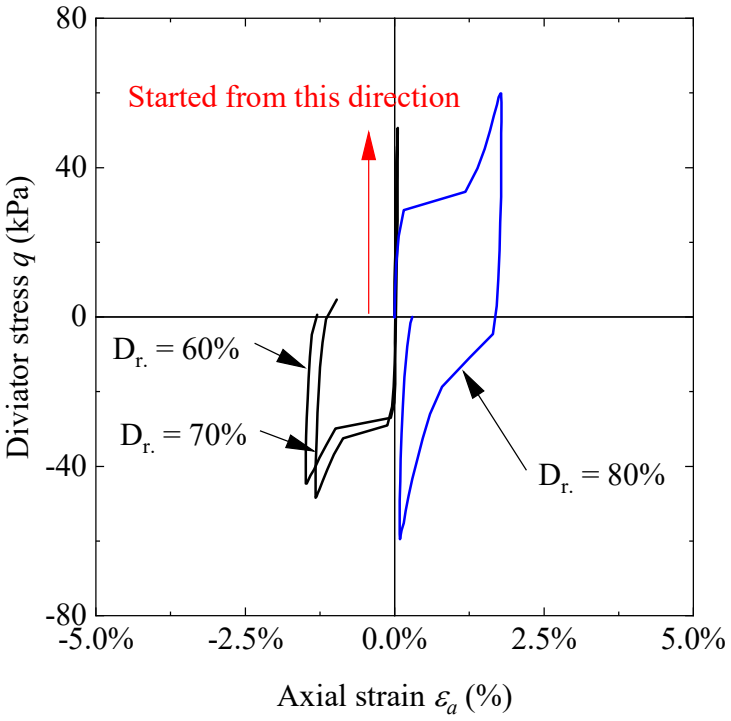

(b) In the first load cycle during second stages

Figure 4.19 Performance of shear stress-strain between first and second cyclic tests

4.2.4 The effect of residual axial strain in first test stage on the performance second stage

There was a noticeable point in the performance between the sand with *Dr* = 80% and *Dr* = 60% (or 70%). The maximum increment of axial strain and the maximum reduction of mean effective stress appeared when the load was at the half cycle in extension direction for the sand with *Dr* = 60% or 70%. However, it in sand with 80% produced an opposite performance, that the greatly changes appeared in compression period. But the final loading direction in the three cases was same that it was retracted from extension direction in first tests, meanwhile, the first load cycle started from the compression direction, as shown in Figure 4.19.

The results also indicated that there was none or very little strain which was produced in the opposite direction where the maximum strain appeared.

There are some researchers such as K. Ishihara and S. Okada (1982), who used the static cyclic tri-axial tests, supposed that the direction of final load in first stage is one of the influence factors to cause the anisotropy inside of particle structure to result in a the great change of liquefaction resistance in second stages. The similar result also was achieved by M. Oda et al. 2001; B. Ye et al. (2015) by using shaking table tests and tri-axial torsional shear tests. In generally speaking base on their results, the mean effective stress would almost not be changed if the cyclic loading starts in the identical direction as the half ending cycle in first stages. However, the if the cyclic lading starts in the direction opposite to the half cycle in first stages, the mean effective stress decreases significantly in second stages.

However, it performed a different result in this study. The significant decreasing appeared in the starting half cycles both direction in compression and extension with a same direction of the final half cycle in first stages. The results in all cases prepared in this section were organized in Table 4.3. The mark “+” is to represent the compressive direction and “-” is to represent the extension direction. And the mark of “0” was added to represent the residual position of axial strain

when first cyclic tests was finished. By considering the measurement accuracy of this system, if the axial strain was less than 0.1%, “0” is used to represent there was non the axial strain in the end of first stages. It is because that there were no visible changes in the axial displacement-time corresponded groups such as indicated in Figure 4.4 and 4.6. There were two types of residual axial strain were arranged in Table 4.3: the first strain was measured immediately at unloading moment in the end of first stage; the other strain was measured after re-consolidation. In the two strains, the first strain could be looked as which was caused by the accumulated changes from liquefaction process; meanwhile, the second strain was caused by the dissipation of excess porewater pressure. The contribution of the two strains are different on liquefaction behaviour. In re-consolidation process, the strain produced in uniform within the change of volume under isotropic confining pressure, which induced the increment of liquefaction resistance commonly. Therefore, the first strain was worthier to discuss. The results could be expressed as follow:

1) The significant increasing of axial strain always appeared together with the significant decreasing of mean effective stress in second stages.
2) The final half cycles produced the identical direction for the position of residual axial strain in most cases. For the cases with the lower relative density Dr = 60% and 70%, the axial strain retracted to initial position in some cases. this behaviour perhaps was caused by the samples also kept in recoverable range while the samples were liquefied (DA = 5%). Moreover, the extension position produced in these cases which was produced by the extensional half load cycle also is very little, that the axial strain ε_a = -0.31% in C-4 and ε_a = -0.17% in C-8. However, the performance became quite different for the denser cases. The residual positions always were accordant with the direction of final half cycles, and the residual axial strain was end at about 3.0% ~ 3.48% of total height.
3) There were lot of significant changes always appeared in the extension direction

in the first half cycle in second stages when the relative density within 60%~70%, even the direction of first cycle in second stages was identical as final half cycles. In the other hand, for the denser sand, the significant changes always appeared in the opposite to the direction of final half cycles.

These behaviours could be improved as that the direction of residual axial strain is the most important factor in the direction for significant changes. If the residual strain is very little, the significant changes would always appear in the extension direction which is commonly considered as the weak direction in cyclic tri-axial tests.

Table 4.3 The Direction of significant changes within the first half of cyclic loading during second cyclic tests corresponding to the conditions in the final half of cyclic loading during first stages

Case No.	Relative density in first stages (%)	Direction of final half cycle	Direction of residual axial strain in first stages	Direction of residual axial strain after re-consolidation	Relative density in first stages (%)	Direction of first half cycle in second stages	Direction of significant decreasing of mean effective stress appeared	Direction of significant increasing of axial strain appeared
C-1	57.96	+	+	+	63.99	+	-	-
C-2	55.67	-	0	+	63.55	+	-	-
C-3	61.94	-	0	+	67.95	+	-	-
C-4	63.87	-	-	-	70.58	+	-	-
C-5	65.78	+	+	+	70.98	+	-	-
C-6	69.21	-	0	+	74.86	+	-	-
C-7	70.17	+	+	+	75.86	+	-	-
C-8	70.56	-	-	+	74.94	+	-	-
C-9	79.68	-	-	-	83.93	+	+	+
C-10	80.13	-	-	-	85.27	+	+	+
C-11	81.22	-	-	-	86.58	+	+	+
C-12	81.27	-	-	-	86.12	+	+	+

4.2.5 Liquefaction behaviours between first and second cyclic tests

As motioned in above, the *DA* = 5% as the failure state for liquefaction was widely used in cyclic tri-axial tests. In study, it also be as the criteria used for the pre-shearing (first cyclic tests) and the final failure in second cyclic tests. This criterion is based on the result that the line of *DA* = 5 % is very closed to and greater than when excess pore pressure ratio reaches 0.95. However, according to the results in second cyclic tests, the excess pore water pressure increased very fast and approaching to 0.95 at only first few load cycles while the axial strain was greatly slower than the excess pore water pressure. The gap between the two indexes would become larger probably until *DA* = 5%. The failure line for liquefaction should be discussed again to take the excess pore water pressure ratio (0.95 and maximum which got to 1.0) and the *DA* = 2% and 5% into discussion. Meanwhile, the comparisons were conducted between the first cyclic tests and second cyclic tests.

At first, the failure lines for first cyclic tests were developed by the cyclic stress ratio and the necessary load cycles in different target indexes. The results were arranged in Figure 4.20 ~ 4.22 for the relative density of 60%, 70% and 80% respectively. It could be found obviously that the results in the sand two lower relative density were very similar both in first and second cyclic tests. In first tests, the failure lines regardless *DA* = 2% to 5% or excess pore water pressure ratio *EPWP* = 0.95 to 1.0 were very close. By a carefully observing, the necessary cycles were from most to least within a very small range for *DA*= 5%, $u/\sigma_{c0}' = 1.0$, *DA* = 2% and $u/\sigma_{c0}' = 0.95$ respectively. And the line for *DA*= 5%, $u/\sigma_{c0}' = 1.0\%$ is very closer than the others. This phenomenon also be confirmed by that the increment rate of axial strain became greater with the cyclic loading applying in first stage especially the loading caused $u/\sigma_{c0}' = 0.95$ or *DA* = 2%.

In second cyclic tests, the results became great different after the pre-sharing which produced liquefaction once. The lines were away from each other and moved to a larger range. The most notably is that the line of *DA* = 5% become far away from the other lines. At the same time, the necessary cycles for causing *DA* = 2% and $u/\sigma_{c0}' = 0.95$ reduced

very significantly, that occurred within only 1 ~ 3 cycles in most cases. As the result, the two lines were almost overlapped in the Toyoura sand.

In addition, the results in the sand with the relative density of 80% were also different to the sand with lower relative densities. The lines for these indexes became more farther away between each other, because the absolute necessary cycles increased greatly with relative density increasing. The difference of these lines became non-negligible in both first and second cyclic tests while the lines for DA= 5%, u/σ_{c0}' = 1.0 also were closer than the others. Besides, the lines for DA = 2% and u/σ_{c0}' = 0.95 separated as well in second cyclic tests. Meanwhile, the necessary cycles for causing DA= 2% became less than the cycles for causing u/σ_{c0}' = 0.95 which is also different to the results in first cyclic tests.

The failure criteria for soil liquefaction adopts the sates when DA = 5% that widely is used by previous researchers as mentioned above. This point could be confirmed because the line of DA = 5% is closed to u/σ_{c0}' = 0.95 mostly based on these results achieved in this study. Moreover, the u/σ_{c0}' = 0.95 used for detecting the correlation with DA = 5%, that could be understand by considering the measurement error in experiments. As the example, the equipment adopted in study can obtained the excess pore water pressure accurately. But the confining pressure was produced by the deference from cell pressure and backpressure, meanwhile the adjustments of the two pressures were also influenced by handle operation. Therefore, DA = 5% as the criteria adopted in the cyclic tri-axial tests is reasonable for non-pre-sheared sample which is as the same as the first cyclic tests in this study.

However, the performances were much different for the pre-sheared (causing liquefaction once) samples. The necessary cycles for causing DA = 2% and u/σ_{c0}' = 0.95, even for causing u/σ_{c0}' = 1.0 became much less than the cycles for causing DA = 5% because the great deformation and excess pore water pressure produced in first few load cycles. Therefore, the criteria for these samples need a further discussion in the future study.

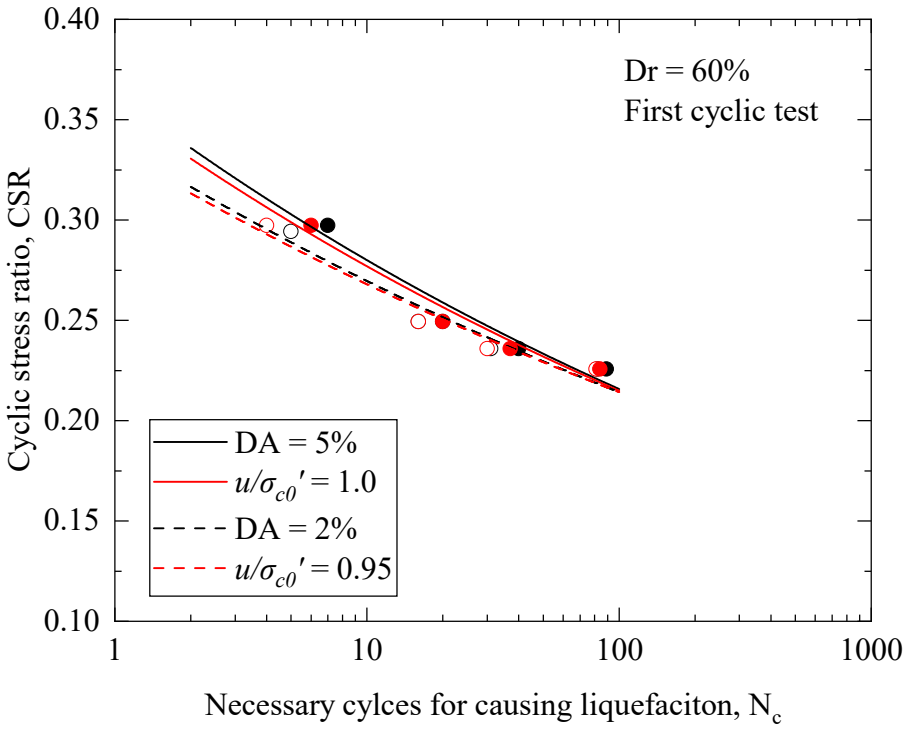

(a) First cyclic tests

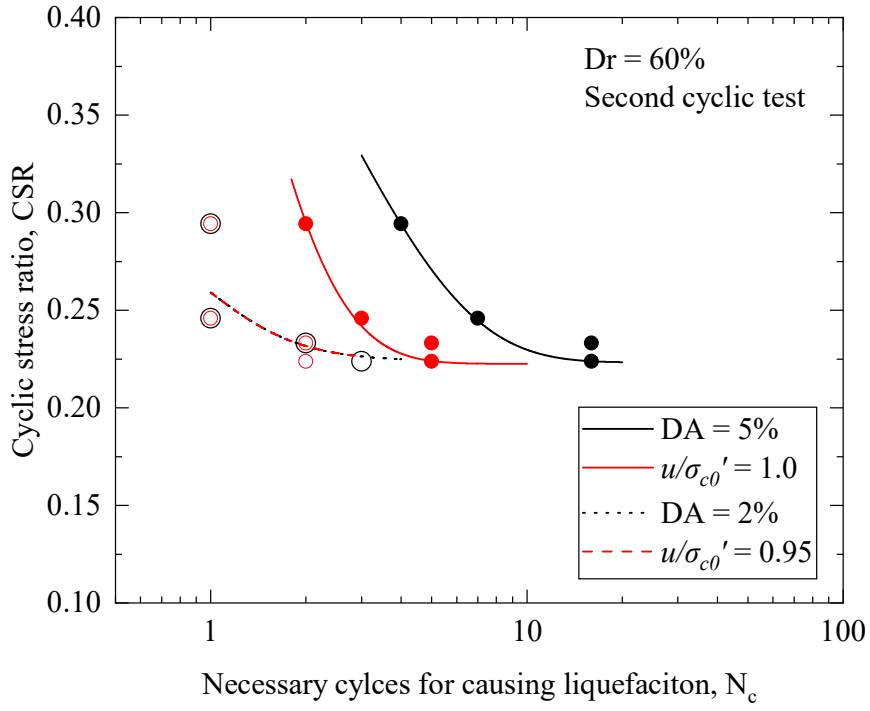

(b) Second cyclic tests

Figure 4.20 Liquefaction behaviours of Toyoura sand with *Dr* = 60% at *DA* = 2%, 5% and u/σ_{c0}' = 0.95, 1.0.

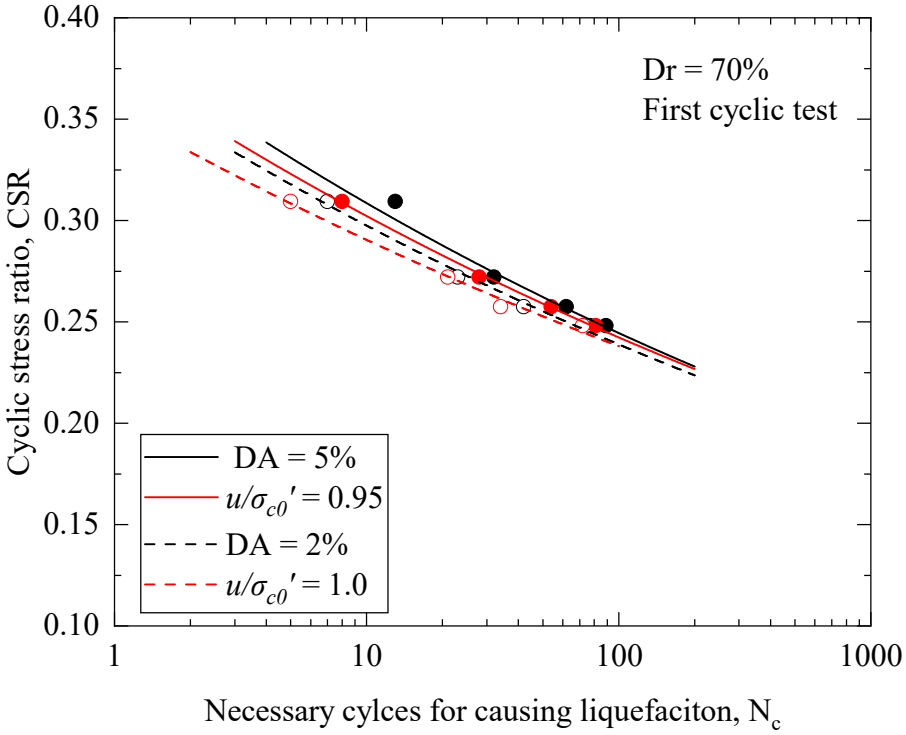

(a) First cyclic tests

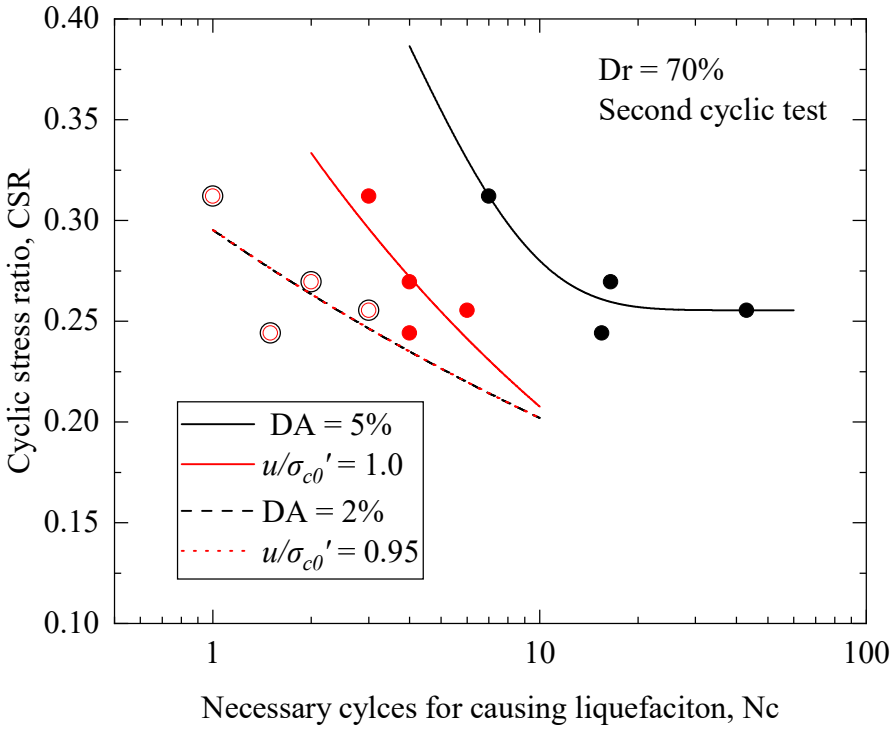

(c) Second cyclic tests

Figure 4.21 Liquefaction behaviours of Toyoura sand with *Dr* = 70% at *DA* = 2%, 5% and u/σ_{c0}' = 0.95, 1.0.

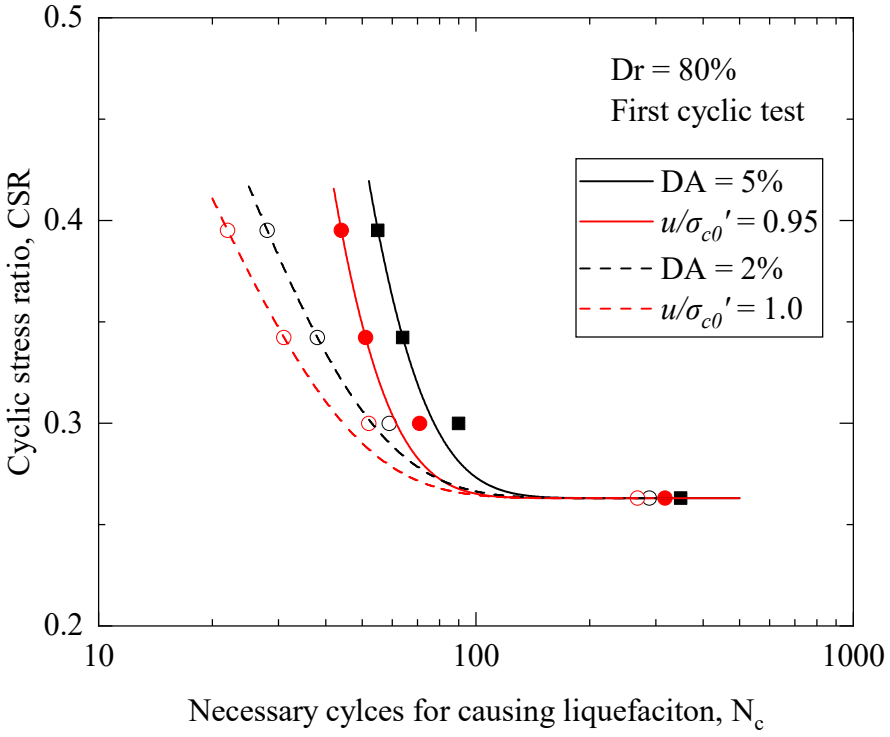

(a) First cyclic tests

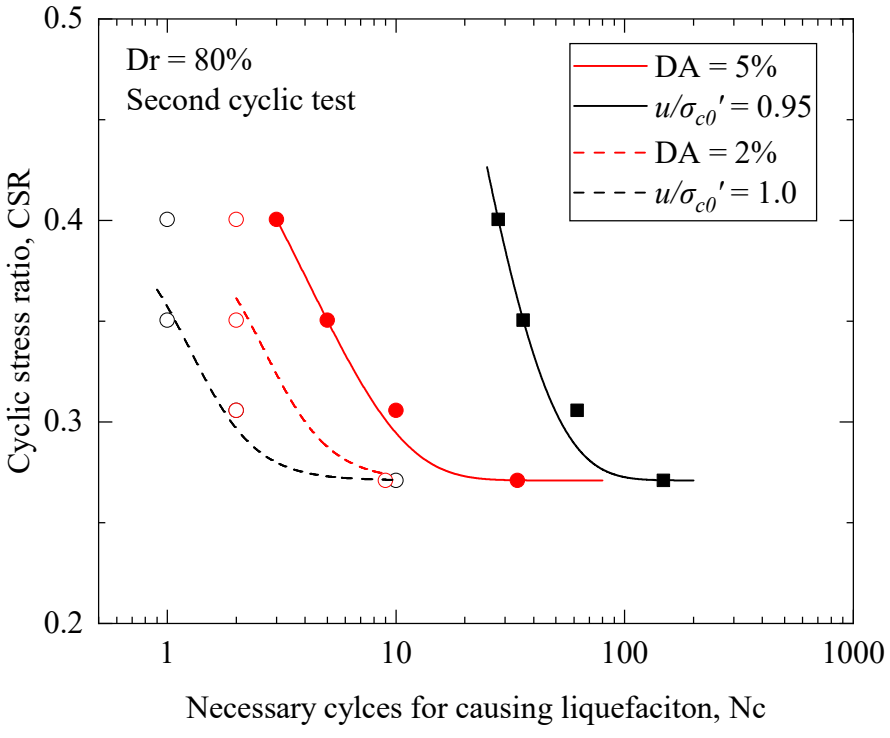

(b) Second cyclic tests

Figure 4.22 Liquefaction behaviours of Toyoura sand with *Dr* = 80% at *DA* = 2%, 5% and u/σ_{c0}' = 0.95, 1.0.

In this study, DA = 5% also was adopted to evaluate the failure state for pre-sheared sample, that consideration was based on the two points. 1) The disasters caused from soil liquefaction was commonly concerned from the ground deformation not directly from the excess pore water pressure ratio; 2) Because the state when DA = 5% could correctly represent the failure state for the sand without pre-shearing, the usage with the same criterion of DA = 5% could make the comparison of the changes od liquefaction behaviours become easier and more convenient.

Based on these considerations, the comparison of the liquefaction behaviours of the sand with initial relative density from 60% ~ 80% was conducted by the results arranged in Figure 4.23.

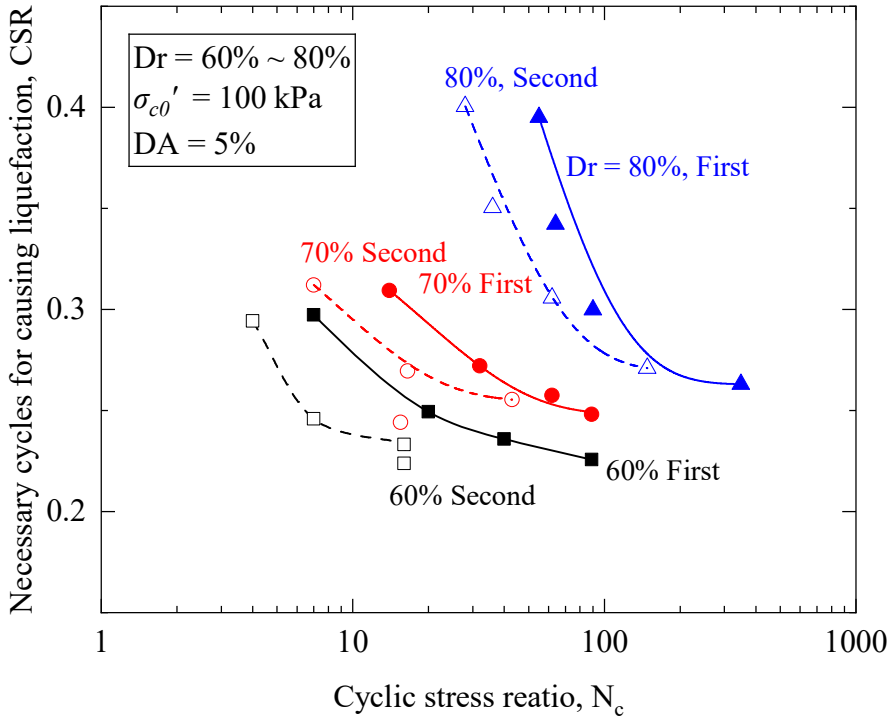

Figure 4.23 Comparison of liquefaction resistances between first and second cyclic tests for Toyoura sand with the relative density: 60% ~ 80%.

The solid lines and dash lines represent the correlation between cyclic stress ratio and necessary load cycles when DA = 5%. At first, the results clearly showed that the

liquefaction resistance was affected by the relative density when the sand had not any pre-shearing. The denser sand owned the greater liquefaction resistance no matter at any cyclic stress ratio. On the other hand, the liquefaction resistance decreased significantly when sand suffered the pre-shearing which produced liquefaction once as in the second cyclic tests. Moreover, it is worth to noting that the relative densities marked in Figure 4.23 were depended on the initial relative densities which were achieved after the first consolidation. These relative densities should be changed by the deformation caused from the dischargement for excess pore water and re-consolidation. After these processes, the relative densities would increase some degrees. These results of this part were arranged and drew in Figure 4.24 for comparing with the initial relative densities. The results directly indicated the change of relative density between the two stages. It could be confirmed that the relative density increased in all cases after liquefied-reconsolidated process. These increments were very depending on the initial relative density. The smaller increment appeared in the denser sands. As the result, increments could be observed that is approximate 6% ~ 8%, 4.4% ~ 5.7%, 4.0% ~ 5.3% for the initial relative density of 60%, 70%, 80% respectively.

According to the discussion in this section, the liquefaction resistance was reduced greatly after pre-shearing (liquefaction once) for saturated Toyoura sand, although the relative density would increase by the discharging of excess pore water. This behaviour needs to pay an enough caution because the denser sand is normally perceived to own a greater liquefaction resistance.

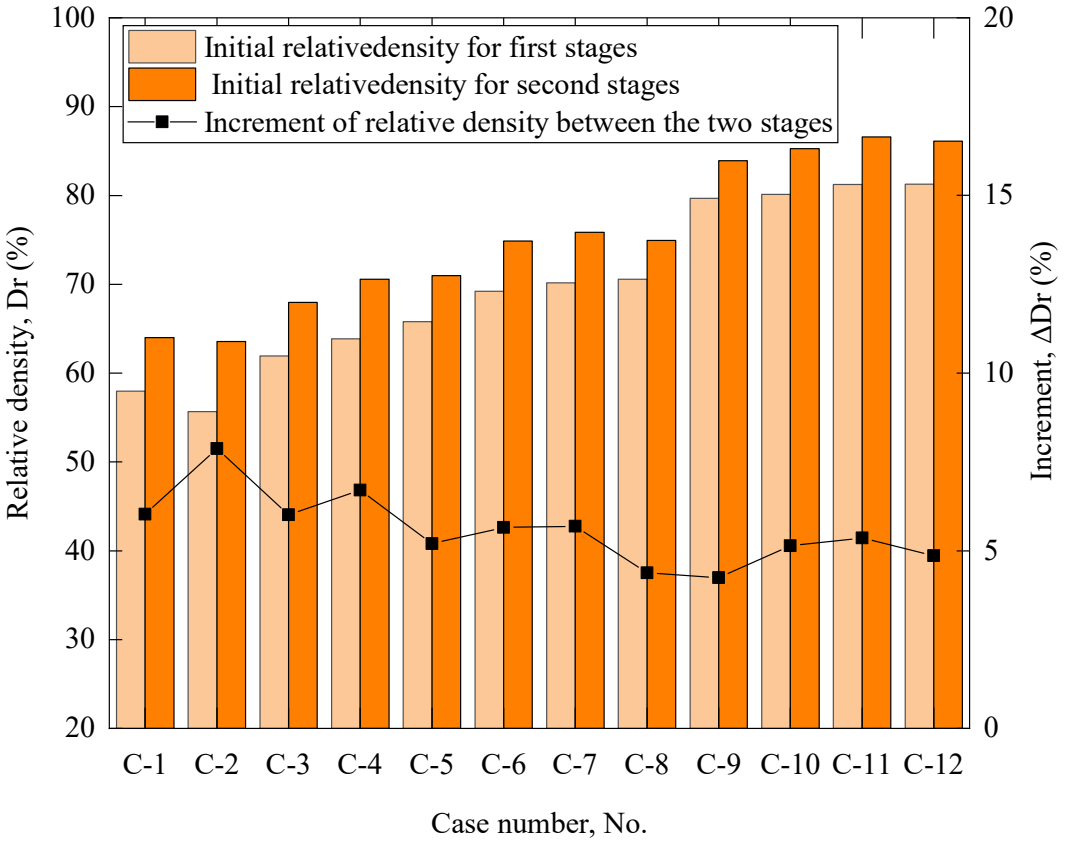

Figure 4.24 Comparison of initial relative density between first and second cyclic tests

4.3 Comparison of liquefaction behaviours between saturated and unsaturated Toyoura sand

The unsaturated samples were prepared as well for making the comparison with the saturated sample which is attempted to generalize the results obtained from saturated samples. However, the saturation degree was unable to control due to limitation of the experiment equipment used in study.

The method of air-pluviation was adopted for the sample's preparation. The saturation degree (B-value) of samples only could be measured when the samples had already been prepared. Thus, the results of saturation degree were obtained by accident in this section that lead the result became very unsteady. Therefore, there were only 4 cases which were tested both with the first and second cyclic tests. And all samples were prepared for the target relative density of 80%. The detail conditions were also arranged

by Table 4.4. The maximum B-value was obtained with around 0.92, meanwhile the minimum B-value was obtained with around 0.65. The B-value in the other 2 cases was distributed at around 0.8. These cases could provide a possibility to detect the influence from different saturation degrees.

The air was relative more than it in saturated samples, at the same time, the volume of air is able to be compressed by back pressure inside of specimen, therefore, the influence from the volume changed of air should not be neglected including the process of consolidation and re-consolidation. So as to influence the calculation for relative density and cyclic stress ratio. Besides, it also affected the recorded excess pore water pressure during the cyclic tests both in first and second stages, that lead the effective stress cannot be achieved correctly.

Due to these reasons, the indexes except B-value which is listed in Table 4.4 only represented nominally. Since the exact value could be obtained by using the equipment in this study, the discussion was only done briefly here. However, the axial strain produced by the cyclic loading could be measured accurately during cyclic test processes. That made a possibility to compare the failure resistance between saturated samples and unsaturated samples by the criterion of $DA = 5\%$.

According to the results shown in Figure 4.25, the behaviours of unsaturated samples were very different to the saturated samples. It could not find a suitable line to describe the entire variation tendency for these samples with a similar relative density while B-value was different. It also could find that the liquefaction resistance in second cyclic tests was different with the results for saturated samples. It became smaller in two samples as same as it in saturated sand. However, there were two cases that the liquefaction resistance became larger than it in first cyclic tests. Moreover, this kind of behaviour maybe depend on the level of applied cyclic loading. The liquefaction resistance became greater when the cyclic stress ratio at a lower level; on the other hand, it became smaller when cyclic stress at a higher level based on the results here.

Table 4.4 Nominal test conditions modified by the changes of specimens' dimensions in consolidations

Case No.	B-Value	Relative density after consolidation D_{r01} (%)	Cyclic stress ratio CSR_{01}	Relative density after re-consolidation D_{r02} (%)	Cyclic stress ratio CSR_{02}
C-1	0.65	82.08	0.270	85.85	0.273
C-2	0.836	78.45	0.279	84.33	0.278
C-3	0.816	78.76	0.301	83.91	0.306
C-4	0.921	77.22	0.328	83.23	0.329

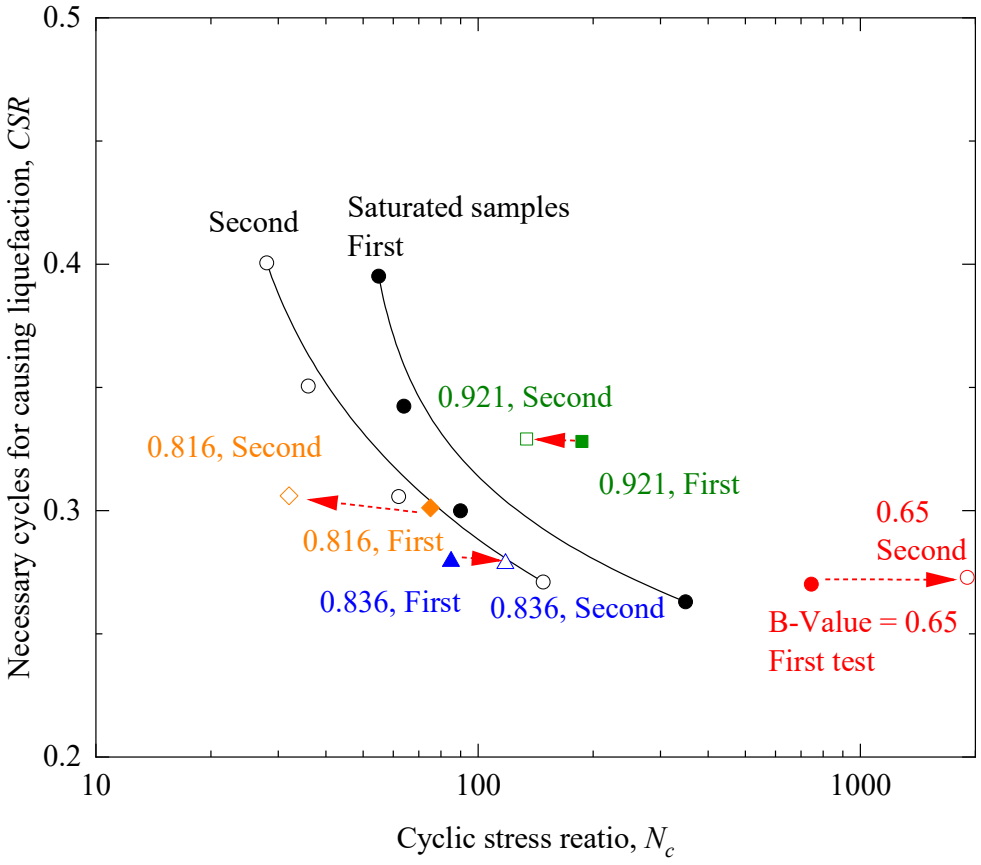

Figure 4.25 Liquefaction behaviours of unsaturated Toyoura sand comparing with saturated samples

Besides, it is noteworthy that two samples with B-value of 0.816 and 0.836 less than the 0.921 in one sample, however the liquefaction resistance was much smaller than the sand with B-value of 0.921. The seemingly contradictory phenomenon also perhaps was due to the limitation of experiment equipment and the manual operation. It most likely produced by the error of the calculation for cyclic stress ratio. That is not only because the exact deformation of specimen cannot be obtained, but also because it affected significantly by the manual operation when confining pressure was being applied. Though the confining pressure was exactly applied during the consolidation progress, the beginning of applying progress was separated to two steps: 1) applied the cell pressure to the target level; 2) adjusted the vertical axial force to the corresponded level. This operation order could result in that the contraction in surrounding would greater than in

vertical direction. In addition, the defamation of specimen was only calculated from the discharged volume of excess pore water that lead to that the calculated difference of volume was much less than the exactly contracted volume. On the other hand, the axial displacement was measured accurately. Thus, the cross area which was used in cyclic stress ratio calculation became greater than the exact area, which leaded to the nominal cyclic stress ratio by calculated results became less than the real level. As the result, the necessary cycles were reduced significantly as the result shown in Figure 4.25.

The existence of air produced the many uncontrolled conditions and irregular behaviours for unsaturated Toyoura sand. The improvement of the experiment equipment and the operation way needs to take into concern in the future study.

4.4 Summarises

Toyoura sand as the material was tested by cyclic tri-axial tests in this chapter. The cyclic tests were set to two steps, that the first cyclic test was to detect the liquefaction behaviours for non-pre-sheared sand, meanwhile this process is to be considered as the pre-shearing for the samples in second cyclic tests. The second cyclic tests were focused on the liquefaction behaviours for pre-sheared sand (liquefied once) and the comparison of these behaviours between the two stages.

The saturated samples were discussed firstly. The liquefaction resistance reduced greatly if the sand was liquefied once and re-consolidated, though the relative density increased after this progress. One of the typical explanations by previous researches is that the direction of cyclic loading especially in the final half cycle, was considered as the major factor to cause the anisotropy after pre-shearing which leaded to the great reduction in second cyclic tests. In this study, the results indicated the closer correlation to the residual positions instead of the load direction after pre-shearing. Of cause the residual position was identical with the direction of final half cycle, however, for the looser sand the residual position retracted to initial position regardless the direction in final cycle. Therefore, the residual position was detected as the prime factor on influencing the

behaviours in second cyclic tests.

Furthermore, the results showed that the failure criterion of DA = 5% need more discussion for second cyclic tests duo to the lines of DA= 5% and u/σ_{c0}' = 1.0% were obviously away between each other.

Finally, the liquefaction behaviours of unsaturated samples were discussed as well. The outcomes showed an irregular result compared with saturated samples. The uncontrollability of residual air could be considered as the prime reason in this study.

References

Bin Ye, Hailong Hu, Xiaohua Bao, Ping Lu. Reliquefaction behavior of sand and its mesoscopic mechanism. Soil Dynamics and Earthquake Engineering 114 (2018) 12–21.

Bin Ye, Jiafeng Lu, Guanlin Ye, 2015. Pre-shear effect on liquefaction resistance of a Fujian sand. Soil Dynamics and Earthquake Engineering, Vol. 77, pp 15-23.

K。 Ishihara, and S. Okada, 1982. Effects of large preshearing on cyclic behavior of sand. Soils and Foundations, Vol. 22, No. 3, pp 109-125.

M. Oda, K. Kawamoto, K. Suzuki, H. Fujimori; and M. Sato, 2001. Microstructural interpretation on reliquefaction of saturated granular soils under cyclic loading. Journal of Geotechnical and Geoenvironmental Engineering, 127(5), pp 416-423.

CHAPTER 5

LIQUEFACTION AND RE-LIQUEFACTION BEHAVIOURS OF KUROBOKU AND BOILED SAND

5.1 Introduction

Based on the liquefaction disasters occurred in the 2016 Kumamoto earthquakes, two typical soils were collected from the affected area (Kumamoto-Aso area) for detecting the liquefaction behaviours. The boiled sand was obtained directly from the liquefied sites where the boiled sand was erupted and deposited above the ground. The boiled sand used in this study was collected from Chikami 1 Chomei, Minami-ku of Kumamoto City where the foundation of residential houses was damaged seriously by soil liquefaction in the earthquakes. Photo 5.1 express the deposition of boiled sand after the earthquakes. The boiled sand expressed the colour with black and charcoal grey mainly, as shown in Photo 5.1 and Photo 2.2 in Chapter 2.

Photo 5.1 The deposition of boiled sand nearby the entrance of residential house (T. Nakano et al. 2017.3)

The volcanic ash was considered as the main component in boiled sand, which was produced from Aso volcano in the region. The ash deposited in Kumamoto-Aso area and formed the unique soil-Kuroboku that widely distributed in the plain and valley area. Therefore, it was worth to detect the physical properties and the behaviour of

liquefaction for this type of volcanic soil (Kuroboku named in following). The Kuroboku used in this study was carried from site nearby the deep landslide in Aso-Bashi Area, as showed in Photo 5.2. It was very closed to the location where Y. Kawaguchi (2018.3) collected in Chapter 2. However, the basic physical properties of Kuroboku may be different even the location was closed, as the Sample A and B tested by Y. Kawaguchi in Chapter 2. Therefore, the sampled Kuroboku was tested by once time for the physical properties in this study.

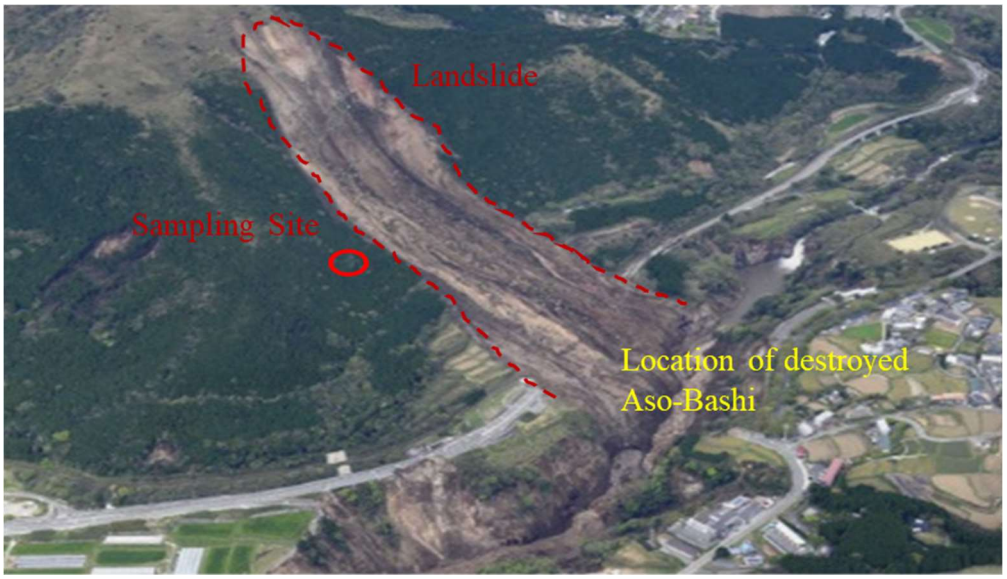

Photo 5.2 Sampling site of Kuroboku nearby landslide in Aso-Bashi Area

This Chapter is consisted with three major parts:

1) Liquefaction and re-liquefaction behaviours of boiled sand.
2) Liquefaction and re-liquefaction behaviours of Kuroboku. Due to very little fines was found in boiled sand, the fines in Kuroboku were sieved out to tested as well. Thus, the effects from fines became to be discussed.
3) The basic physical properties were tested for boiled sand and Koroboku with fines and without fines.
4) Brief comparison the liquefaction behaviours between the two typical soils and Toyoura sand.

5.2 Basic physical properties of Kuroboku and boiled sand

The basic physical properties were investigated firstly, that the specific gravity G_s, the analysis of grain size, the liquid-plastic limit, and the maximum and minimum void ratio e_{max}, e_{min} were investigated in this section. The Kuroboku with fines was be excluded from maximum and minimum tests due to the great influence from the fines in a great quantity.

5.2.1 Specific gravity

The specific gravity was tested according to the criterion of JGS 0111 (or JIS A 1202). Photo 5.3 (a) to (d) shows the important steps in the test process, that could understand the basic principle of this experiment by using boiled sand.

The volume of pycnometer with stopper was determined by manufacturer for each sample. Photo 5.3 (a) exhibits the measurement of the weight of pycnometer was filling with distilled water (de-aerated). Them, the boiled sand was carried into the pycnometer and filled by water at approximately 2/3 in height. Moved the pycnometers to a pan; heat the pycnometers under water environment to carry out the air in boiled sand, as indicated in Photo 5.3 (b). When air was completely cleared, the pycnometers were filled by de-aerated water again. The weight also was measured again, as shown in Photo 5.3 (c). After that, the boiled sand was washed out by de-aerated water into the beaker, as Photo 5.3 (d), and oven-dried theses samples within one day. The dried weight of samples was measured finally.

The influence of temperature was concerned in this experiment. The gravity G_s was obtained by Equation 5.1 and 5.2.

$$m_a = \frac{\rho_w(T)}{\rho_w(T')} \times (m'_a - m_f) - m_f \tag{5.1}$$

$$G_s = \frac{m_s}{m_s + (m_a - m_b)} \times \rho_w(T) \tag{5.2}$$

Where, m_f is the weight of pycnometer; m_a and $\rho_w(T)$ are the weight and the corresponded water density measured in Photo 5.3 (c); m'_a and $\rho_w(T')$ are the weight and the corresponded water density measured in Photo 5.3 (a); m_s is the weight of oven-dried boiled sand.

(a) Filled water

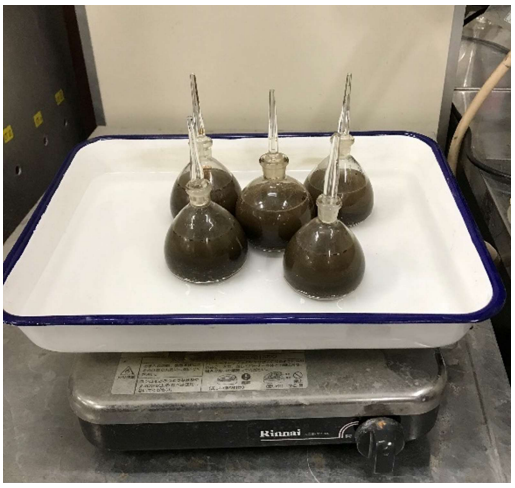

(b) Deaerating

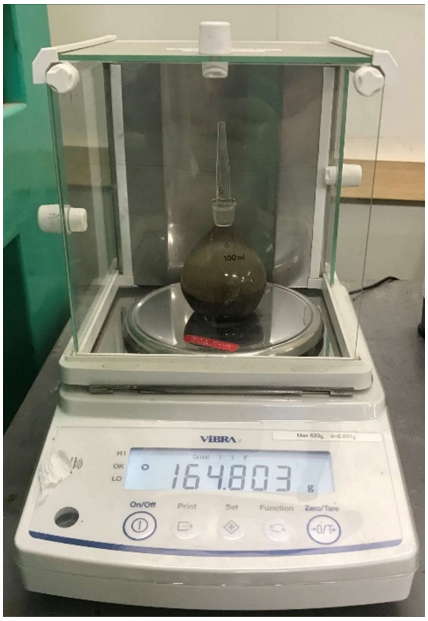

(c) Filled water with soil

(d) Washing out soil

Photo 5.3 Key steps for specific gravity experiment (Boiled sand)

5.2.2 Distribution of grain size

Due to a mass of fines included in Kuroboku, meanwhile, the measure error may be increased during the sieving and washing, because the fines most likely absorbed on the greater particles specially for the grain size closed to 0.075 mm. There two method of the investigation were performed in this study to attempt to find the exact distribution of grain size.

The first method was using sieve analysis and settling analysis, which were proposed by JGS 0131 (JIS A 1204). The second method was the equipment developed by Shimadzu Company (Laser diffraction particle size analyser SALD-3100), that could direct read the accumulated grain size. Photo 5.4 and Photo 5.5 displays a full view of this equipment and the feeding open. The soil sample needs to be dilute by distilled water and put it into the feeding open.

This equipment utilized the characteristics of refraction and scattering from the laser which is irradiating at the soil particles. The light intensity would be caught by this equipment and recorded by PC. The maximum grain size less than 2 mm is suitable for the analysis by using this equipment.

Photo 5.4 Full view of Laser diffraction particle size analyser (SALD-3100)

Photo 5.5 Feeding open of Laser diffraction particle size analyser (SALD-3100)

Two Kuroboku samples and the boiled sand were tested by the two methods. The results and comparison were showed in Figure 5.1. In General speaking, the results tested by sieve analysis and settling analysis were found that the grain size was a little smaller in each percentage of accumulated weight. In this study, the test by laser analysis was unified and adopted as the major method for results discussion, that could make the comparison become easier. There were also two samples collected nearby each other, while the grain size distribution also very similar.

On the hand, concerning on categories of soil particles, the results showed that:

1) For the boundary between sand and silt (D =0.075 mm): there was only approximately 10% of fines discovered in boiled sand; and approximately 65% for Kuroboku A and 45% for Kuroboku B.
2) For the boundary between clay and silt (D =0.005 mm): the component of clay was discovered with a very littler in three samples. Moreover, there were

only 2.86% and 2.74% were found in Kuroboku A and B respectively; and 0.7% was found in boiled sand.

According to the findings, the particles belonging to sand and silt were consisted the two typical soils in Kumamoto-Aso area. The soiled soil could be looked as sandy soil principally and involved with some silt particles. Kuroboku has the component between silt and sand with around half-to-half in weight. The fines were operated to sieved out from Kuroboku B in this study, the component of fines reduced to 25%, meanwhile, the component of clay also reduced greatly to approximately 1.0%. This component became very closed to boiled sand.

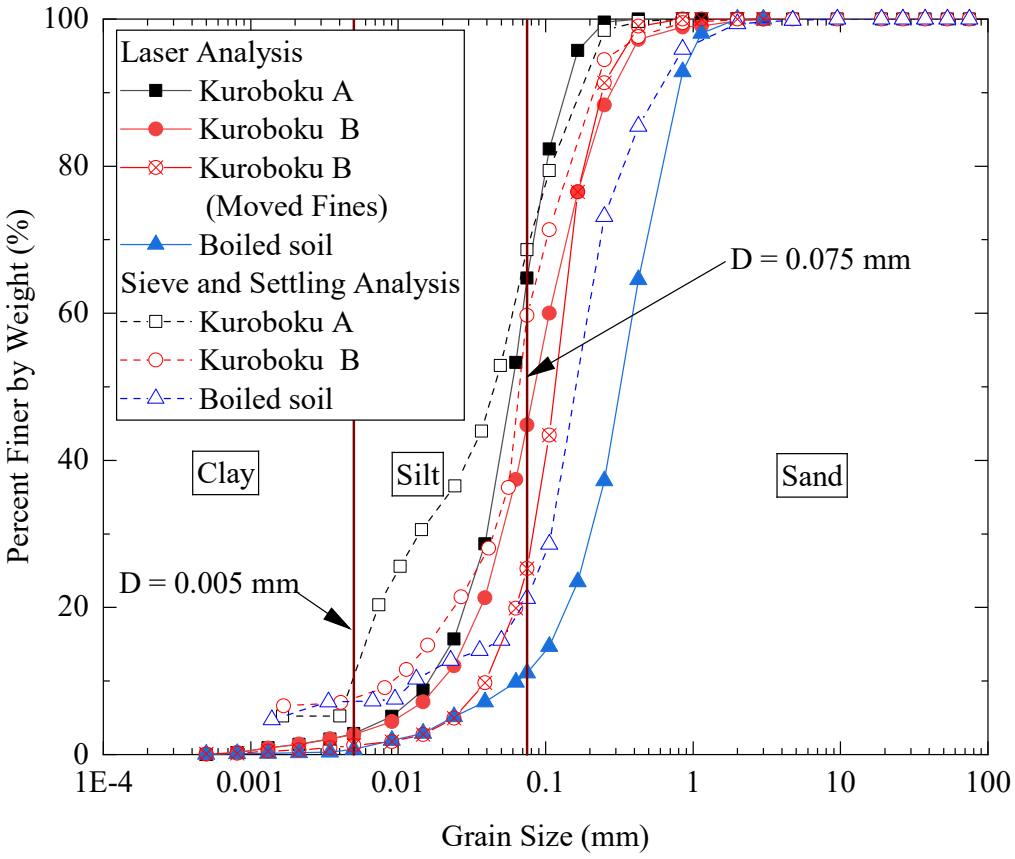

Figure 5.1 Cumulative grain size distribution of Kuroboku and boiled sand

5.2.3 Liquid limit and plastic limit of Kuroboku and boiled sand

The liquid limit LL and plastic limit PL of Kuroboku A and B were used the results tested by R. Yamamoto depended on the in-situ investigation for the landslide in Aso-Bashi Area (N. Yasufuku, et al. 2018.7.). The Kuroboku B moved out fines and boiled sand was investigated according to the criterion of JGS 0141 (JIS A 1205). Photo 5.5 shows the photograph during the tests process.

(a) Sample's preparation for Liquid Limit test

(b) Sample's preparation for Plastic Limit test

Photo 5.6 Sample's preparation for the experiment of Liquid Limit and Plastic Limit.

5.2.4 Summaries of the basic physical properties of the two soils

Because there were very less fines in Kuroboku B moved out fines and boiled sand, the maximum and minimum void ratio, e_{max}, e_{min}, were survey by the way as same as sand, based on JGS 0161 (JIS A 1224).

End here, the basic physical properties including the specific gravity G_s, the analysis of grain size, the liquid-plastic limit, and the maximum and minimum void ratio e_{max}, e_{min} were completely to detected. Except the grain size distributions, which were arranged in Section 5.2.2, the other properties were summarised and arranged with Figure 5.2 and Table 5.1. According to the classification of JGS 0051-2009, the three types of soils included Kuroboku A and B, and Kuroboku B moved out fines was classified to MH, silt with a high liquid limit. Meanwhile, Kuroboku B moved out fines was very near to the boundary between ML and MH, low limit and high limit.

Table 5.1 Basic physical properties for the typical soils related to liquefaction disasters in the 2016 Kumamoto Earthquakes

Sample	Specific gravity, G_s	Max. void ratio, e_{max}	Min. void ratio, e_{min}	Liquid Limit, *LL* (%)	Plastic Limit, *PL* (%)	Plastic Index, *PI*
Kuroboku A	2.390	Non	Non	212.5	146.3	66.2
Kuroboku B	2.320	Non	Non	157.3	112.1	45.2
Kuroboku B moved out fines	2.320	2.351	1.594	59.3	57.2	2.0
Boiled sand	2.755	1.618	0.951	NP	NP	NP
Toyoura	2.643	0.977	0.606	NP	NP	NP

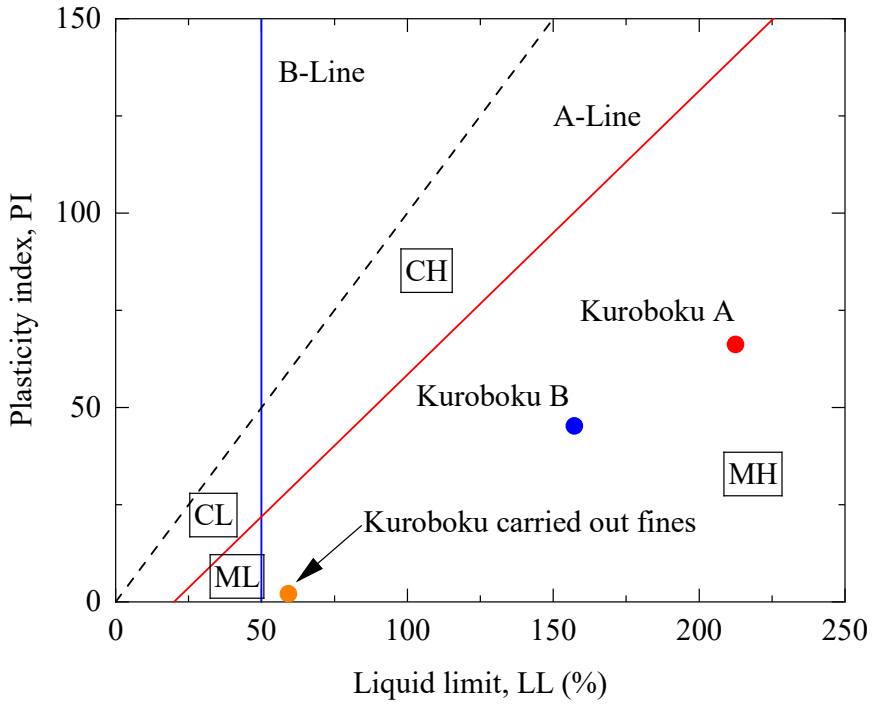

Figure 5. 2 Plasticity Chart of Kuroboku A and B, and Kuroboku B moved out fines.

5.3 Liquefaction behaviours of Kuroboku and boiled sand

The behaviours including liquefaction and re-liquefaction were investigated in section. The soil samples were prepared with saturated state. The Kuroboku B moved out fines and boiled sand was made based on the target relative densities, while, the Koroboku A was made according to the void ratio due to the fines abounding.

The preparation method for the specimens of Kuroboku B moved out fines and boiled sand was using water pluviation and CO_2 to make sure the samples were sufficiently saturated, that was as same as the method used for the saturated Toyoura sand.

The method for Kuroboku A was distinctive to others, because CO_2 was unable to pass through the specimen due to the very high suction produced by the fines. Therefore, the specimens were made by tamping, and the sample was separated to 5 equal mass with weight. The void was attempted to control by the

certain volume and the certain weight. However, the result of void ratio was very sensitive to the volume, though the change was very small. as a consequent, the void ratio became very difficult to control. Instead of using CO_2, the double negative pressure method, as introduced in Chapter 3, was adopted to saturate the specimens. Also because of the high suction, the water might not run freely inside of the specimen. The B-value measured here may represent the excess pore water pressure at the border region.

Thus, the saturation degree for Kuroboku A was the nominal result in this study. Depending on the understandings, three specimens with a similar void ratio were selected to discuss the test results under the three typical test conditions:

1) the axial strain with the amplitude in double directions DA = 5% was controlled between first and second cyclic tests, to detect the performances of excess pore water pressures.
2) The excess pore pressure was produced as much as possible. Let it become most closed to excess pore pressure ratio u/σ_{c0}' = 1.0 to detect the performance on deformation.
3) Applied a small pre-shearing to detect the change of the cyclic resistance. The similar shear strain produced between first and second cyclic test stages was controled.

The detailed test conditions were summarized and arranged by Table 5.2. In addition, the confining pressure was set by two level for Kuroboku B moved out fines: 50 kPa, 70 kPa in consolidation process. Although, in common, the confining pressure was considered has not the relation to cyclic resistance at the same cyclic stress ratio for sands. But there were the fines still had been contained approximately 25% inside of specimen, even if the operations were conducted for carrying out. These fines may perform different cohesions under different confining pressures in consolidation or reconsolidation.

Table 5.2 Exact test conditions modified by the changes of specimens' dimensions in consolidations

Case No.	Soil Types	B-Value	Relative density after consolidation D_{r01} (%)/ void ratio e_{01}	Cyclic stress ratio CSR_{01}	Relative density after re-consolidation D_{r02} (%)/void ratio e_{01}	Cyclic stress ratio CSR_{02}
C-1	Kuroboku A	0.977	1.43	0.246	1.16	0.250
C-2	Kuroboku A	1	1.32	0.294	Non	Non
C-3	Kuroboku A	1	1.28	0.288	1.14	0.297
C-4	Kuroboku B moved out fines	0.941	59.49%	0.312	70.93%	0.583
C-5	Kuroboku B moved out fines	0.964	61.38%	0.430	73.00%	0.394
C-6	Kuroboku B moved out fines	0.968	63.85%	0.403	74.04%	0.416
C-7	Kuroboku B moved out fines	0.976	64.01%	0.356	75.64%	0.504
C-8	Kuroboku B moved out fines	0.948	71.03%	0.403	81.12%	0.609
C-9	Kuroboku B moved out fines	0.942	85.25%	0.362	95.80%	0.579
C-10	Boiled sand	0.963	59.88%	0.251	70.81%	0.247
C-11	Boiled sand	0.911	62.21%	0.209	73.06%	0.198
C-12	Boiled sand	1	63.96%	0.151	74.69%	0.155
C-13	Boiled sand	0.945	65.45%	0.295	74.10%	0.297
C-14	Boiled sand	0.979	77.43%	0.302	84.48%	0.304
C-15	Boiled sand	0.982	77.86%	0.241	84.71%	0.176
C-16	Boiled sand	0.934	78.50%	0.255	85.03%	0.391
C-17	Boiled sand	0.952	80.47%	0.210	89.03%	0.205

5.3.1 Performances of Kuroboku in cyclic tests

From C-1 to C-3, there were three cases tested for the Kuroboku, which was unabridged for the grain size distribution. The content of fines was measured up to around 65% by weight. The it was classified as the silt with a very high liquid limit. The performances were arranged in Figure 5.3.

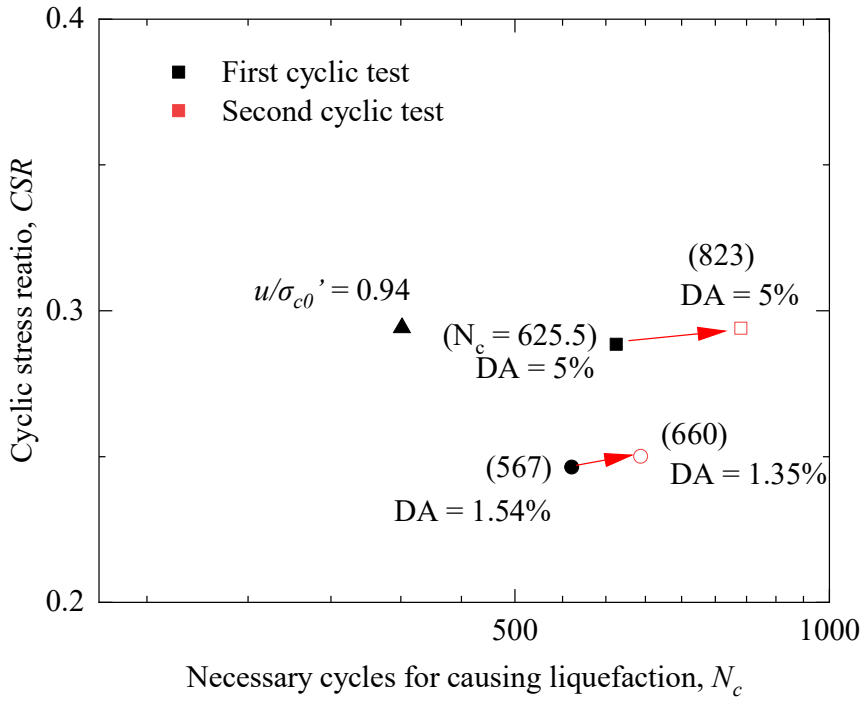

Figure 5.3 Cyclic resistance of Kuroboku by different loading conditions

In C-3, the specimen was applied the cyclic loading until the axial strain with amplitude in double directions reached DA = 5%, while the excess pore pressure u/σ_{c0}' = 0.842. Then, the sample was consolidated again with drainage. The void ratio increased some level from 1.28 to 1.14, which lead the cyclic stress ratio also increased in a small level. After that, the cyclic loading was applied again to cause the DA = 5% once time and stopped the test. It could be found that the necessary cycles increased significantly from 625.5 to 823 even if the cyclic stress ratio increased. The similar behaviour could be discovered in C-1. The cyclic resistance (at DA = 1.35) increased

as well when the sample was pre-sheared with DA = 1.54%. The results indicated the cyclic resistance would go up by the pre-shearing within $DA \leq 5\%$ because of the existence of fines.

If the sample was detected to find the maximum excess pore pressure in possibility, such as C-2 in this study, the very large deformation occurred. The axial strain with amplitude in double directions rose to 25.68%. Photo 5.7 shows the situation after first cyclic stage. The necking appeared at the middle of specimen in height. It can not recover when unloaded lead to an unavailability for second test stage.

Photo 5.7 The necking appeared when Kuroboku pre-sheared to DA = 25.68%

5.3.2 Liquefaction behaviours of Kuroboku removed fines

The initial considering was to move out all fines from Kuroboku, to obtain a similar grain size as it in boiled sand. However, it was found that was very difficult and impossible by sieving and washing. Therefore, the sample was tested with the decreased

fines, containing approximately 25%, in this study. The samples were divided to two groups. The first one including four cases, which were prepared with relative density around 60%, were supposed to investigate the general behaviour in liquefaction and re-liquefaction. The other two cases were used to find the effects from different relative densities. The cyclic test results were arranged by DA = 5%, as shown in Figure 5.4. And the typical stress path with cyclic loading and the relation between shear stress-strain, collected from the samples with initial relative density D_r = 60% and 70%, were presented from Figure 5.5 to Figure 5.8.

Regardless in first stages or second stages, the liquefaction resistance was affected by relative density greatly. Approximately 10% in relative density increased after first liquefaction stage and re-consolidation whether the samples were prepared with an initial relative density of around 60%, 70%, or 85%. As the same time, the liquefaction resistance also increased greatly with increasing of the relative density.

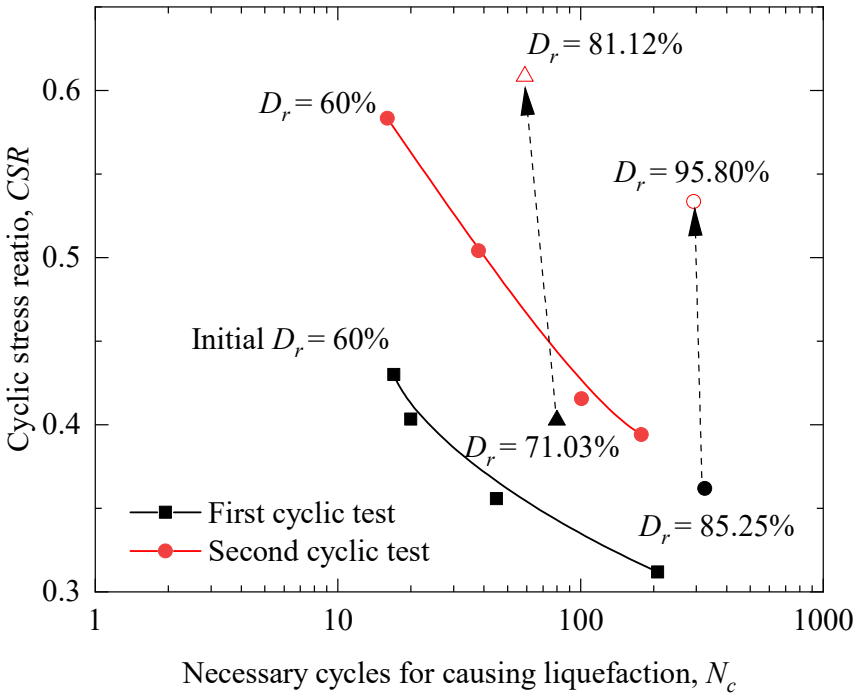

Figure 5.4 Liquefaction and re-liquefaction behaviours of Kuroboku moved out fines

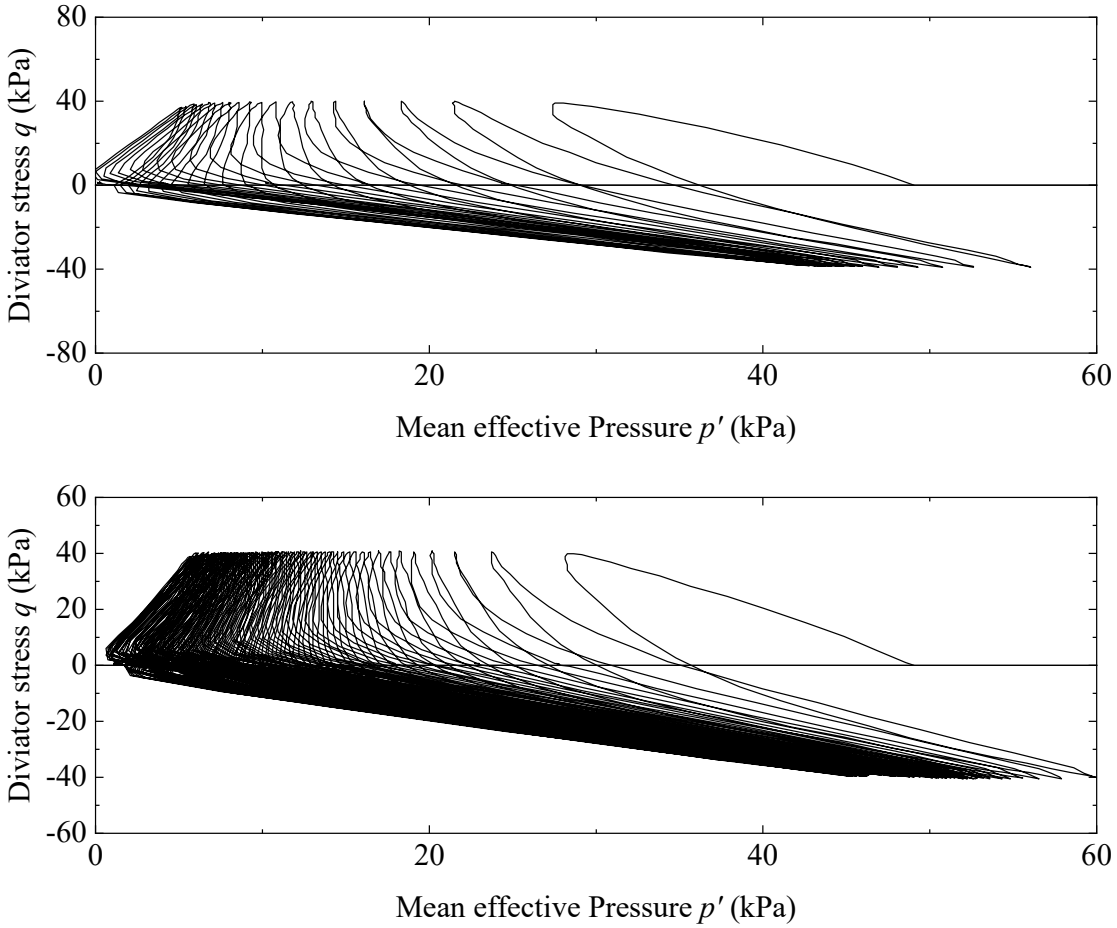

Figure 5.5 Stress path of first and second cyclic testes for Kuroboku moved out fines with initial relative density D_r = 60%

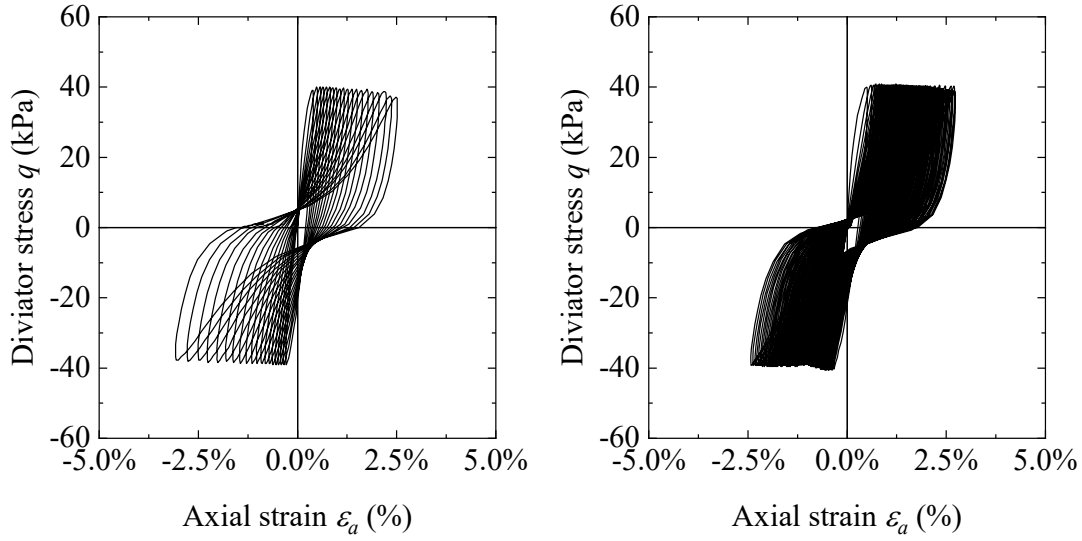

Figure 5.6 Shear stress-strain relation between first and second cyclic tests for Kuroboku moved out fines with initial relative density D_r = 60%

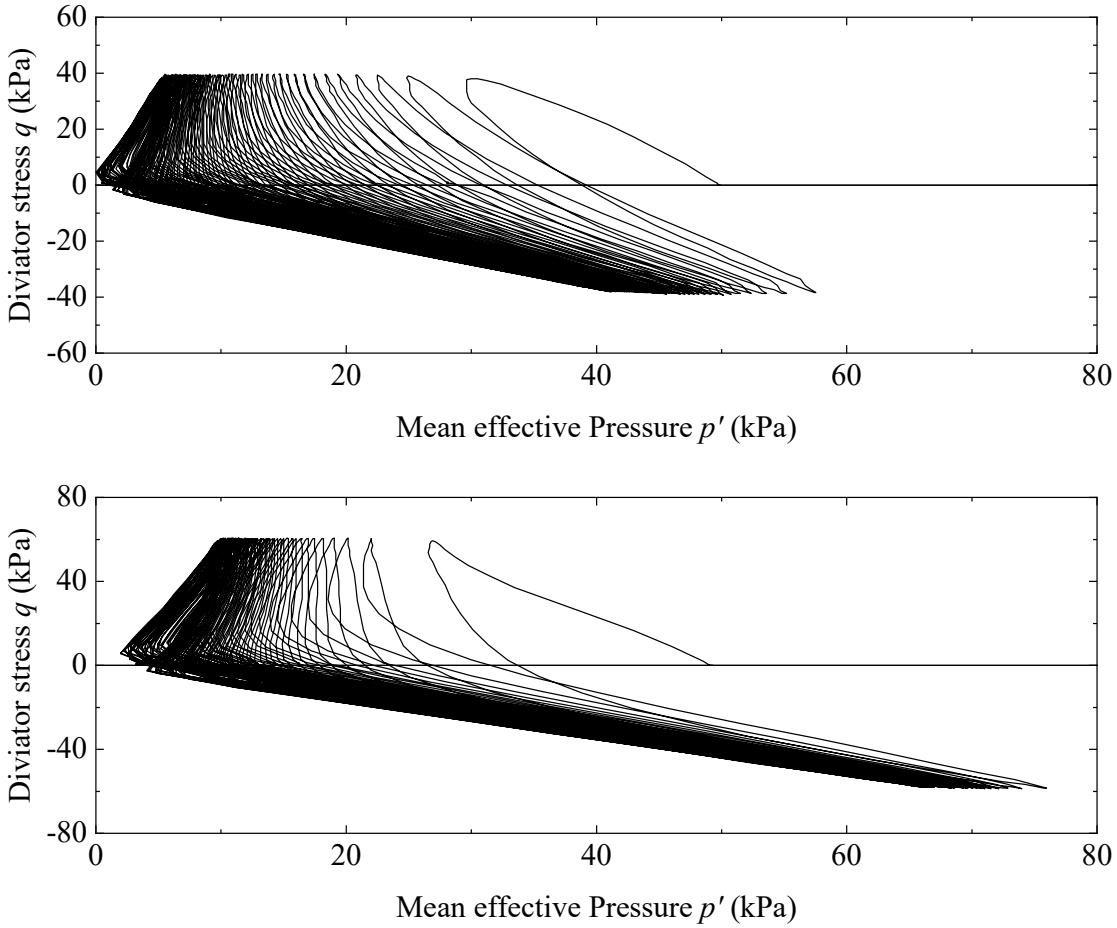

Figure 5.7 Stress path of first and second cyclic testes for Kuroboku moved out fines with initial relative density D_r = 70%

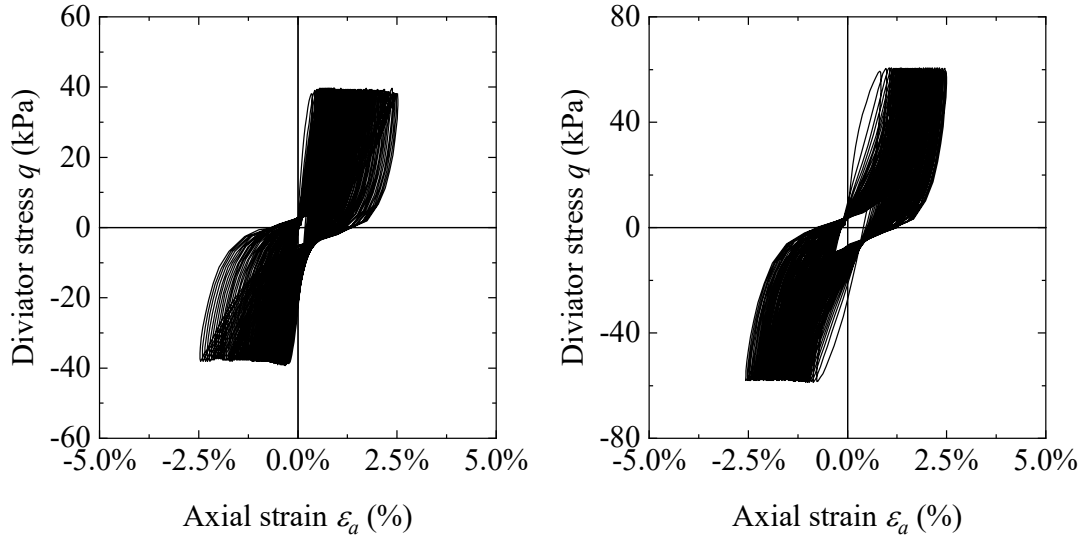

Figure 5.8 Shear stress-strain relation between first and second cyclic tests for Kuroboku moved out fines with initial relative density D_r = 70%

It also could be found that, the failure states of the sample with the initial relative density of 70% and 85%, were very closed to the failure line for the sample with initial relative density D_r = 60% in second cyclic test stage while the it increased to around 70%. These results appeared occasionally in this study or not, that needs more test results and more discussion in future.

Stress path in first several cycles between first and second test stages looked very similar. The reduction of mean effective stress started from the compression direction of first loading. The difference appeared from that mean effective stress reduced to approximately half from initial. The decreasing became difficult in second test stage and result in a higher liquefaction resistance than it in first stage. The behaviour could be discovered in the samples with the relative densities in this study. Moreover, whether in first or second stage, the mean effective stress internal specimen produced a greater level than the initial confining pressure, that did not appear in any case of Toyoura sand. Thus, this performance should be caused by the fines which still were contained in Kuroboku samples.

5.3.3 Liquefaction behaviours of boiled sand

Boiled sand was prepared to two relative densities of around 60% and 80%. By the similar method as for Kuroboku, the results were arranged in the Figures from 5.9 to 5.13.

Liquefaction resistance for first test stages did not affected basically by the relative density between 60% and 80%. The failure lines were very closed. This behaviour could also be extended to the performance in second test stages. The liquefaction resistance in second stages was raised, however, the difference was very small. The resistance could be looked without changes in general consideration. In addition, the liquefaction resistance in second stages decreased with decreasing of cyclic stress ratio. It would become less than it in first stages when the cyclic stress ratio decreased to lower than 2.0 for the sample with D_r = 60%.

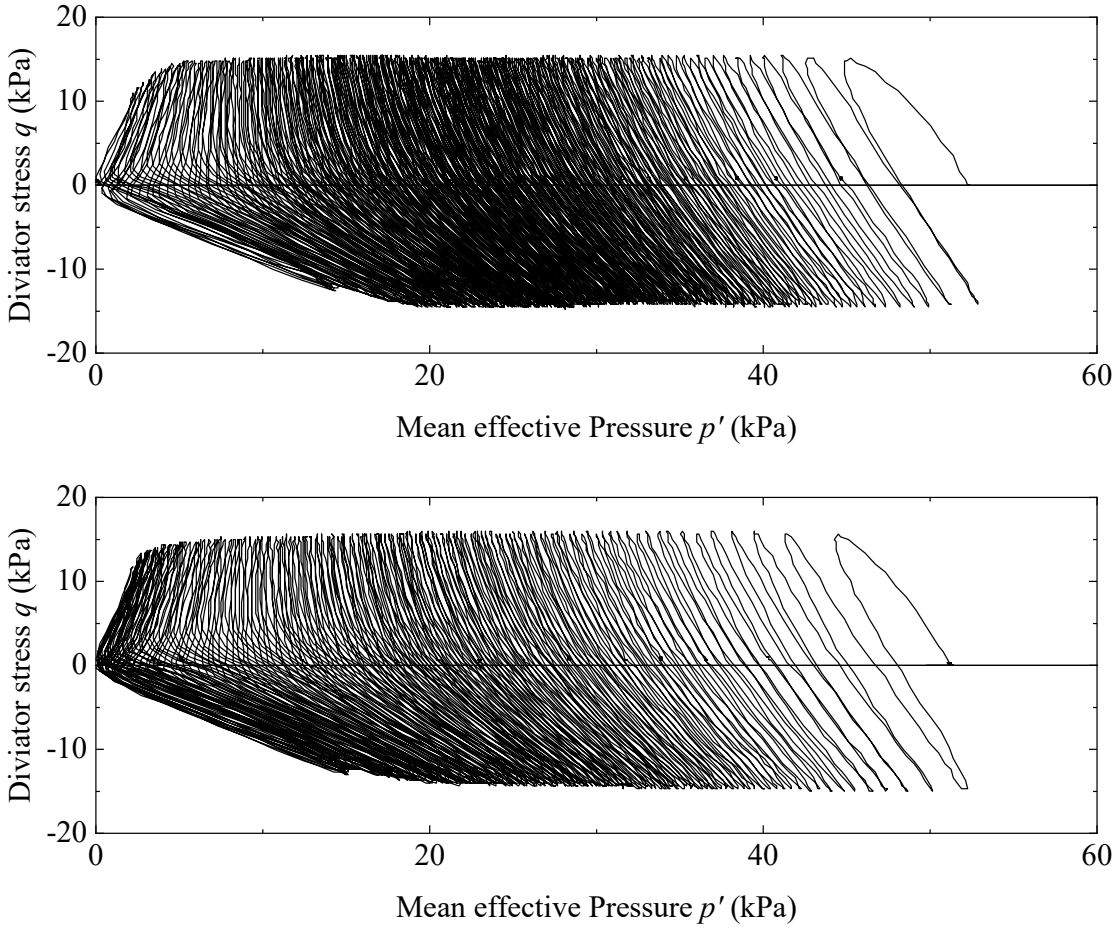

Figure 5.9 Stress path of first and second cyclic testes for boiled sand with initial relative density D_r = 60%

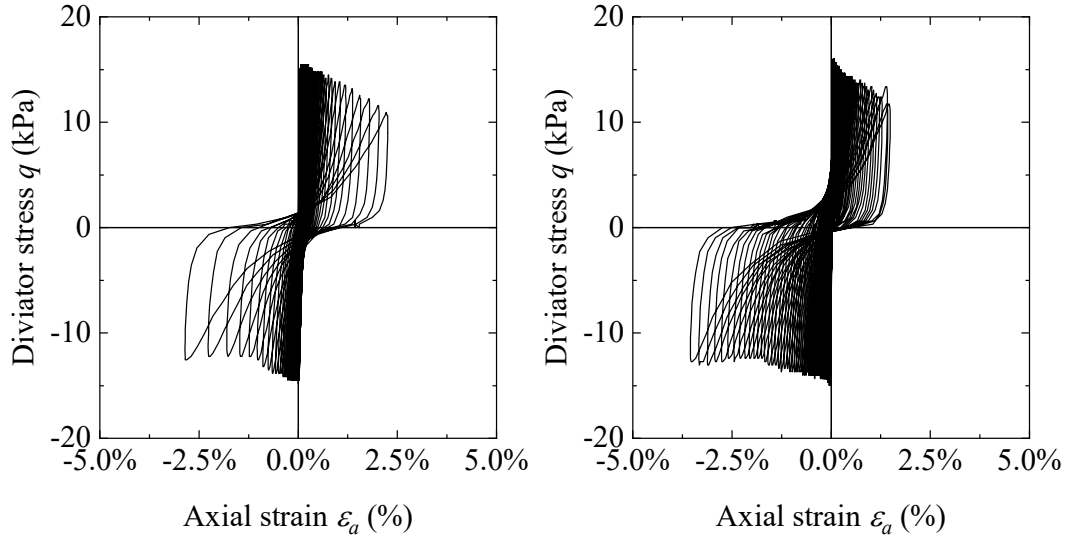

Figure 5.10 Shear stress-strain relation between first and second cyclic tests for boiled sand with initial relative density D_r = 60%

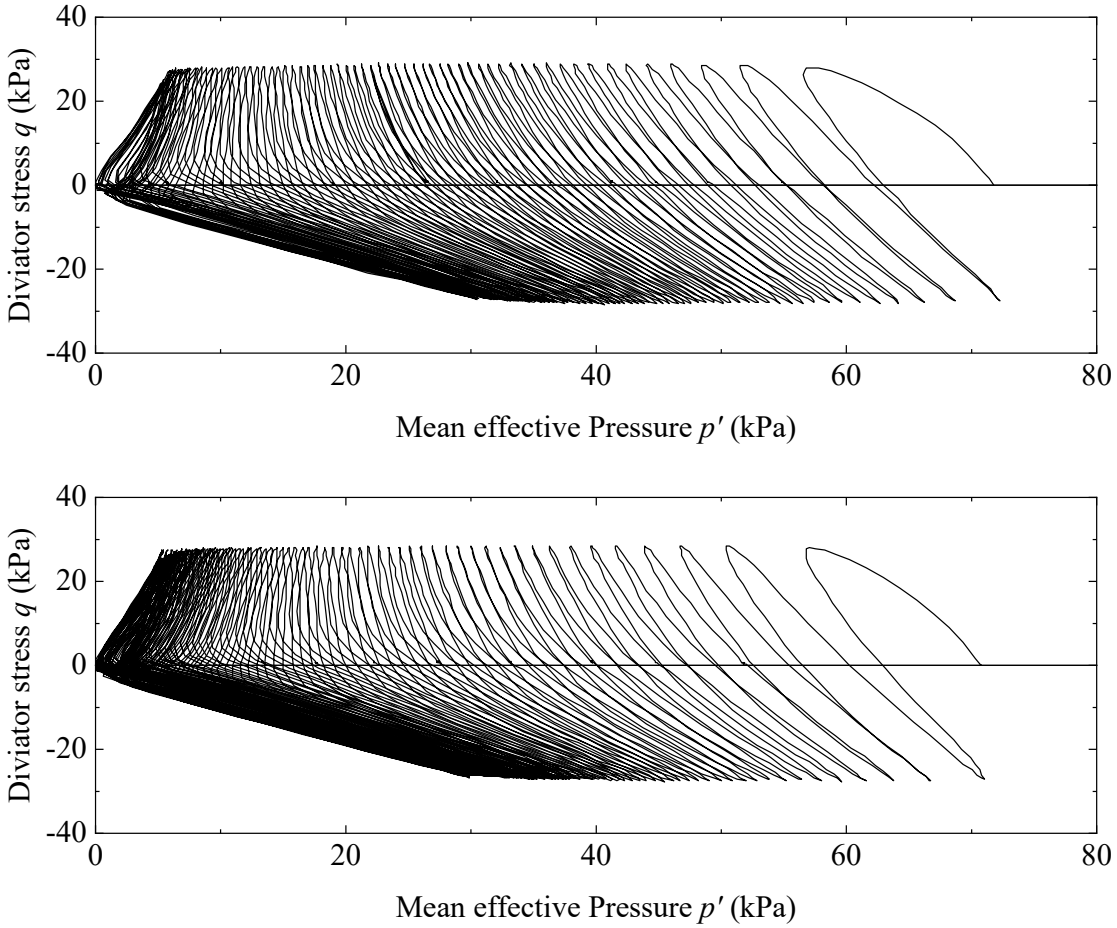

Figure 5.11 Stress path of first and second cyclic testes for boiled sand with initial relative density D_r = 80%

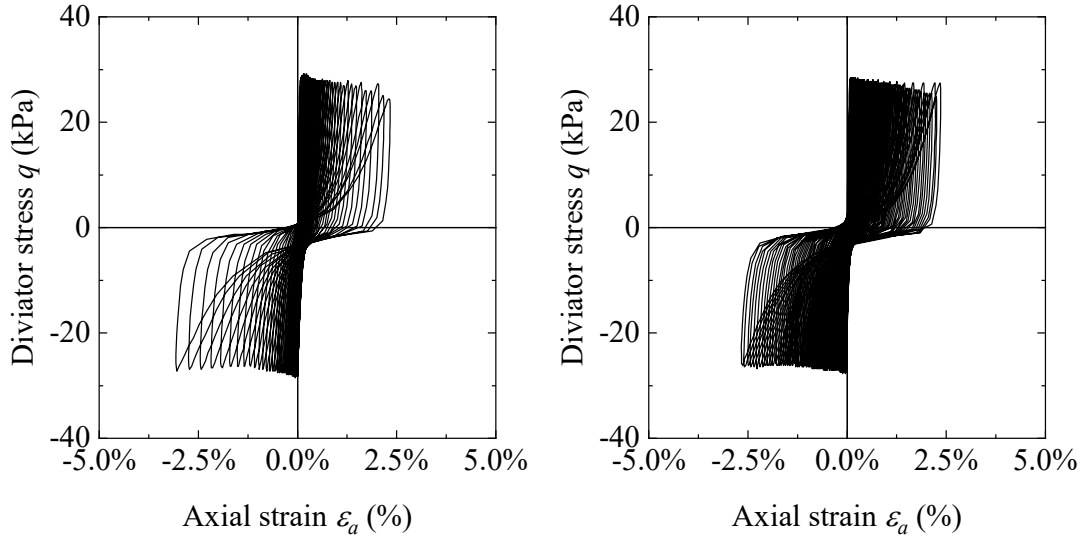

Figure 5.12 Shear stress-strain relation between first and second cyclic tests for boiled sand with initial relative density D_r = 80%

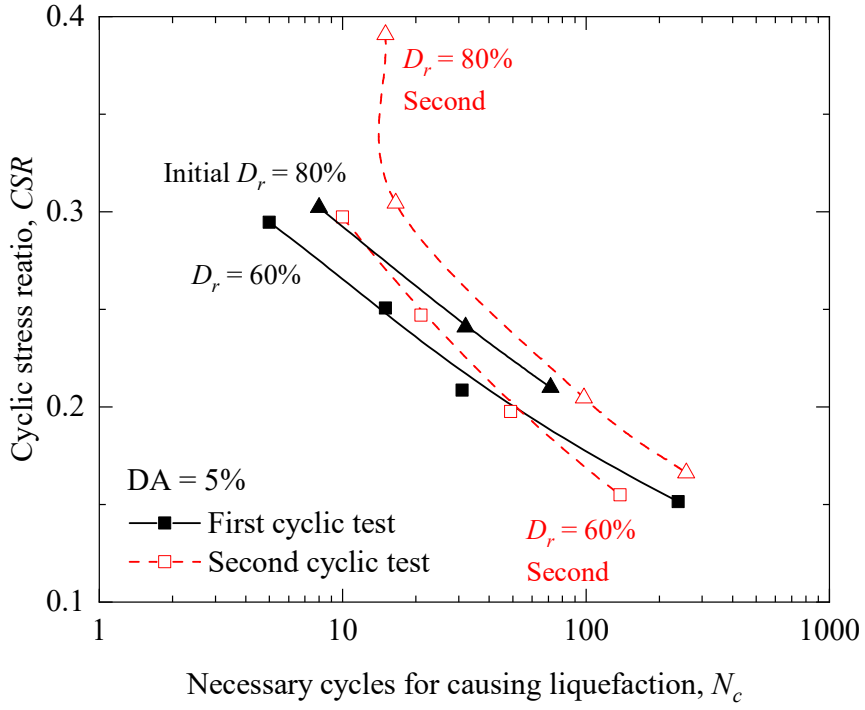

Figure 5.13 Liquefaction behaviours of boiled sand in liquefaction and re-liquefaction tests

Stress path was different to the path of Kuroboku moved fines. It looks similar as the stress path in Toyoura sand during first cyclic test stages. The relation of strain-stress performed as well. The difference produced in second cyclic tests because the liquefaction resistance reduced significantly in Toyoura sand. The strain in second stages became more uniform by each cyclic loading.

The excess pore water pressure was not produced greater than the initial confining pressure in all cases. The cohesion could be neglected by comparing to samples of Kurobiku moved fines.

5.4 Comparison of liquefaction behaviours between Toyoura sand, Kuroboku, and boiled sand

In order to investigate the liquefaction behaviour of the local soils in Kumamoto-Aso area, especially for detecting the potential influence from the volcanic particles

which deposited in this area. It is worth to compare the liquefaction behaviour between Toyoura sand, Kuroboku, and boiled sand. Toyoura sand was regarded as the base to find the relative differences in liquefaction potential. The failure line of DA = 5% was used here. The result of Toyoura sand was compared with Kuroboku removed fines in Figure 5.14, and compared with boiled sand in Figure 5.16.

Kuroboku owned the greatest liquefaction resistance compared to the others for the contribution of fines around 25%. Meanwhile, the fines also provided the cohesion according to the results showed in Figure 5.5 and Figure 5.7, that the mean effective pressure was produced greater than initial confining pressure. Therefore, pure kuroboku could be consider as a soil that is difficult to be liquefied.

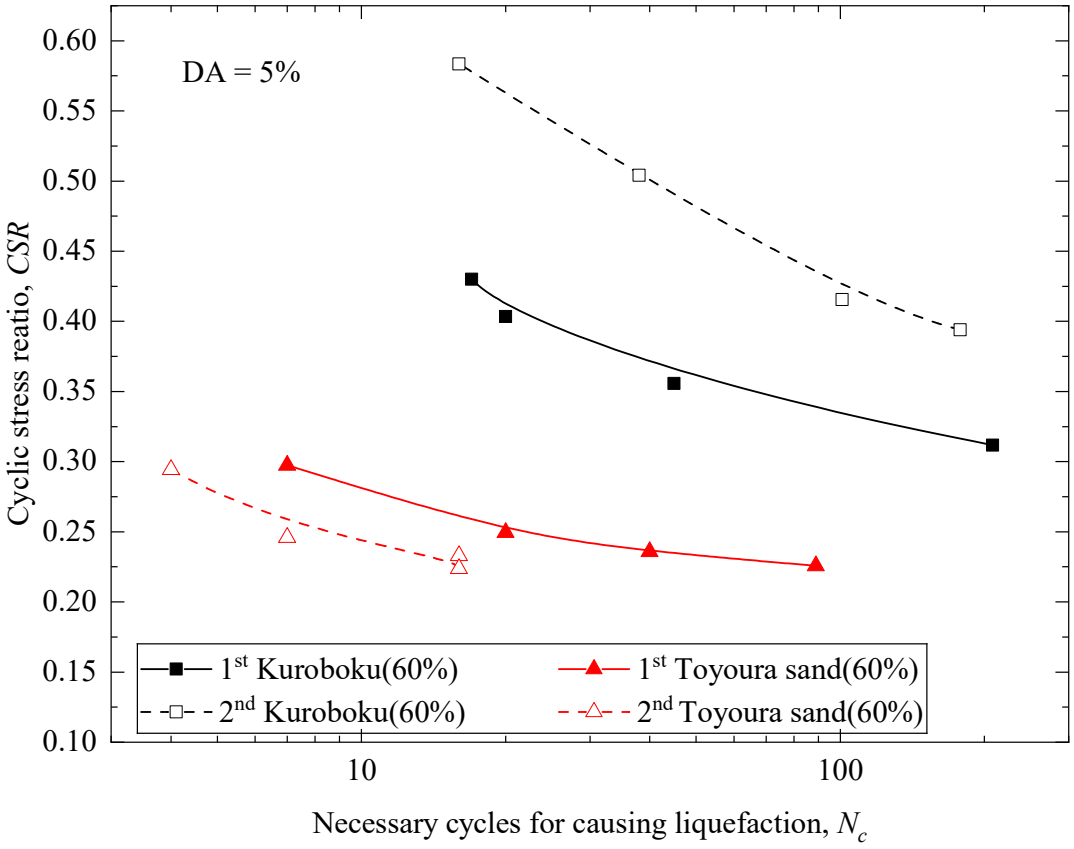

Figure 5.14 Comparison of liquefaction behaviour between Toyoura sand and Kuroboku

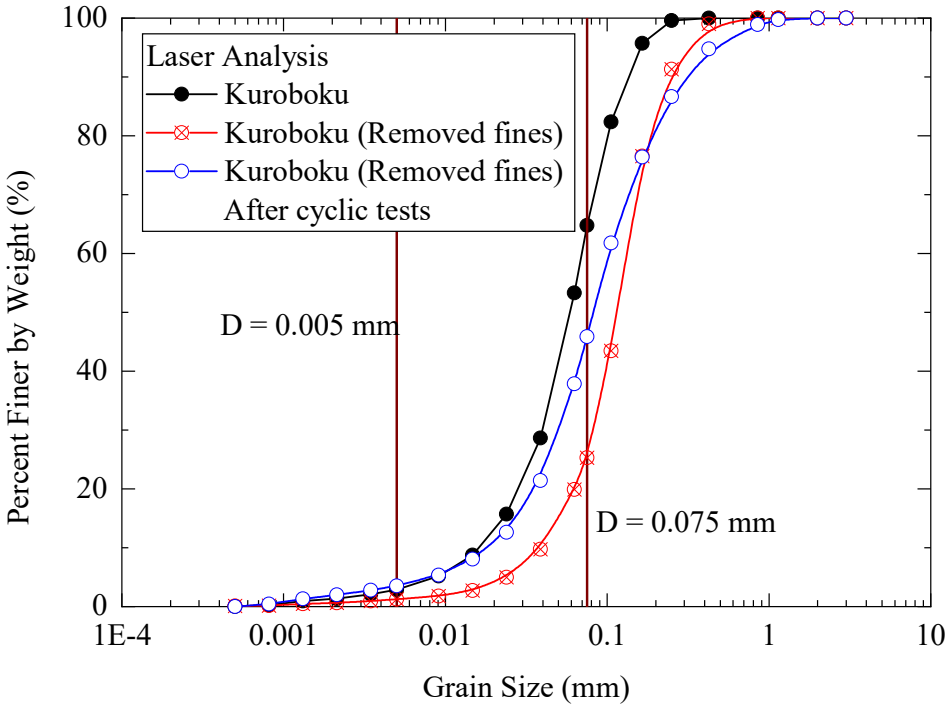

Figure 5 15 Grainsize distribution of Kuroboku after cyclic test

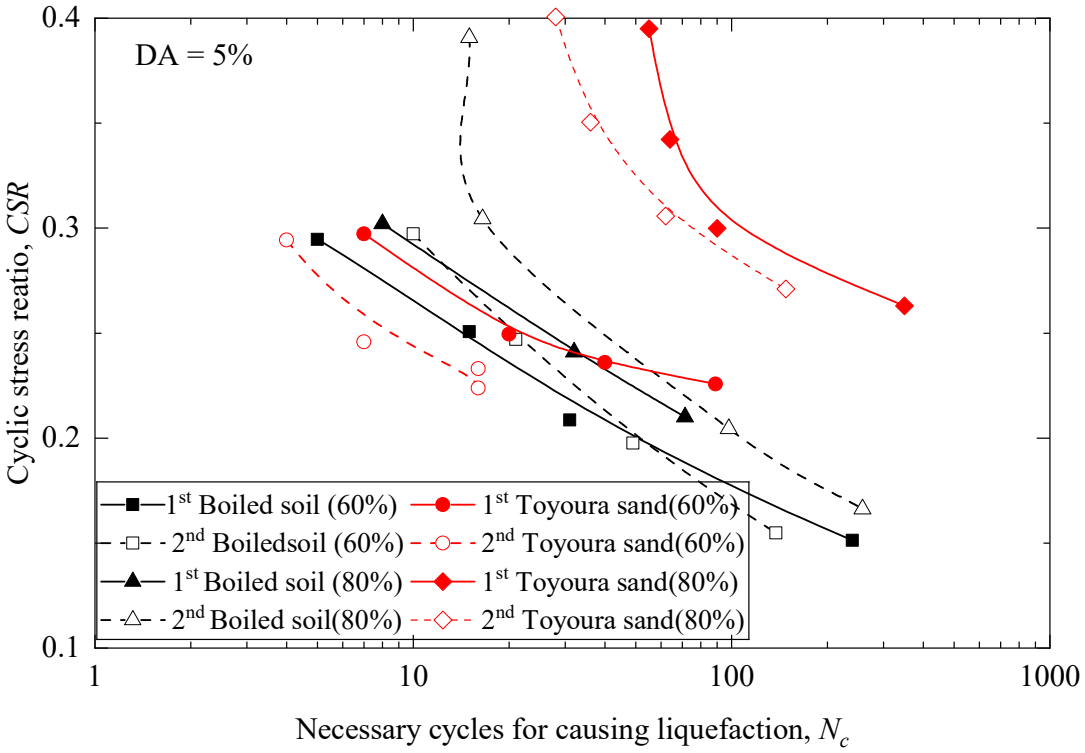

Figure 5.16 Comparison of liquefaction behaviour between Toyoura sand and boiled sand.

Figure 5.15 showed the fines content increased from approximately 25% to 50% after cyclic tests. Many particles were crushed by the cyclic loading during test process. At the same time, the grain distribution also became better than the initial state. As the result, the liquefaction resistance of Kuroboku removed fines increased significantly in second liquefaction stages.

In the other hand, although the boiled sand as a soil was considered containing the volcanic particles, the test results showed a very low liquefaction resistance comparing to Toyoura sand, even if there was about 10% of fines contained. It may be because the exact void is much greater than Toyoura sand. The void ratio was tested from 1.618 to 0.951 for boiled sand while from 0.977 to 0.606 for Toyoura sand. The boiled sand always kept with a void ratio nearly 2 times as Toyoura sand. The change of liquefaction resistance also was very small. This small increment was depended on the completely drainage and enough consolidation after first liquefaction. In real disasters, such in the 2016 Kumamoto earthquakes, the two shocks may come within a short interval, the liquefaction resistance might be reduced furtherly in the ground.

5.5 Summarizes

Based on the recurrence of liquefaction in the 2016 Kumamoto Earthquake, the two local soils were tested for investigating the basic physical properties and liquefaction behaviours. The sand boiled in liquefied site in this earthquake was selected to represent the typical ground where was prone to liquify in Aso-Kumamoto Area. Kuroboku, a representative volcanic soil in Aso-Kumamoto Area, was selected to discuss effects from the volcanic grains contained in boiled sand.

The results showed that the boiled sand could be classified as a sandy soil contained with fines. Kuroboku is a kind of silt with a high liquid limit.

In general, Kuroboku cannot be liquefied because of the great cohesion produced by fines. It still had a very high liquefaction resistance even if the fines were removed. Moreover, the liquefaction resistance increased in second liquefaction stages, which

was most possibly caused by the particle crushing during cyclic loading.

Boiled sand owned the lowest liquefaction resistance in the three soils in spite of approximately 10% of fines contained. The liquefaction resistance of boiled sand was not depended on the relative density greatly, which was also different to the other soils. At the same time, the liquefaction resistance didn't not change greatly between first and second liquefaction stages.

Therefore, the volcanic grains were proved that would not produce an adverse effect on liquefaction resistance of boiled sand. The great void ratio affected the behaviours potentially due to the similar the specific gravity between fine sand and boiled sand measured in this study.

References

中野武大，劉浩，永瀬英生，廣岡明彦，友久徹也．熊本地震における噴砂の液状化特性に関する事例的研究． 土木学会西部支部研究発表会, III(060), pp 371-372. 2017.3. In Japanese.

川口裕子. Master thesis: 阿蘇大橋地区における火山灰質土の力学特性と複合災害を想定した斜面の安定性評価への適用 2018.3. 九州大学. In Japanese.

JGS 0111-2009 (JIS A1202: 2009): Test method for density of soil particles.

JGS 0131-2009 (JIS A1204: 2009): Test method for particle size distribution of soils.

N. Yasufuku, R. Ishikura, A. Alowaisy, G.J. Liu, O.A. Putra, R. Yamamoto, 2018.7. In situ investigation for the landslide in Aso-Bashi Area, 2018.7.16.

JGS 0141-2009 (JIS A1205: 2009): Test method for liquid limit and plastic limit of soils.

JGS 0161-2009 (JIS A1224:2009): Test method for minimum and maximum densities of sands.

JGS 0051-2009: Method of classification of geomaterials for engineering purposes.

CHAPTER 6

EFFECTS OF SHEARING HISTORY ON THE ESTIMATION OF LIQUEFACTION POTENTIAL USING SHEAR WAVE VELOCITY

6.1 Introduction

Velocity of shear wave was used to evaluate the liquefaction potential depended on the data of liquefied sites recorded in the historical earthquakes and the empirical analysis (R.D. Andrus, and K.H. stoke II 2000; R.D. Andus et al. 2004). They proposed three boundary lines to separate the regions to liquefaction and non-liquefaction. At the same time, the component of fines also was taking into considering based on the in-situ investigations and related reports. However, the shear wave velocity adopted in their studies, mostly were investigated after the earthquakes. Thus, the results were difficult to reflect the accuracy for the ground experienced a relative great shear history or pre-shearing, if there were more than one shocks during the earthquakes in their studies. But the influence can not be neglected by the results tested by Ishihara and Okada (1978, 1982) and Bin Ye et al. (2018).

Because of the non-repeatability of real earthquakes at a same site, this study used the bender elements coupled with the cyclic tri-axial tests to try to find the correlation between the propagation of shear wave and liquefaction potential in soils. The pre-shearing also could be controlled easily. The main results were summarized in this Chapter.

In this section, the measuring method of shear wave with cyclic tri-axial test was introduced firstly. The adoption of velocity or amplitude was discussed as well.

Concerned on the shear-wave-based evaluation, the effects of shear history or pre-shearing was analysed primarily in this study. For undrained test (looks like the liquefaction occurring in earthquake), the pre-shearing normally could be categorized two major types: (1) the excess pore water pressure is discharged completely, that could be corresponded to the ground suffered the earthquakes with a relative long interval. (2) the excess pore water pressure remains in soil, that could be the same with some sites in the 2016 Kumamoto earthquakes struck by two great shock within a relative short interval. The two patterns of the influences

were discussed respectively in second.

A comparison between the test results achieved in this study and the boundary lines supposed by Andrus and Stoke (2000, 2004). The conversion approach was necessary for the results obtained in laboratory experiments to compare with the filed-based data. This these contents were discussed in the final part of this Chapter.

Kuroboku including the samples moved out the fines showed a very high resistance on liquefaction behaviour. The resistance became even more higher than it in initial, after being pre-sheared with the small strains and liquefied once time. Therefore, the test materials of Toyoura sand and boiled sand in the 2016 Kumamoto earthquakes were tested in this study.

6.2 Measurement of shear wave in cyclic tri-axial test apparatus

6.2.1 Shear wave velocity

The full-scale consistence of the test equipment has been illustrated in Chapter 3 already. The couple of bender elements were assembled with the porous stone in both sides of upper and lower, as shown in Figure 6.1. The elements were inserted into the test samples, meanwhile, the two elements needed to be perfectly set in the identical direction. The datum line was marked on the rubber membrane to help the set up during the preparation progress. Photo 6.1 shows a prepared sample after dissembling of mould.

The measuring method utilized in this study was based on the criterion supposed by Japanese Geotechnical Society (JGS: 0544). A single signal of sine wave was produced from the function generator, and it was sent to the amplifier where it was amplified to 20 times. Then the signal was inputted from the upper bender element. The shear wave propagated into the specimen with non-destructivity, and it would be detected by the bender element at lower. After that,

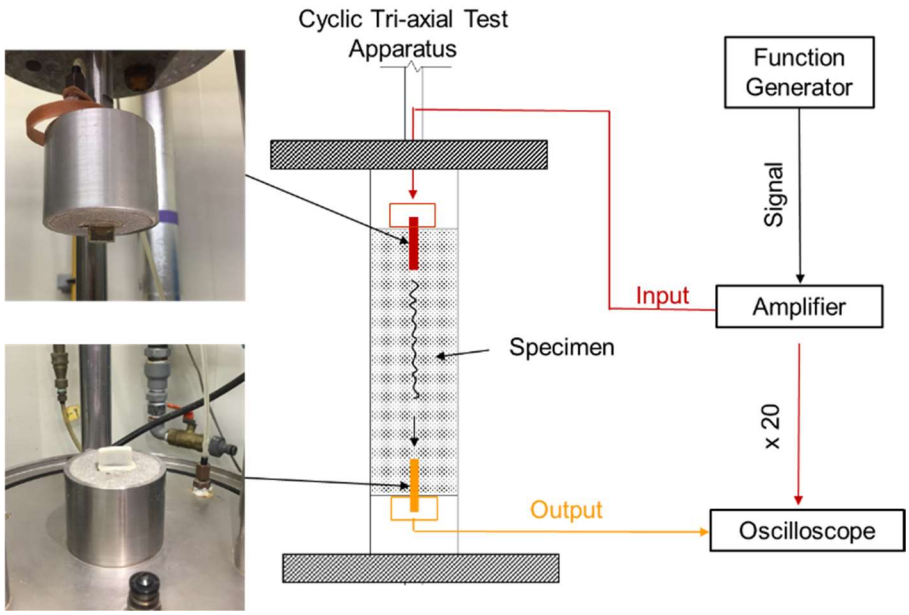

Figure 6.1 Illustration of cyclic tri-axial test apparatus with bender elements.

Photo 6.1 Bender elements were set up in the identical direction by datum line marked in rubber membrane.

the signal was delivered to the digital oscilloscope. There is another way for the signal, that the amplified signal was delivered to the digital oscilloscope directly from amplifier. The necessary time for the arriving of the two signals obviously was different. The arrival time passed though the specimen should be delayed by comparing to the electrical signal, the velocity of which is approximately 2.3×10^{8} m/s. This velocity also was much greater than the velocity propagating in soils which is only located at the magnitude of $\times10^{2}$ m/s. The delivery time in the system by electric signal could be ignored related to the time in specimen. Therefore, the delivery time ΔT in specimen could be obtained from the result shown in Figure 6.2, which was carried from the result measured in this study. The delivery time was defined as the peak to peak, which was more simply than the method supposed in JGS: 0544. The difference was verified by using the results measured in this study, meanwhile, make the calculation became easier.

By Equation 6.1 and 6.2, the velocity of shear wave (V_s) propagating in specimen was obtained.

$$V_s = \frac{L}{\Delta \mathrm{T}} \tag{6.1}$$

$$L = H_s - 2H_{BE} \tag{6.2}$$

Where, L is the propagation distance; H_s is the height of specimen at measuring the velocity of shear wave; H_{BE} is the height of bender elements inserted into specimen. $2H_{BE}$ means the distance L is defined as the top to top between the bender elements at upper and lower.

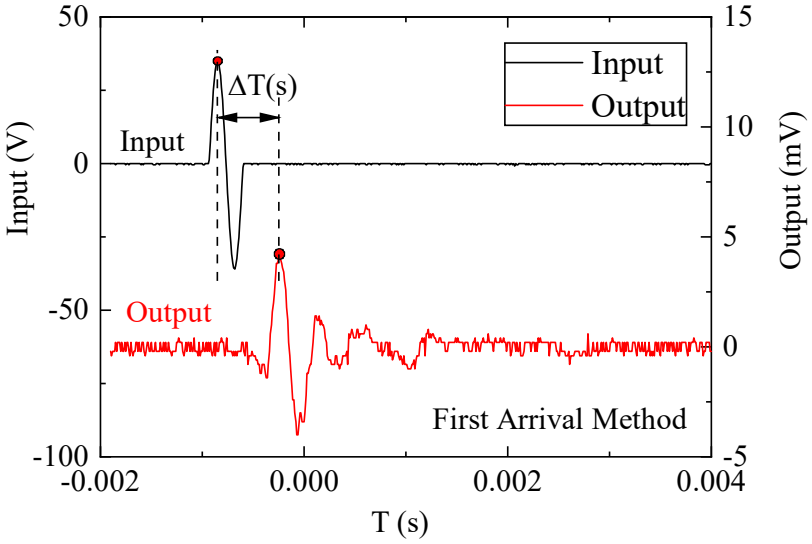

Figure 6.2 Definition of ΔT from the results of bender elements.

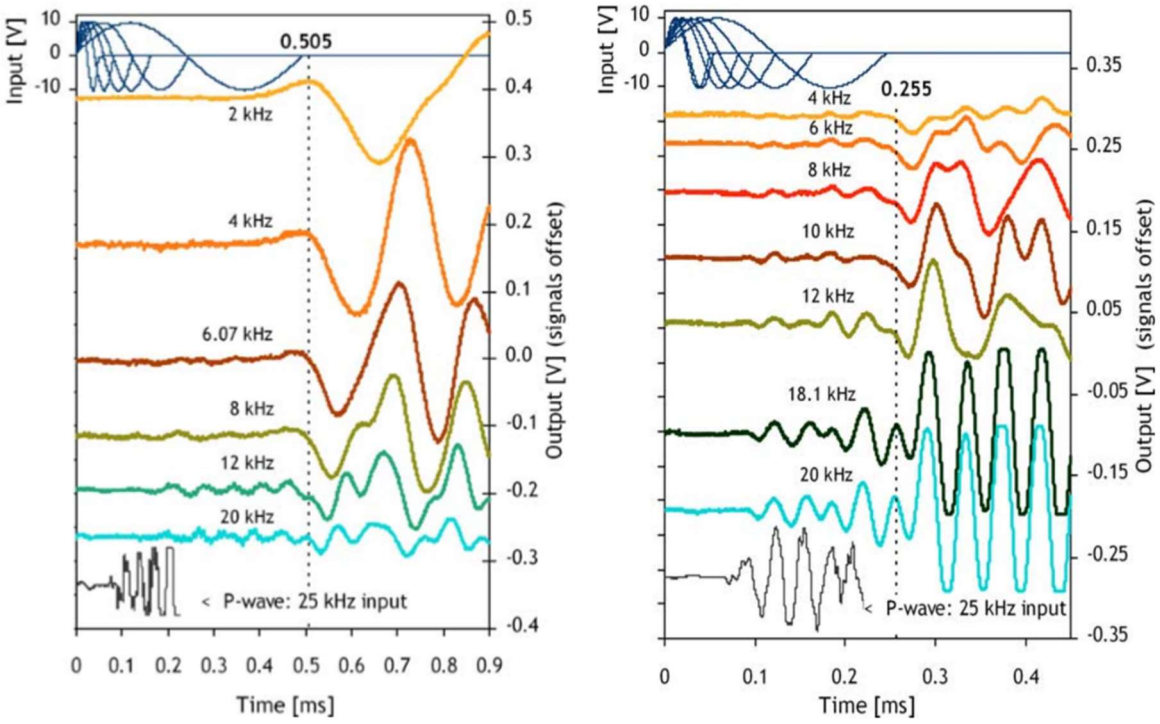

(a) σ_c = 100 kPa (b) σ_c = 800 kPa

Figure 6.3 Comparison of the amplitudes at the outputted frequency of 2, 4, 6.07, 8, 12, 18.1, 20 kHz. (Residual soil, tri-axial test) (Fonseca et al. 2009)

6.2.2 Discussion for the applicability of velocity and amplitude as the index

The amplitude of the outputted signal also could be obtained from Figure 6.2. The order of magnitude of the outputted signal lost approximately 4 magnitudes from inputted signal. The attenuation was very great. Moreover, the attenuation of amplitude also was very depended on the frequency of the inputted signal. (A.V. Fonseca et al. 2009). The similar results also were obtained in this study.

The amplitude trended to increases with decreasing of the frequencies inputted signal under the confining pressure of 100 kPa. At the same, the confining pressure influenced the performances as well. At 800 kPa, the amplitude changed to increase with increasing of the frequency until the frequency became very great to around 20 kHz. The amplitude became steadier, that was without a visible change between 18.1 kHz and 20 kHz in frequency. Taken as a whole, the performance of amplitude can not be looked as the reliable index if it is used to evaluate the liquefaction potential.

On the contrary, the performance of velocity dose not greatly depend on the frequency of inputted signal. Figure 6.4 shows the velocities measured at the different frequencies by 2, 3, 4, and 5 kHz. The two tests were carried from two samples of Toyoura sand prepared with the relative density around 60% under the confining pressure u/σ_{c0}' = 100 kPa.

The velocity performed similarly by each inputted frequency in the two tests. The velocity also changed very small comparing to the amplitude, that were situated at the range of 190 ~ 225 m/s for all frequencies. Therefore, the velocity is steadier than amplitude in tri-axial compression apparatus, that could be looked as a well index for estimating liquefaction potential. The frequency f = 5 kHz was adopted in this study according to the suggest proposed by JGS: 0544.

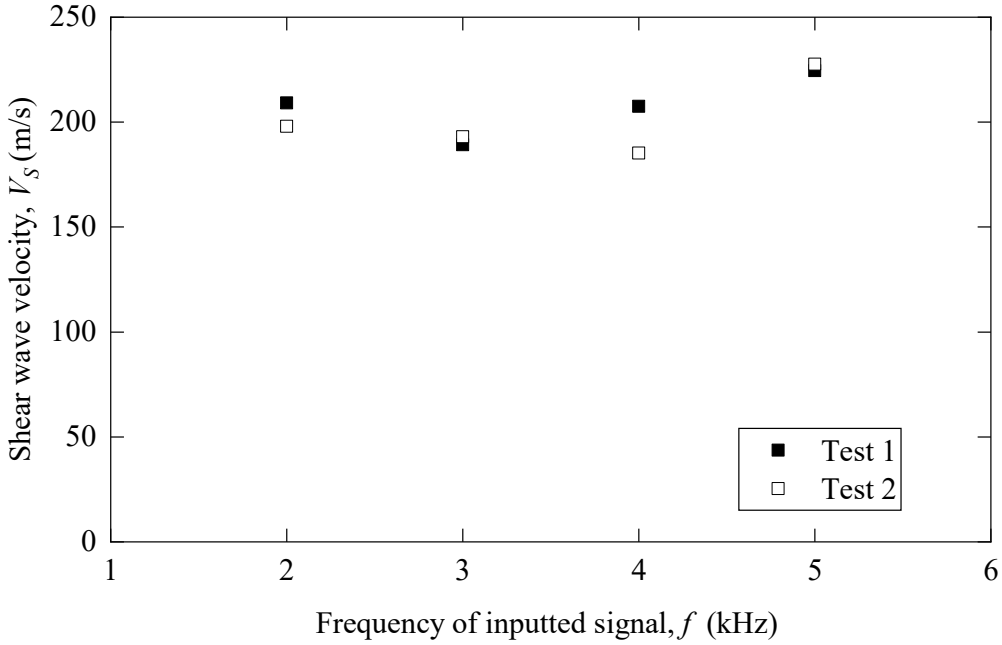

Figure 6.4 Comparison of the velocity at the outputted frequency of 2, 3, 4, 5 kHz. (Toyoura sand)

6.3 Correlation between shear wave velocity and liquefaction potential

There were two types of pre-shearing as mentioned in above, which were detected the correlation to shear wave velocity.

6.3.1 Correlation between V_s and B-value

The samples were tested by bender elements at the checking of B-value, after first consolidation and after re-consolidation. The index of B-value represents the saturation degree in soil, thereby, influences the liquefaction resistance significantly in general. The boiled sand was tested under completely saturated sate for all cases in this study. Thus, the results from Toyoura sand were expressed only.

The correlation was detected from the oven-dried conditon to completely saturated condition (B-value is very closed to 1.0). Because the B-value can not directly be controlled due to the limitation of the equipment in this study, the B-

value was achieved by air pluviation accidently. As the result, there were lack of data situated at lower saturation degrees. The B-value at the range of 0.6 ~ 1.0 were plotted in Figure 6.5 with the correlation to shear wave velocity. The saturation degrees were obtained by the Equation 6.3 (Lade and Hernandez 1977).

$$B = \frac{1}{1 + nK_s[S_r / K_w + (1 - S_r)/u_a]} \tag{6.3}$$

Where, n is porosity, 0.43; K_s is the bulk modulus of soil skeleton, 6.7 × 10^4 kPa; K_w is the bulk modulus of water, 62.23 × 10^6 kPa; u_a is the absolute pressure in pore fluids, 343 kPa for saturated sand and 98 kPa for partially saturated sand.

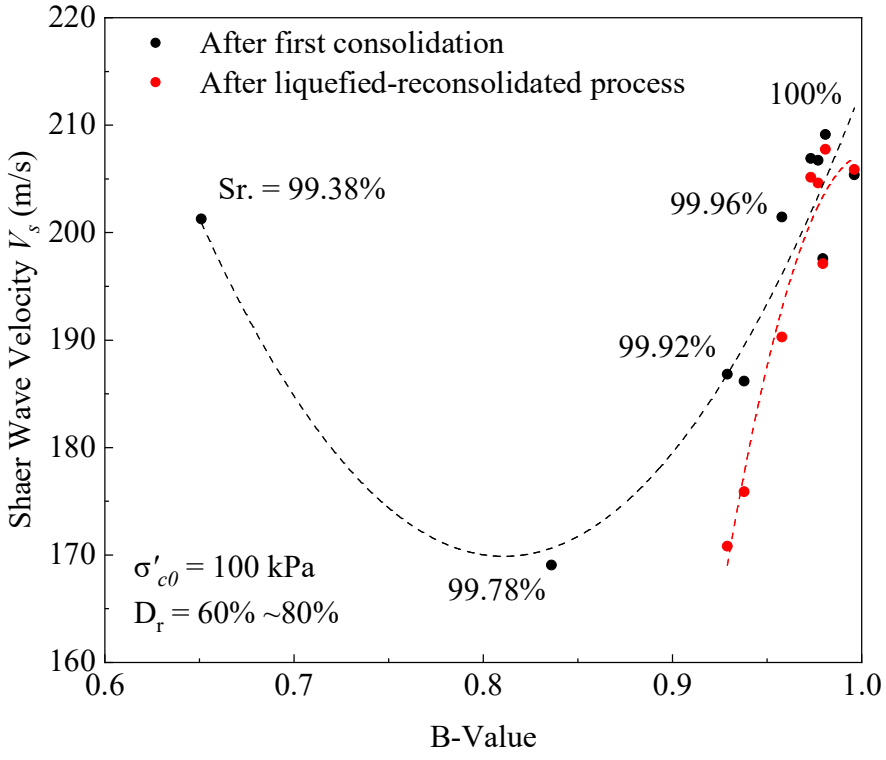

Figure 6.5 Comparison of V_s after first consolidation and re-consolidation under different B-Value.

Based on the calculated results, B-value could accurately represent the saturation degree even if the degree is very closed to 100%. The velocity was checked both after the first consolidation and re-consolidation. For the line of first consolidation, the shear wave velocity had a valley when B-value at around 0.75 ~ 0.85. Meanwhile, the velocity in oven-dried sand was measured at around 270 m/s, when the relative density was 80% under the confining pressure of 100 kPa. Therefore, it could be predicted that the shear wave velocity decreases with increasing of the saturation degree on the whole, and a valley may appear at the range of 0.75 ~ 0.85 just before sand is considered completely saturated for liquefaction test in cyclic tri-axial apparatus (B-value ≥ 0.95 is needed commonly). For the line of re-consolidation, because the samples with a low B-value were not tested secondly in this study, there were only the results from the samples with a high B-value. The variation tendency was looked as same as it of first consolidation. Therefore, the velocity of shear wave could be deemed to estimate the liquefaction potential by the view of saturation degree.

6.3.2 Evaluation for soils in liquefaction and re-liquefaction

Liquefaction resistance of Toyoura sand and boiled sand were finished to discuss in Chapter 4 and Chapter 5. The results majorly showed that:

1) The liquefaction resistance of boiled sand was very similar at different relative densities of 60% and 80%, as well as, between first liquefaction and re-liquefaction.
2) In test of Toyoura sand, the liquefaction deduced significantly in re-liquefaction process.
3) In the comparison of the two soils, Toyoura sand with initial Dr = 60% owned a similar liquefaction resistance as boiled sand no matter of the relative densities and it in first or second cyclic tests. For Toyoura sand with initial D_r = 80%, the higher resistance occurred even though it

decreased greatly in the re-liquefaction test process.

The evaluation by using shear wave velocity was based on these results and discussed in this section. The comparison for Toyoura sand was conducted firstly, and results were arranged in Figure 6.6. The velocities were very similar between the two processes. Therefore, the shear wave velocity can not clearly indicate the change of liquefaction resistance for the sand liquefied once time with a sufficient drainage consolidation.

Figure 6.7 shows the performance of shear wave velocity in boiled sand. The tendency of the variation between B-value and shear wave velocity was similar as the relation in Toyoura sand, that the velocity increased accompanied the increasing of B-value. However, the level was decreased from the range of 170 ~ 210 m/s to 150 ~ 200 m/s.

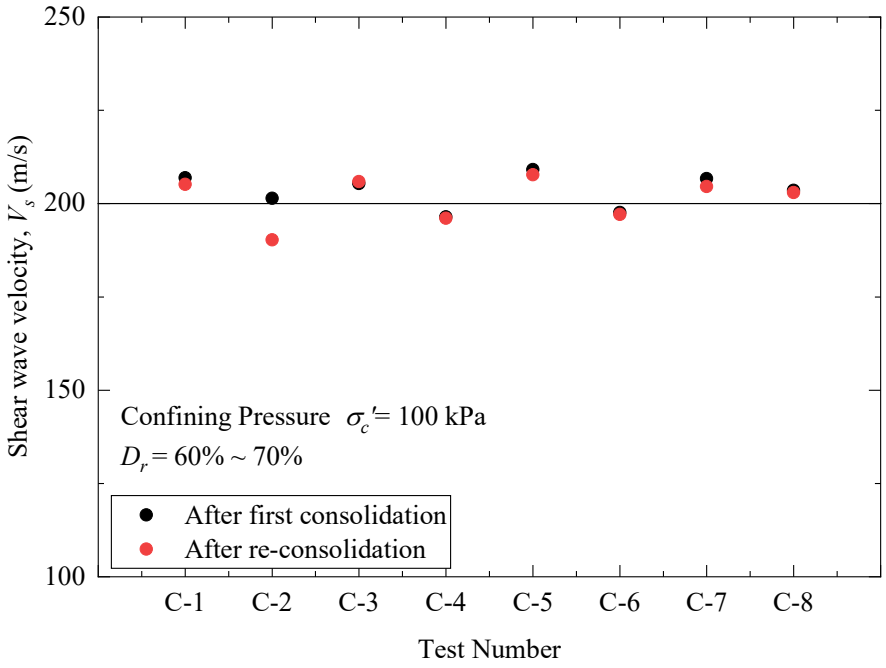

Figure 6.6 Comparison of shear wave velocity between first consolidation and re-consolidation.

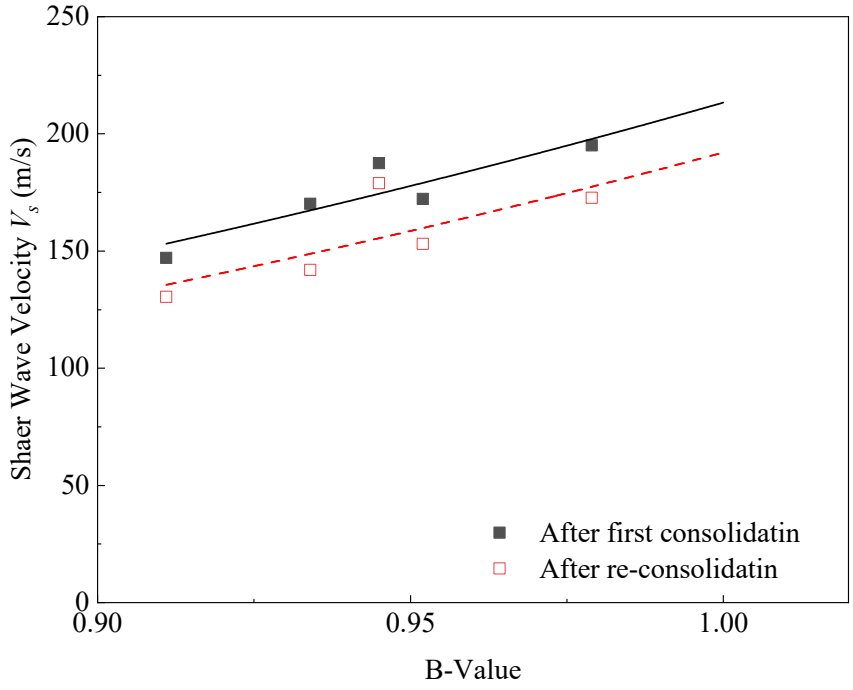

Figure 6.7 Comparison of shear wave velocity between first consolidation and re-consolidation with B-value

Shear wave velocity was widely used in-situ investigation for detecting the shear modulus G in ground using the relation defined by Eq. 6.4.

$$G = \rho V_s^2 \tag{6.4}$$

Where, ρ is the density of soil. Meanwhile the shear modulus also is depended on the void ratio e and confining pressure σ_c', (Tatsuoka et al. 1979), which can be expressed by:

$$G = A\frac{(2.17-e)^2}{1+e}\sqrt{\sigma_c'} \tag{6.5}$$

Where, A is the empirical constant, adopted as 550 for the normal

consolidated soil (Tokimatsu et al. 1986). When the soil's void ratio $e \leq 2.17$, shear modulus would decrease with increasing of the void ratio. In this study, the samples of Toyoura sand were prepared by the relative densities of around 0.7 ~ 0.75; while the samples of boiled sand were prepared by around 1.1 ~ 1.2. The void ratio of boiled sand samples was smaller than the Toyoura sand samples with more than 50% in the tests. This may induce the reduction of shear wave velocity in boiled sand by comparing to it in Toyoura sand.

The performance of velocity between after first consolidation and after re-consolidation was different to the results in Toyoura sand. The velocity after re-consolidation always reduced with some degree in all test cases which is opposite to the liquefaction resistance increased with some degree in cyclic tests. This phenomenon only could be explained by the influence from fines of approximately 10% in boiled sand. This point was also discussed in the final part of this Chapter with the proposed boundary for different contents of fines.

6.3.2 Evaluation for the soil remained excess pore water pressure

In earthquakes, the excess pore water pressure increases by the shaking, at the same time, the effective stress decrease from the initial state. If the excess pore water pressure remains in the ground after the earthquake, the current effective stress will not rise back to the initial state, that may cause a reduction of liquefaction resistance when next earthquake comes. Therefore, the most important issue is that, is there a correlation between shear wave velocity and current effective stress, if the shear wave velocity is expected to use in the estimation.

Besides, the shear wave velocity also decreased during the cyclic loading, as a typical result achieved in study, shown in Figure 6.8. The test was started from Nc = 0, while the velocity had the maximum value at around 200 m/s. Then, the velocity decreased smoothly and gently in most portion. However, when the soil was near liquefaction, the velocity decreased very faster in few cycles and

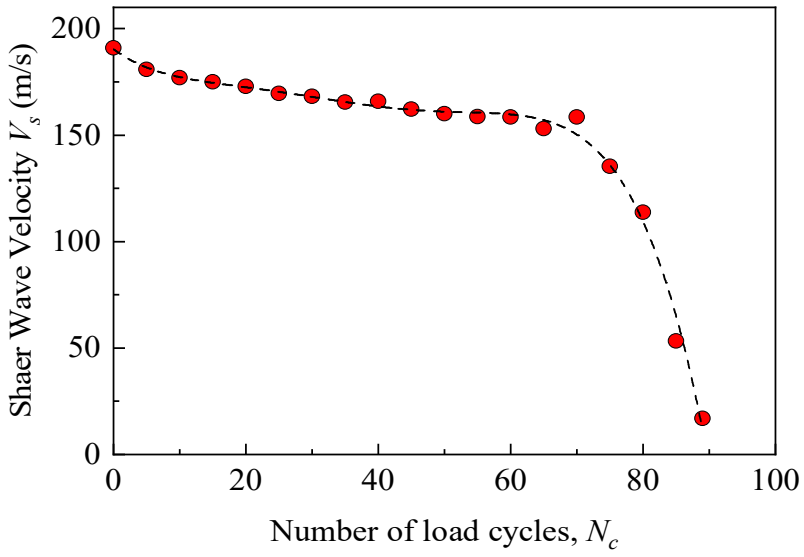

Figure 6.8 Variation of shear wave velocity during cyclic loading (Toyoura sand with D_r = 60%).

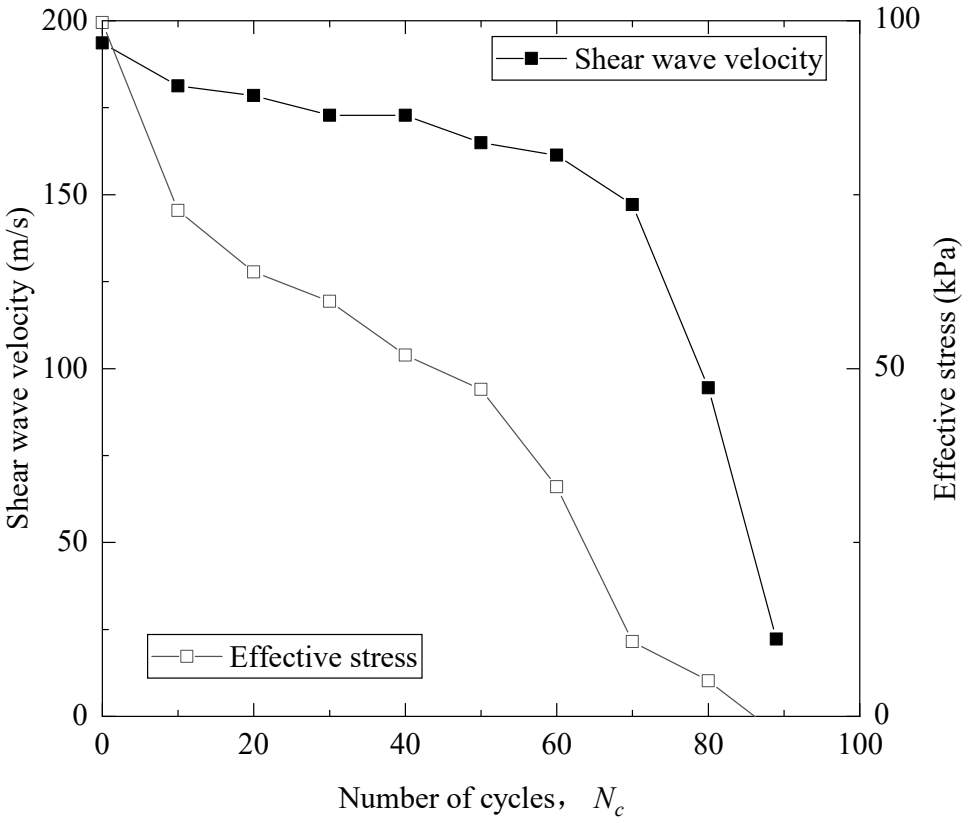

Figure 6.9 Variation of effective stress together with shear wave velocity during cyclic loading (Toyoura sand with D_r = 70%)

approaching to 0. Figure 6.9 shows the effective stress was decreasing together with the shear wave velocity during cyclic loading. Therefore, the correlation between effective stress and shear wave velocity could be built. The results between Toyoura sand and boiled sand were arranged and compared in Figure 6.10.

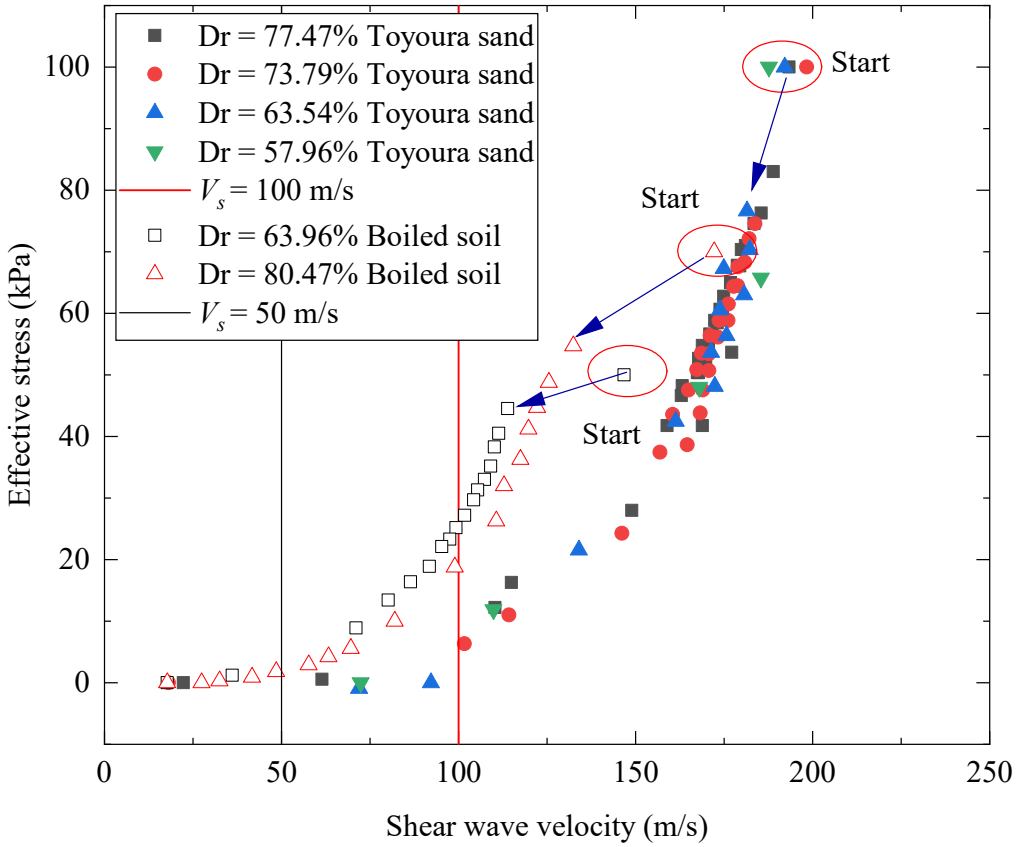

Figure 6.10 Correlation between effective stress and shear wave velocity in Toyoura sand and boiled sand

Four samples of Toyoura sand with the relative density from around 60% to 80%, and two samples of boiled sand with the relative density of around 60% and 80% were tested. The results indicated that the influences from relative density were very small, even it could be neglected in the samples of Toyoura sand. At a given velocity of shear wave velocity, the residual effective stress or the excess pore water pressure remaining could be regarded uniquely for each soil.

Comparing the performance between Toyoura sand and boiled sand, the shape moved to left on the whole to produce two critical velocity of shear wave. The key velocity for Toyoura sand is 100 m/s. The effective stress reduced to almost 0 before this velocity. The similar situation appeared in boiled sand at around 50 m/s. Meanwhile, it also indicated that the effective stress was different at the same shear wave velocity between the two soils. Furthermore, if the correlation in sand was set as the datum line, the initial state in boiled sand was singular for the tendency in entire. The two points of boiled sand with Dr = 60% and 80%, where the velocity measured after consolidation just before the cyclic test, were very closed to the line formed by Toyoura sand. This behaviour was only produced in the boiled sand or not that also be worth to discuss later.

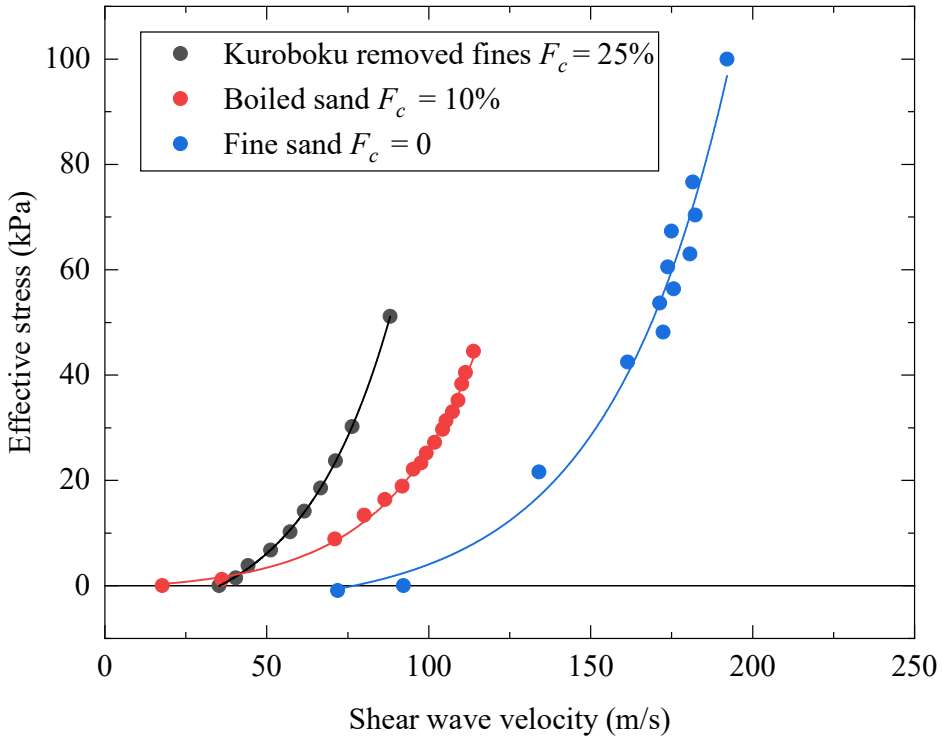

Figure 6.11 Characteristic curves for soils with different fines contents

In order to furtherly discuss the effect from fines, Kuroboku contained approximately 25% of fines was carried for comparing. The curves selected

typically from test materials were compared and arranged in Figure 6.11. As discussion in above, the characteristic curve was unique in a certain soil, which was not depending on the change of void ratio and confining pressure. However, the results indicated the characteristic curves depended on the fines content heavily. Under a certain effective stress, the shear wave velocity performed a lower level with the increasing of fines content. Meanwhile, a similar residual effective stress can not directly represent the residual liquefaction resistance in different soils. Therefore, the shear wave velocity, as the indicator, was applicable to a certain ground with because the characteristic curve may be unique for the ground with different grain distribution and fines contents.

6.4 Comparison of the Laboratory-based and the Filed-based results on liquefaction estimation using shear wave velocity

The shear wave velocities relating to the liquefaction potential were clarified by the discussions in above. Now, the velocities after the first and second consolidation have been obtained, as well as, the correlation to the excess pore water pressure remained in soils. The comparison is necessary for this study, to discuss the applicability of the data from laboratory and the accuracy of the field-based results in empirical simultaneously.

6.4.1 Conversion from laboratory-based data to field-based data

In order to compare data from laboratory and field, both shear wave velocity and liquefaction resistance needed to be converted to the field conditions by the following expressions:

Stress-corrected shear-wave velocity

For shear wave velocity to be considered as the index, much depends on the state of stress in the soil (Hardin and Drnevich, 1972). It could be corrected with the reference overburden stress in a similar way as the traditional procedure for

correcting SPT blow count and CPT trip resistance by (Robertson et al., 1992; Andrus and Stokoe, 2000):

$$V_{s1} = V_s C_v = V_s \left(\frac{P_a}{\sigma_v'}\right)^{0.25} \tag{6.6}$$

Where, V_{s1} = Overburden stress-corrected shear wave velocity; V_s = measured shear wave velocity in situ; C_v = conversion factor to correct V_s for overburden pressure; P_a = reference stress of 100 kPa; σ'_v = effective overburden stress. In field investigation, σ'_v determined majorly by depth and ground water level, is corresponded to the σ'_h with K_0 = lateral earth pressure coefficient at rest.

$$\sigma_h' = K_0 \sigma_v' \tag{6.7}$$

Where, σ'_h = horizontal effective stress; The velocity at which shear wave propagates along the soil in current condition can be determined by the empirical formula (Roesler, 1979; Bellotti et al. 1996).

$$V_s = C_s \sqrt{F(e) \sigma_a'^{na} \sigma_b'^{nb} \sigma_c'^{nc}} \tag{6.8}$$

Where, $F(e)$ = void ratio function; σ'_a = principal effective stress along the propagation direction; σ'_b = principal effective stress in the direction of particle motion; σ'_c = the effective principal stress which acts on the plane defined by the propagation direction of shear wave and particle motion; and C_s = constant determined empirically. Since the cyclic tri-axial tests in this study were conducted under isotropic condition, $nc \approx 0$; and $na \approx nb \approx n$ according to experimental results presented by Roesler (1979), Stokoe et al. (1985) and Bellotti et al. (1996).

Thus, σ_c' could be neglected, and Eq. (6.8) could be simplified to,

$$V_s = C_s\sqrt{F(e)(\sigma_a'\sigma_b')^n} \tag{6.9}$$

In cyclic tri-axial tests, $\sigma_a' = \sigma_v' = \sigma_1'$ and $\sigma_b' = \sigma_h' = \sigma_3'$ based on the installation direction of bender elements as shown in Photo 1. Therefore, $\sigma_1' = \sigma_3' = \sigma_m'$, σ_m' = mean effective stress, for isotropic conditions; $K_0\sigma_1' = \sigma_3'$, for anisotropic conditions. Therefore, shear wave velocity achieved by Eq. (6.9) for isotropic and anisotropic conditions can be determined respectively, by

$$V_s = C_s\sqrt{F(e)\sigma_m'^{2n}} \tag{6.10}$$

$$V_s = C_s\sqrt{F(e)K_0^{\,n}\sigma_1'^{2n}} \tag{6.11}$$

Substituting $\sigma_1' = P_a$ into Eq. (6.6) and Eq. (6.11)

$$V_{s1} = V_s = C_s\sqrt{F(e)K_0^{\,n}P_a^{2n}} \tag{6.12}$$

Solving C_s by Eq. (6) and substituting it into Eq. (6.12)

$$V_{s1} = V_s K_0^{0.5n}\left(\frac{P_a}{\sigma_m'}\right)^n \tag{6.13}$$

Therefore, the stress-corrected shear wave velocity is calculated from the velocities measured in cyclic tri-axial tests using Eq. (6.13) by assuming n = 0.25 for typical saturated soils. K_0 was assumed to be around 0.5 based on the in-situ

data from historical liquefied sites (Andrus and Stokoe, 2000; Zhou and Chen, 2007). The confining pressure of 100 kPa was adopted as effective mean stress σ'_m for the stress states after normal consolidation and liquefied-reconsolidated process in this study. For the cases of pre-shearing with undraining process, confining pressure was modified by the produced excess pore water pressure using Eq. (6.13).

Conversion of liquefaction resistance between laboratory and field data

Field-based liquefaction resistances were based on the observation of the occurrences at the ground such as ground settlement, sand boils, footing inclinations during or just after earthquakes. A strain of around 5% with double amplitude produced in the specimen was considered as the criterion to evaluate the liquefaction resistance in cyclic tri-axial tests. The correlated criterion between the two kinds of results was discussed by comparing the data from laboratory and field (Seed et al., 1983; Tokimatsu and Uchida, 1990; Idriss, 1999). Seed et al. suggested the liquefaction resistance be based on the representative number of cycles of different earthquake magnitudes, as shown in Table 2. The equivalent Nc = 15 was adopted in this study for comparing with the field-based data at Mw = 7.5.

Table 6.1 Number of cycles representative of different magnitude earthquakes

Magnitude	**Number of representative cycles at 0.65 τ_{max}**
8.5	26
7.5	15
6.75	10
6	5-6
5.25	2-3

The obtained cyclic resistance from tri-axial tests also need to be the converted to field results. Seed (1979) and Kramer (1996) proposed the following equation

$$CRR = 0.9 \times C_r \times CRR_{tx} \tag{6.14}$$

Where CRR = cyclic resistance ratio in field; CRR_{tx}= cyclic resistance ratio in tri-axial tests, indicated by the cyclic stress ratio CSR at Nc = 15; C_r = conversion factor, proposed as 0.63 for normal consolidated sandy soil by Seed. Therefore, the laboratory-based data could be evaluated using field-based correlation.

6.4.2 Comparison of results including the soils with pre-sharing

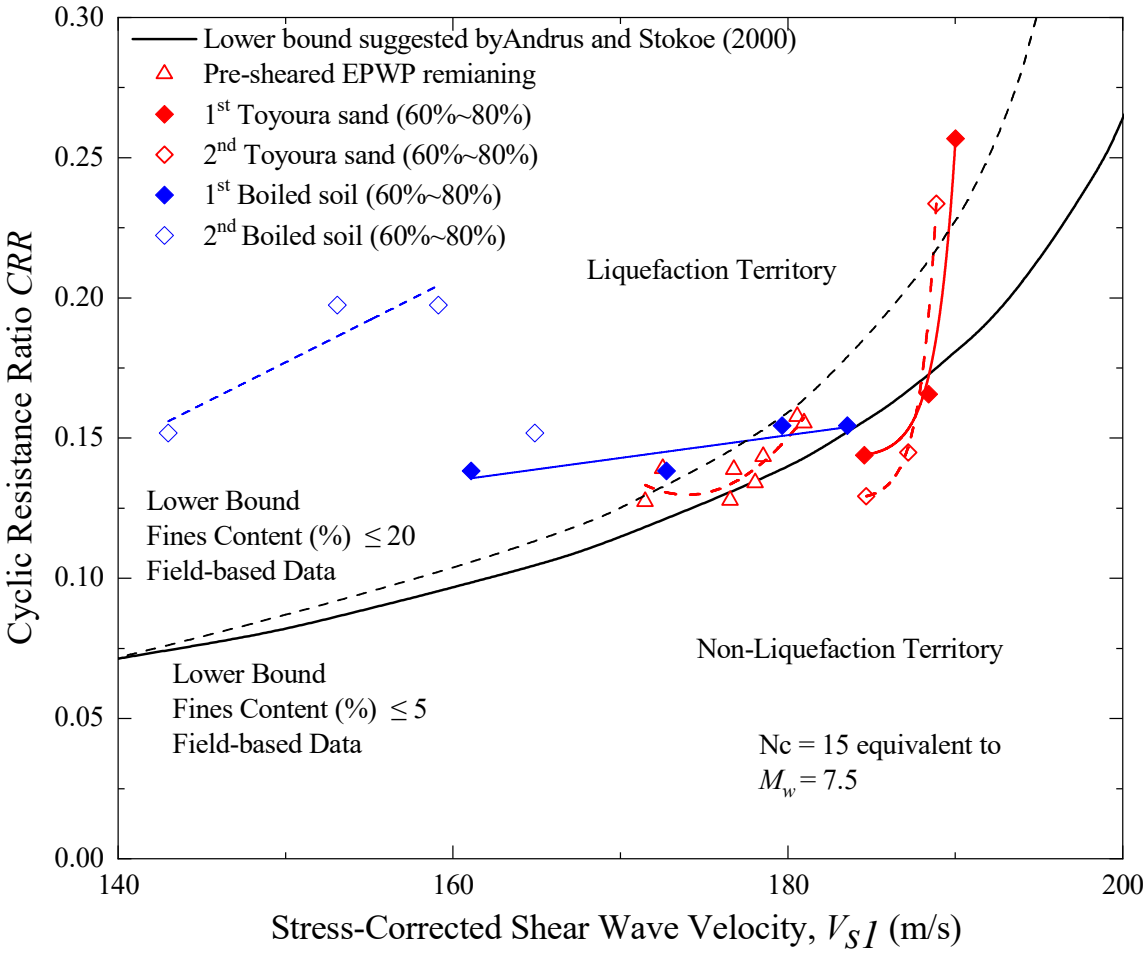

Figure 6.12 Comparison between lower-bound curve supposed by field data (R.D. Andrus and K.H. Stokoe 2000) and laboratory-based data.

The resistances of samples in first and second cyclic tests, as well as, the excess pore water pressure remained samples were arranged in Figure 6.12. The results carried out the influences of the confining pressure where the soils situated to find the correlation between liquefaction resistance and shear wave velocity simply. The behaviours could be looked only affected by the physical properties of soils.

The corresponding cures were monotonous in expressing the variation tendency for each group. The liquefaction resistance also increased with increasing of stress-corrected shear wave velocity in generally. Therefore, it could be accepted that the shear wave velocity could be used to evaluate liquefaction potentials.

The results between Toyoura sand and boiled sand were quite different. For the excess pore pressure discharged cases and non-pre-sheared cases of Toyoura sand, the two curves overlapped in a small range at around 190m/s. Meanwhile, a small change of stress-corrected shear wave velocity may cause a great change in liquefaction resistance. The boiled sand without pre-shearing expressed a similar performance as the sand was pre-sheared and remained with excess pore pressure. The slope for these samples were very gentle, that make the velocity can evaluate the change of liquefaction accurately.

In boiled sand, the liquefaction resistance increased however a slower velocity was performed in re-liquefaction stage. This phenomenon also was caused by an increment of fines content in most possibly. The particles of boiled sand may crush slightly during the cyclic loading as well, because the considerable volcanic grains were contained. According to the discussion from above, the fines would reduce the shear wave velocity, which caused a deduction of shear wave velocity in re-liquefaction stages.

In addition, the correlation in Toyoura sand extended out to the lower boundary which was developed based on the field-based data. The similar results were observed by Christopher et al. (2008), who used Providence silts with a very high fines content $Fc \geq 95\%$. Therefore, this liquefaction evaluation method still

needs more corrections and improvements in future works.

6.5 Summarises

The correlation between shear wave velocity and liquefaction resistance, particularly for the soils with shearing history, was investigated in this Chapter. The results showed the shear wave velocity can indicate B-value and the liquefaction resistance determined by relative density well.

In the pre-sheared cases, shear wave velocity was difficult to indicate the change of liquefaction between liquefaction and re-liquefaction stages. For fine sand, the accuracy was highly requested, because the resistance changed greatly within a very range of velocity. For boiled sand, the estimation method may be influenced by the potential particle crushing.

In the excess pore water pressure remained cases, the shear wave velocity could indicate the change of residual effective stress accurately. In a ground with a certain distribution of grains, the correlation was relying on the relative densities and confining pressures.

References

A.V. Fonseca, C. Ferreira, and M. Fahey, 2009. A framework interpreting bender element tests, combining Time-Domain and Frequency-Domain Methods. Geotechnical Testing Journal, Vol 32, No. 2, pp 91-107.

B.O. Hardin, and V.P. Drnevich, 1972. Shear modulus and damping in soils: design equations and curves. Journal of Soil Mechanics & Foundations Div, ASCE, **98**(SM7), 667-692.

Bin Ye, Hailong Hu, Xiaohua Bao, Ping Lu. Reliquefaction behavior of sand and its mesoscopic mechanism. Soil Dynamics and Earthquake Engineering 114 (2018) 12–21.

Bin Ye, Jiafeng Lu, Guanlin Ye, 2015. Pre-shear effect on liquefaction

resistance of a Fujian sand. Soil Dynamics and Earthquake Engineering, Vol. 77, pp 15-23.

F. Tatsuoka, T. Iwasaki, S. Fukushima, and H. Sudo, 1979. Stress modulus and damping of sand under cyclic loading. Soils and Foundations, Vol. 19, No. 2, pp 29-43.

H.B. Seed, 1979. Soil liquefaction and cyclic mobility evalution for level ground during earthquakes. Journal of Geotechnical and Geoenvironmental Engineering, **105**(GT2), 201-225.

H.B. Seed, I.M. Idriss, 1983. Evaluation of liquefaction potential using field performance data. Journal of Geotechnical Engineering, ASCE, **109**(3), 458-482.

I.M. Idriss, 1999. An update to the Seed-Idriss simplified procedure for evaluating liquefaction potential. Proc., TRB Worshop on New Approaches to liquefaction, FHWA-RD-99-165, Federal Highway Administration, U.S.A.

JGS 0544: 2011. Method for laboratory measurement of shear wave velocity of soils by bender element test

K Ishihara, S Okada, 1982. Effects of large preshearing on cyclic behavior of sand. Soils and Foundations, Vol. 22, No. 3, pp 109-125.

K. Ishihara, and S. Okada. 1978. Effects of stress history on cyclic behavior of sand. Soils and Foundations, Vol. 18, No. 4, pp 31-45.

K. Tokimatsu, and A. Uchida, 1990. Correlation between liquefaction resistance and shear wave velocity. Soils and Foundations, JGS, **30**(2), 33-42.

K. Tokimatsu, T. Yamazaki, and Y. Yoshimi, 1986, Soil liquefaction evaluations by elastic shear moduli. Soils and Foundations, Vol. 26, N0. 1, pp 25-35.

K.H. Stokoe II, S.H.H. Lee, and D.P. Knox, 1985. Shear moduli measurements under true triaxial stresses. Advances in the Art of Testing Soils Under Cyclic Conditions. Detroit, ASCE.

P.K. Robertson, D.J. Woeller, and W.D.L. Finn, 1992. Seismic cone

penetration test for evaluating liquefaction potential under cyclic loading. Canadian Geotechnical Journal, **29**(4), 686-695.

P.V. Lade, and S.B. Hernandez, 1977. Membrane penetration effects in undrained tests. Journal of the Geotechnical Engineering Division, ACSE, Vol. 103, No. GT2, pp 109-125.

R. Bellotti, M. Jamiolkowski, D.C.F Lo Presti, and D.A. O'Nell, 1996. Anisotropy of small strain stiffness in Ticino sand. Geotechnique., **46**(1), 115-131.

R.D. Andrus, and K.H. Stokoe II, 2000. Liquefaction resistance of soils from shear-wave velocity. Journal of Geotechnical and Geoenvironmental Engineering, 126(11), 1015-1025.

R.D. Andrus, and K.H. Stokoe II, and C.H. Juang, 2004. Guide for shear wave-based liquefaction potential evaluation. Earthquake Spectra, 20(2), 285–308.

S.K. Roesler, 1979. Anisotropic shear modulus due to stress anisotropy. Journal of the Geotechnical Engineering Division, **150**(7), 871-880.

S.L. Kramer, 1996. Geotechnical Earthquake Engineering, Prentice Hall, Upper Saddle River, New Jersey 07458, 369-375.

Y.G. Zhou, and Y.M. Chen, 2007. Laboratory investigation on assessing liquefaction resistance of sandy soils by shear wave velocity. Journal of Geotechnical and Geoenvironmental Engineering, ASCE, **133**(8), 959-972.

D.P. Baxter, A.S. Bradshaw, R.A. Green, and J.H. Wang, 2008. Correlation between cyclic resistance and shear-wave velocity for providence silts. Journal of Geotechnical and Geoenvironmental Engineering, 134(1), pp 37-4,

CHAPTER 7

CONCLUSIONS AND FUTURE WORKS

7.1 Conclusions

The motivation for this study was the serious disasters induced by soil liquefaction in the 2016 earthquakes. A lot of sites were liquefied twice by the two great shocks. According to the investigation by JGS organised just after the earthquake, the results reported the damages were expanded greatly in the mainshock, even if some site struck by the similar intensity between the two shocks. Therefore, there were some researchers thought that the serous damages appeared in mainshock was mainly because of the foreshock as the pre-shearing for the ground when mainshock came. The pre-shearing may cause liquefaction in some sites, which were indicated by the report of investigation, or only produced an excess pore pressure where liquefaction did not occur in foreshock. But the effects did not disappear in mainshock.

The recurrence of liquefaction in a same site is not uncommon in Japan, that the related studies have been introduced in Chapter 1. The excess pore water pressure remained in the ground when main shock came, that was considered by some researchers. The idea was depended on the relative short interval between foreshock and mainshock. However, there was not a direct evidence to prove it.

Besides, the volcanic soils were suspected influencing on the liquefaction behaviour greatly in the earthquake, that was depended on the observation and investigation for the boiled sand in liquefied sites. The liquefied sites mostly located at the plain where is nearby Aso volcano. Meanwhile, the boiled sand expressed a black or grey colour for being contained with the black soil particles.

This study was done following the two concerns. Kurobuku, a typical volcanic soil distributed in Kumamoto-Aso are, was carried as one of the test materials to be detected the liquefaction behaviour for the concern from volcanic component in liquefied ground. Boiled sand and Toyoura sand were also carried into the tests. Boiled sand was used to represent the typical soil condition for the liquefied ground in the 2016 kumamoto earthquakes. And Toyoura sand as the

standard in Japan represented the sandy ground which is thought very easily to be liquefied. For the concern of the influence from pre-shearing, cyclic tri-axial tests were conducted. The test samples were applied two serious of cyclic loading to cause liquefaction two times. This provided a comparing for the change of liquefaction resistances between liquefaction and re-liquefaction. It is very meaningful for the ground if it was liquefied in history.

The behaviours of Toyoura sand, Kuroboku and boiled sand concerning with pre-shearing were obtained from cyclic tri-axial tests. The results were summarised as follow:

1) For Toyoura sand, the liquefaction resistance reduced in re-liquefaction stage even if the relative density increased with some degree. However, the resistance in Kuroboku and boiled sand increased after experiencing pre-shearing or liquefied once.
2) The increment of liquefaction resistance in Kuroboku and boiled sand was different. The resistance in Kuroboku increased more greatly than in boiled sand, including those samples which were decreased the content of fines. The absolute content of fines may affect this.
3) The absolute liquefaction resistance between the three soils also very different. Kuroboku had the greatest resistance. The smallest resistance was discovered in boiled sand though it contained approximately 10% of fines. Moreover, for the boiled sand, the greater relative density can not provide a higher liquefaction resistance by the results comparison between D_r = 60% and 80%. With a same initial relative density, the samples of Toyoura sand expressed a greater liquefaction resistance than boiled sand even the resistance in second liquefication stage.

Duo to the lowest liquefaction detected for boiled sand, the soil deposited at the liquefied sties in the 2016 earthquakes can be considered very easily to be liquefied. The soil even was weaker than Toyoura sand. Additionally, if

liquefaction occurs or excess pore water pressure produced in ground, the fines are prone to be suspended in water and erupted out to surface. It reduces the fines content inside of ground, that reduced the liquefaction resistance furtherly. The great reduction of liquefaction resistance in mainshock may be caused by this reason possibly.

In addition, the evaluation method by using shear wave velocity was discussed. The velocity of shear wave could be directly obtained in field investigation without any destructivity for ground. Because of the reliability and convenience in investigation, it was discussed with the correlation to the liquefaction potential of test samples, including the samples without any pre-shearing, with the pre-shearing causing liquefaction once, and with a pre-shearing which remained excess pore water pressure. The results indicated that the evaluation would be difficult to use the shear wave velocity for the samples experienced liquefaction and re-consolidation.

In the other hand, the shear wave velocity was performed as an accuracy indicator for the excess pore water pressure produced in cyclic tests. It could indicate the residual effective stress with no disturb by the changes of relative density. However, the performance also determined by the physical properties of soils. In other words, in a ground with a certain distribution of grains, the shear wave velocity could be considered as the reliable indicator.

The results from the bender element test in cyclic tri-axial test apparatus were discussed in a simulated in-situ condition finally. Commonly, a higher liquefaction resistance was represented by a higher velocity. There was a greater accuracy for boiled sand than Toyoura sand.

7.2 Future works

Some unclear points and problem have already proposed with the results analysis in above Chapters. There are three points in most important was mentioned here again for the future works.

1) First problem is related to the explaining for the reduction of liquefaction resistance in re-liquefaction stages (Bin Ye et al. 2018). They considered the relative movement between water and sand particle was vertically to lead to long axes of particles trended to be vertical as well. However, the state before first event, the specimen which was prepared by water pluviation, also dissipate from the top of water surface to the bottom. The water also could be looked as flowing upward relating to sand particles. The behaviours trended to be different greatly. This point also needs more investigation in future works
2) For the criteria of liquefaction resistance. DA = 5% was widely used by researcher. The validity also was verified by the results in this study for the sample without liquefaction experience. The excess pore pressure produced very faster than axial strain, which lead to the necessary number of cycles for causing DA = 5% became much more than $u/\sigma_{c0}' = 1.0$. Therefore, this behaviour still needs to discussed using other soils furtherly.
3) The boundary of sand for the liquefaction estimation by using stress-correlated shear wave velocity also need to be discussed by using more results. The performance of Toyoura sand in this study and the Providence silts (Christopher et al. 2008) broke the boundary based on laboratory tests. The phenomenon was produced from the difference between laboratory and in-situ conditions or the potential defects existing in empirical analysis in field-based data, that should be detected in future for improving this evaluation method.